Interannual Variability of Air-Sea Fluxes of Carbon Dioxide and Oxygen

by

Galen Anile McKinley

B.S. Civil Engineering (1995)
Rice University

Submitted to the Department of Earth, Atmospheric and Planetary Sciences
in partial fulfillment of the requirements for the degree of

Doctor of Philosophy in Climate Physics and Chemistry

at the

MASSACHUSETTS INSTITUTE OF TECHNOLOGY

June 2002

Author .....
Department of Earth, Atmospheric and Planetary Sciences
May 3, 2002

Certified by .....
John C. Marshall
Professor
Thesis Supervisor

Accepted by .....
Ronald G Prinn
Head, Department of Earth, Atmospheric and Planetary Sciences

Interannual Variability of Air-Sea Fluxes

of Carbon Dioxide and Oxygen

by

Galen Anile McKinley

B.S. Civil Engineering (1995)

Rice University

Submitted to the Department of Earth, Atmospheric and Planetary Sciences
on May 6, 2002, in partial fulfillment of the
requirements for the degree of
Doctor of Philosophy in Climate Physics and Chemistry

Abstract

The currently observed increase in atmospheric CO_2 due anthropogenic emissions is substantially slowed by natural processes that incorporate CO_2 into the terrestrial biota and the ocean. Year-to-year changes in the CO_2 growth rate that exceed variations in the fossil fuel source indicate a significant variability in these global CO_2 sinks. However, the enormous complexity of the terrestrial and oceanic biogeochemical systems that absorb atmospheric CO_2 makes these sinks extremely difficult to understand and precisely quantify. Many techniques, including the interpretation of the relative changes in atmospheric CO_2 and O_2/N_2, ocean modeling, and atmospheric data inversions, have been employed to estimate the mean and variability of global CO_2 sinks. However, uncertainty remains large. The goal of this thesis is to improve understanding of global CO_2 sinks by considering (1) the error in the atmospheric O_2/N_2 partitioning method due to the neglect of interannual variability in the air-sea fluxes of O_2, and (2) the interannual variability of the ocean CO_2 sink. A global, high-resolution ocean general circulation model is used to estimate the magnitude and understand the mechanisms of interannual variability in air-sea fluxes of both CO_2 and O_2. I find that the global variability in the fluxes of both gases are dominantly forced by large-scale physical processes governing upper ocean dynamics, particularly El Niño / Southern Oscillation (ENSO) and, for O_2, the North Atlantic Oscillation (NAO). Estimates of the extremes of CO_2 and O_2 flux variability for the period 1980-1998 are $\pm 0.5 \times 10^{15}$ grams Carbon/yr (PgC/yr) and $-70/+100 \times 10^{12}$ mol/yr (Tmol/yr), respectively. Global O_2 flux variability implies up to a 1.0 PgC/yr error in estimates of interannual variability in land and ocean CO_2 sinks derived from atmospheric O_2/N_2 observations. This error is significant for estimates of annual sinks, but it is cumulatively negligible for estimates of mean sinks from October 1991 to April 1998. Increasing convergence of estimates of land and ocean carbon sink variability from independent methods is also found.

Thesis Supervisor: John C. Marshall
Title: Professor

Acknowledgments

I dedicate this thesis to the memory of my mother, Elizabeth Anderson McKinley. From my earliest days, she taught me to believe in myself and to strive for the highest goals. Her commitment and support nurtured the skills that have now allowed me to achieve this goal. I am eternally grateful for her constant love and for her many sacrifices on my behalf.

I thank Mick Follows for his endless patience and careful guidance throughout this project. John Marshall provided invaluable advice at critical junctures. I also thank my other committee members, Ed Boyle, Ray Najjar, and Carl Wunsch for their time and thoughtful comments.

Chris Hill and Alistair Adcroft helped me with countless MITgcm details. Working with Stephanie Dutkiewicz made sense of so many modeling troubles. I thank Dimitris Menemenlis, Tony Lee, and Ichiro Fukumori at the Jet Propulsion Laboratory for the global model output, and for their endless willingness to answer my questions. I am grateful to Chris, along with Scott and Greg from TechSquare, for keeping PLEIADES up and running.

For all their help in small and large ways, I thank Bud Brown, Helen Deitrich, Takamitso Ito, Samar Khatiwala, Charmaine King, Lisa McFarren, Linda Meinke, and Rong Zhang. Alexandre Ganachaud and Arnaud Czaja both provided invaluable guidance and comments along the way. I thank Michael Bender, Glenn Flierl, Roger Francey, Hernan Garcia, Niki Gruber, Ralph Keeling, Corinne LeQuéré, Andrew Manning, and Peter Rayner for illuminating discussions and for their willingness to provide me with their data and results with me.

There are many friends and acquaintances who have helped to make MIT a wonderful place to be. I thank you all. I send a special thanks to Alex, Doiniţa, and Anatole Ganachaud; Christophe, Emilia, and Sasha Herbaut; Amy Casher, Syusanna Koyfman, and Gail Kopelman; and Momo. My Dad and sister, Turi, have been constant sources of care and support throughout this time.

Last in this list, but first in my heart, I thank my husband, Juan Botella Arriaga, for his love, commitment, and patience through all the ups and downs of the past 5 years. Gracias, mi amor.

Contents

List of Figures

List of Tables

Chapter 1

Introduction

Multiple lines of evidence suggest that the observed increase in the global atmospheric CO_2 concentration [*Conway et al.*, 1994a; *Keeling and Whorf*, 2000, 2001] may have significantly contributed to the 0.6°C warming of Earth in the past century [*Arrhenius*, 1896; *Manabe and Wetherald*, 1967; *Schimel et al.*, 1995; *Mahlman*, 1998; *Sarmiento et al.*, 1998; *Prentice et al.*, 2001]. Predictions of future warming compiled by the Intergovernmental Panel on Climate Change (IPCC) range from 1.4 to 5.8°C for 1990-2100. Although highly uncertain, predicted impacts of future global warming include sea level rise due to the thermal expansion of seawater and the melting of glaciers and polar ice caps; alterations in global snow and ice cover; shifts in the hydrologic cycle; increases in the frequency and severity of both extreme weather events and El Niño conditions in the equatorial Pacific; and weakening of the thermohaline circulation. [*Albritton et al.*, 2001]

The increase of atmospheric CO_2 is modulated by the natural carbon cycle such that only about half of the CO_2 emitted due to anthropogenic fossil fuel combustion, cement production and land use change remains in the atmosphere [*Tans et al.*, 1990; *Sarmiento and Sundquist*, 1992; *Bender et al.*, 1996; *Keeling et al.*, 1996; *Rayner et al.*, 1999; *Francey et al.*, 2001; *Manning*, 2001]. The remaining CO_2 is taken up into the ocean due to the solubility of CO_2 in seawater and into the terrestrial biosphere due to a net increase in biomass. The enormous complexity of the terrestrial and oceanic biogeochemical systems involved in these CO_2 sinks makes them difficult to understand and quantify. Independent estimates of sink magnitudes and geographical distributions differ significantly and have large error bars. If future greenhouse warming due to anthropogenic CO_2 emissions and

associated climate changes are to be predicted, these CO_2 sinks into the land biota and ocean must be quantified and their driving mechanisms need to be understood.

Further, observations indicate that the growth rate of atmospheric CO_2 varies on interannual timescales significantly more than do CO_2 emissions [*Conway et al.*, 1994b; *Keeling et al.*, 1995]. The substantial variability in CO_2 sinks indicated by these observations is also poorly understood. It is important that the interannual variability of CO_2 sinks is better quantified so that valuable clues to the mechanisms driving the sinks might be uncovered. This knowledge is crucial for the prediction of future changes in global CO_2 sinks that may alter the rate of CO_2 buildup in the atmosphere, the magnitude of global warming and the severity of climate change.

A variety of independent methods have been developed to address the challenge of estimating the magnitudes and understanding the mechanisms of the global CO_2 sinks. *Takahashi et al.* [1997, 1999] use in-situ oceanic measurements of the atmosphere / ocean ΔpCO_2 combined with estimates of the wind-dependence of gas exchange to calculate the mean CO_2 sink into the ocean and its geographical distribution. These observations have been combined with atmospheric data and atmospheric circulation models to estimate both the land and ocean sinks [*Tans et al.*, 1990]. Ocean general circulation models with parameterized biogeochemistry have also been used to refine estimates of the mean ocean CO_2 sink [*Sarmiento and Sundquist*, 1992; *Sarmiento et al.*, 1998], and to estimate its variability [*Winguth et al.*, 1994; *LeQuéré et al.*, 2000, 2001].

Atmospheric measurements of decreasing O_2/N_2 have been combined with measurements of the CO_2 increase to estimate the mean land and ocean sinks [*Keeling and Shertz*, 1992; *Keeling et al.*, 1996; *Bender et al.*, 1996] as well as their variability [*Battle et al.*, 2000; *Manning*, 2001] in the 1990's. Using archived air samples and snowpack (firn) gas measurements, the O_2/N_2 data set has been extended as far back as 1977 in the Southern Hemisphere [*Langenfelds et al.*, 1999; *Battle et al.*, 1996]. An assumption crucial to the O_2/N_2 method is that global net air-sea O_2 fluxes are negligible over the period of the sink estimate. This thesis will be the first test of this assumption.

Atmospheric inversion techniques have been employed to estimate CO_2 sinks into the land biosphere and the ocean. *Rayner et al.* [1999] and *Francey et al.* [2001] use atmospheric

$\delta^{13}C$[1], CO_2, and O_2/N_2 to estimate the mean sinks, their interannual variability, and their geographical distribution. In *Fan et al.* [1998] and *Bousquet et al.* [2000], only atmospheric CO_2 measurements are used to make similar estimates.

Land carbon sinks can be estimated from studies of terrestrial ecosystems. In-situ forestry studies tend to indicate a significantly smaller mean terrestrial biota sink [*Schimel et al.*, 1995] than do other methods based on ocean and atmospheric data and models. Land surface models may also be used to estimate the mean and variability of the land CO_2 sink and to predict its future change [*Schimel et al.*, 2000; *Melillo et al.*, 1993].

Many other studies have estimated CO_2 sink magnitudes, investigated regional details, and evaluated interannual variability. Yet, the magnitudes of the mean sinks and their variability remain unclear, and error bars are still large. For the mean land sink, estimates range from 0.4 ± 1.1 PgC/yr for 1977-1985 [*Battle et al.*, 1996] to 3.3 ± 1.6 PgC/yr [*Bender et al.*, 1996] for 1991 to 1994; and for the mean ocean sink from <1.0 PgC/yr [*Tans et al.*, 1990] for 1981 to 1987 to 2.3 ± 0.7 PgC/yr [*Langenfelds et al.*, 1999] for April 1978 - January 1997. Decadal shifts and interannual variability of in sink magnitudes [*Battle et al.*, 2000] may be to some degree responsible for the wide range of estimates.

I focus on two aspects of the quantification of global CO_2 sinks that relate to interannual variability in air-sea fluxes of O_2 and CO_2: (1) the potential error in the use of atmospheric O_2/N_2 in the estimation of both the mean and variability of CO_2 sinks due to interannual variability of air-sea O_2 fluxes; and (2) the magnitude and driving mechanisms of variability in the global ocean CO_2 sink. A suite of biogeochemical ocean models are used to estimate interannual and decadal variability in air - sea fluxes of O_2 and CO_2, and to understand the mechanisms driving the flux variability.

1.1 Using Atmospheric O_2/N_2 to Estimate CO_2 Sinks

Timeseries measurements of atmospheric O_2/N_2 have allowed significant advancement to be made in quantifying aspects of the global carbon cycle. Precise atmospheric measurements of O_2/N_2 and CO_2 in a sparse global network have been used to study the global CO_2 cycle and estimate CO_2 sink magnitudes [*Keeling and Shertz*, 1992; *Keeling et al.*, 1996; *Bender*

[1] $\delta^{13}C_{sample} = [\frac{(^{13}C/^{12}C)_{sample}}{(^{13}C/^{12}C)_{standard}} - 1] \cdot 1000$

et al., 1996; *Battle et al.*, 2000; *Manning*, 2001]. CO_2 sinks into the terrestrial biota (B) and the ocean (O) are estimated using atmospheric data and the following two simplified equations that describe the global atmospheric carbon and oxygen budgets.

$$\Delta CO_2 = F - O - B \tag{1.1}$$

$$\Delta O_2 = \alpha_F F - \alpha_B B \tag{1.2}$$

Here, ΔCO_2 (ΔO_2) is the observed global change in the atmospheric CO_2 (O_2) concentration, F is the global source of CO_2 due to the burning of fossil fuels. The factor α_F is the O_2:C molar ratio describing O_2 utilization and CO_2 production with fossil fuel burning, and α_B is the O_2:C ratio for O_2 production and CO_2 utilization with terrestrial photosynthesis. ΔO_2 is measured as O_2/N_2 in the atmosphere. It is assumed that over the time period these equations are applied, there is no net air-sea O_2 flux, and for this reason Equation 1.2 has no term to describe the ocean's interaction with atmospheric O_2.

Studies using this method and different data sets over various time periods have made various estimate for the CO_2 sinks into the ocean and terrestrial biota. For the period July 1991 to July 1994, *Keeling et al.* [1996] estimate global land and ocean sinks of 2.0 ± 0.9 PgC/yr and 1.7 ± 0.9 PgC/yr, and use the north - south gradient of O_2/N_2 and CO_2 to infer that the land biota sink is primarily in the temperate northern latitudes. For 1991-1994, *Bender et al.* [1996] find global land and ocean sinks of 3.3 ± 1.6 PgC/yr and 1.1 ± 1.6 PgC/yr, respectively. *Manning* [2001], in an update of the *Keeling et al.* [1996] study, finds land and ocean sinks of 1.62 ± 0.58 PgC/yr and 1.51 ± 0.41 PgC/yr, an average for July 1991-July 1999. *Manning* [2001] extends the O_2/N_2 method to estimate the interannual variability of the CO_2 sinks by assuming that Equations 1.1 and 1.2 are valid over each annual cycle.

Battle et al. [1996] and *Langenfelds et al.* [1999] use measurements from air trapped in the firn at the South Pole and in air archives at Cape Grim, Tasmania to extend the O_2/N_2 record back to 1977. *Battle et al.* [2000] use these data sets and atmospheric $\delta^{13}C$ to infer a significant decadal shift in the terrestrial sink of CO_2 wherein the land biosphere is neutral to CO_2 in the 1980's and has a sink of 1.4 ± 0.8 PgC/yr from mid-1991 to mid-1997.

The approach used in all these studies assumes that the global atmospheric oxygen concentration can be described by only a land photosynthetic source and a fossil fuel sink. However, evidence exists that variability of air-sea fluxes of O_2 may not be negligible on interannual timescales. In the study of *Bender et al.* [1996], O_2/N_2 data from two stations at 41°S are shown to have a large seasonal cycle with substantial interannual variability (21% of the mean). In a latitude with minimal terrestrial influence, the only remaining forcing for O_2 cycle variability is the ocean. These observations support the hypothesis that interannual variability in air-sea fluxes of O_2 may not actually be negligible.

There are several physical mechanisms which may allow for interannual and longer timescale air - sea flux variability of O_2.

- *Local Balance*: [*Bender et al.*, 1996] A net efflux of O_2 from the ocean occurs in the warm months when photosynthesis exceeds respiration and the euphotic zone becomes supersaturated with O_2. Some organic matter sinks below the euphotic zone and is oxidized, creating an undersaturated reservoir beneath. Deep mixed layers of the cold months bring this undersaturated water to the surface and a net influx of O_2 from the atmosphere occurs [*Jenkins and Goldman*, 1985]. In the interpretation of joint timeseries measurements of atmospheric CO_2 and O_2/N_2, a local balance of warm month efflux and the cold month influx has been assumed over each annual cycle. However, it is likely that temporary storage and deficit occurs due to the advection of anomalies, and because mixed layer depths and productivity rates change on various timescales. *Dutkiewicz et al.* [2001] illustrate the relationship of significant changes in phytoplankton productivity to physical processes in the North Atlantic.

- *Stationary Fluxes*: [*Bender et al.*, 1996] Local O_2 flux imbalances over each annual cycle due to organic matter sinking into isopycnals below the depth of deepest winter convection will to some degree be compensated for by the ventilation of O_2 undersaturated waters along that isopycnal in high latitudes. However, isopycnal ventilation has a decadal timescale. A possibility of temporary storage or deficit with decadal timescales exists through this mechanism.

- *Temperature variability*: Efflux of O_2 occurs in summer and influx in winter due to the inverse relationship of solubility and temperature. Sea surface temperatures vary

interannually, and therefore a potential for flux variability due to thermal forcing also exists. However, the effect of temperature variability on atmospheric O_2/N_2 may be effectively cancelled by proportional changes in the air-sea flux of N_2.

- *Net O_2 outgassing*: Observations of decreasing in-situ O_2 concentrations in the North Pacific [*Keller et al.*, 2002; *Emerson et al.*, 2001] and global modeling studies [*Plattner et al.*, 2001; *Matear et al.*, 2000; *Sarmiento et al.*, 1998] indicate that global warming is driving a net O_2 outgassing from the ocean. Increasing upper ocean stratification has been found to be primarily responsible for the net outgassing. The studies of *Plattner et al.* [2001] and *Keeling and Garcia* [2002] find that this global net O_2 outgassing implies a correction to the most recent IPCC sink estimates for 1990-2000 [*Manning*, 2001] that shifts 0.7 PgC/yr and 0.2 PgC/yr, respectively, of carbon uptake from the land sink to the ocean sink.

Via the above-mentioned mechanisms, variability in meteorological forcing, influencing the ocean through convective and advective changes, SST anomalies, gas transfer coefficients, and productivity changes may be linked to air - sea O_2 flux variability. Coordinated regional climate shifts associated with the North Atlantic Oscillation, the El Niño / Southern Oscillation cycle and the Antarctic Circumpolar Wave may drive variability in air - sea fluxes of O_2.

For the short timeseries used for mean calculations with O_2/N_2, and especially for calculations of the interannual variability in the sinks, there may be significant error due to the interannual variability in O_2 air-sea fluxes. This neglected variability could disturb the assumed balance between fossil fuel emissions of CO_2 and uptake by the land biota and ocean solubility. Hitherto, it has not been possible to incorporate the error due to the neglect of air-sea gas flux variability into atmospheric data / modeling studies because this variability has not been quantified. The first goal of this thesis is to estimate the global interannual variability in air-sea O_2 fluxes and to evaluate the error the neglect of this variability imparts to O_2/N_2 estimates of CO_2 sinks.

1.2 Interannual Variability of the Sink of CO_2 into the Ocean

The variability of the CO_2 sink in the oceans has been the subject of some controversy in the recent past. *LeQuéré et al.* [2000] point out that ocean observation and model-based estimates of ocean CO_2 sink variability [*Winguth et al.*, 1994; *Lee et al.*, 1998; *LeQuéré et al.*, 2000] are all significantly smaller that atmosphere inverse model estimates [*Francey et al.*, 1995; *Keeling et al.*, 1995; *Rayner et al.*, 1999; *Joos et al.*, 1999].

The recent atmospheric inversion study of *Francey et al.* [2001], updating the work of *Rayner et al.* [1999], indicates a substantially smaller ocean CO_2 sink variability than previous atmospheric inversion studies. Recalibration of $\delta^{13}C$ data at Cape Grim, better gross flux estimates and new smoothing routines are responsible for the smaller estimate of ocean flux variability (Roger Francey, personal communication). Data issues such as these may be the root cause of the discrepancy pointed out by *LeQuéré et al.* [2000]. However, the cause may be that the models are too coarse in resolution, have overly crude forcing, or are otherwise unable to capture the physical variability of the ocean that actually causes air-sea CO_2 flux variability. For example, the model of *LeQuéré et al.* [2000, 2001] may be limited in its capacity to capture the physical variability of the ocean outside the tropics because model temperature and salinity are restored to climatological values beneath the mixed layer at a rapid 1 month timescale everywhere away from the coasts and outside 10°S to 10°N. This means that physical variability in the model of *LeQuéré et al.* [2000, 2001] is likely damped in the middle and high latitudes.

Model estimates presented by *Winguth et al.* [1994], *LeQuéré et al.* [2000] , and *LeQuéré et al.* [2001] indicate that the equatorial Pacific drives the majority of the global CO_2 flux variability. Physical changes associated with the El Niño / Southern Oscillation cycle explain a significant portion of the air-sea flux variability in this region. Further, the equatorial Pacific observations summarized by *Feely et al.* [1997] indicate a CO_2 flux variability in this region that is similar in magnitude to the model estimates of the global flux variability, suggesting that this region may indeed be globally dominant. However, another interpretation of this comparison is that model variability is only realistic in the tropics.

In addition, other recent studies question the dominance of the equatorial Pacific in the global air-sea CO_2 flux variability. A study of data from the Bermuda Atlantic Timeseries

Station in the North Atlantic indicates the potential for significant CO_2 flux variability associated with the North Atlantic Oscillation (Niki Gruber, personal communication). It is possible that the properties of previous ocean models have made them unable to capture this type of extratropical variability.

In summary, there remain several outstanding questions regarding the magnitude and mechanisms of the variability of air-sea CO_2 fluxes. It is particularly unclear how the different properties of ocean general circulation models might change flux variability estimates. Therefore, the second goal of this thesis is to provide a new model estimate of air-sea CO_2 flux variability using a fully prognostic, high-resolution ocean general circulation model. I will consider the contributions of basin-scale regions of the ocean to CO_2 flux variability, evaluate the driving mechanisms in these regions, and determine whether the properties of this model makes it better able to capture the full extent of CO_2 flux variability.

1.3 Summary

The importance of variability in air-sea fluxes of O_2 to estimates of global CO_2 sinks has not been investigated. Assumptions neglecting O_2 air-sea flux variability in the use of atmospheric O_2/N_2 data to determine CO_2 sinks need to be tested and the error resulting from these assumptions needs to be quantified. In face of a dearth of oceanic measurements, alternative methods must be used. In this thesis, I use an ocean general circulation model with parameterized biogeochemical processes in an effort to provide reasonable bounds for the O_2 air-sea flux boundary condition.

In addition, significant questions remain about the variability of the global ocean CO_2 sink and the mechanisms responsible for this variability. This work provides an updated estimate of the ocean CO_2 sink variability by using a fully prognostic, high-resolution ocean general circulation model.

In **Chapter 2** (published as *McKinley et al.* [2000]), the question of O_2 flux variability is initially addressed using a regional model of the North Atlantic for 1987-1995. The model estimates a significant O_2 flux variability in this region and the results suggest that global interannual variability in O_2 fluxes may be large.

The physical model driving the offline global biogeochemical model is evaluated in

Chapter 3. The biogeochemical model for phosphorus, O_2, and CO_2 is then described. As part of this description, the derivation of a spatially inhomogeneous export parameter that improves the model agreement with the nutrient climatology is discussed.

Estimates of the variability of global air-sea fluxes of CO_2 and O_2 for 1980-1998 from the global biogeochemical model are detailed in **Chapter 4**. A significant flux variability exists for both gases. Large-scale physical changes in the equatorial Pacific associated with the El Niño / Southern Oscillation cycle dominate the global air-sea flux variability of both CO_2 and O_2. Variability in global O_2 fluxes is also driven to a significant degree by convective variability in the North Atlantic that is typically associated with the North Atlantic Oscillation. The global CO_2 flux variability is minimally impacted by rapid physical changes in the North Atlantic because shifts in biogenic export eliminate DIC anomalies before CO_2 gas exchange is significantly altered. Carbonate reactions are responsible for slowing CO_2 gas exchange and allowing time for the biogenic response.

In **Chapter 5**, I find that estimates of air-sea flux variability of O_2 and CO_2 are changed only slightly in 1997-1998 by the use of a new version of the physical model that has been constrained by satellite altimetry. The minimal change in gas flux variability is due to the altimetric constraint having little impact on the physical state of the model below the surface layer.

The impact of air-sea O_2 flux variability on the calculation of land and ocean CO_2 sinks and their variability using atmospheric O_2/N_2 is quantified in **Chapter 6**. The impact is found to be significant on interannual timescales, but negligible for mean sinks calculated over the period October 1991 - April 1998. In addition, it is shown that the most recent estimates of the variability of CO_2 sinks from separate methods agree that the global land sink of CO_2 is significantly more variable (approximately ± 2 PgC/yr) than the ocean sink (less than ± 1 PgC/yr).

Chapter 2

Interannual Variability of the Air-Sea Flux of Oxygen in the North Atlantic

This chapter appeared in full as McKinley, G.A., M.J. Follows and J.C. Marshall, Interannual variability of the air-sea flux of oxygen in the North Atlantic, *Geophysical Research Letters, 27*(18), 2933-2936, 2000.

In studies using timeseries observations of atmospheric O_2/N_2 to infer the fate of fossil fuel CO_2, it has been assumed that multi-year trends in observed O_2/N_2 are insensitive to interannual variability in air-sea fluxes of oxygen. We begin to address the validity of this assumption by investigating the magnitude and mechanisms of interannual variability in the flux of oxygen across the sea surface using a North Atlantic biogeochemical model. The model, based on the MIT ocean general circulation model, captures the gross patterns and seasonal cycle of nutrients and oxygen within the basin. The air-sea oxygen flux exhibits significant interannual variability in the North Atlantic, with a standard deviation (0.36 mol m^{-2} y^{-1}) that is a large fraction of the mean (0.85 mol m^{-2} y^{-1}). This is primarily a consequence of variability in winter convection in the subpolar gyre.

2.1 Introduction

The variability of air-sea O_2 fluxes has recently become of particular interest since observed atmospheric O_2/N_2 trends have been used to estimate the partitioning of the sink of fossil fuel CO_2 between the ocean and terrestrial biosphere [*Keeling et al.*, 1996; *Bender et al.*, 1996]. These studies indicate that approximately one-third of anthropogenically produced CO_2 is taken up by the global land biota (2.0 ± 0.9 Pg carbon y^{-1} ($PgCy^{-1}$);[*Keeling et al.*, 1996]). *Keeling et al.* [1996] also use the meridional gradient of O_2/N_2 and CO_2 to infer that the sink in the Northern Hemisphere land biota is approximately the same magnitude (1.9 ± 0.9 $PgCy^{-1}$) as the global sink. Forest inventory studies, however, suggest a smaller global land biota sink (0.5 ± 0.5 $PgCy^{-1}$, [*Schimel et al.*, 1995]).

A key assumption made by *Keeling et al.* [1996] and *Bender et al.* [1996] is that multi-year trends in observed O_2/N_2 are insensitive to interannual variability in the global, annual mean air-sea oxygen flux. The global atmospheric balance for CO_2 and O_2/N_2 is assumed to be comprised only of the long-term trends imparted by fossil fuel combustion, land biota and ocean CO_2 uptake. However, data suggests that interannual variability may be significant. *Bender et al.* [1996] study atmospheric O_2/N_2 data from two stations at 41°S and interpret a large seasonal cycle with substantial interannual variability (21% of the mean). At a latitude with minimal terrestrial influence, the likely source for O_2 variability is air-sea exchange.

The magnitude of interannual variability in air-sea oxygen fluxes has yet to be estimated either globally or regionally. Although the impact of interannual variability on CO_2 sink estimates will be reduced by forming multi-year averages, the timescale on which interannual variability is negligible also remains an unknown.

In this study we focus on air-sea O_2 flux variability in a model of North Atlantic ocean. Our goals are two-fold. Firstly, to examine the regional interannual variability of air-sea O_2 fluxes. Is there potential for a significant uncertainty in estimates of fossil fuel CO_2 partitioning due to the assumption that interannual variability in air-sea O_2 fluxes can be neglected? Secondly, we elucidate the physical mechanisms underlying the model's variability.

2.2 North Atlantic Biogeochemical Model

We use a North Atlantic biogeochemical model based on the MIT ocean general circulation model (MITgcm) [*Marshall et al.*, 1997b,a] integrated globally at one degree horizontal resolution, with 21 vertical levels, and initialized with *Levitus and Boyer* [1994] climatology. It was forced with 12-hourly, reanalyzed wind stress and heat flux fields during the period 1979-1996, and a nine-year segment (1987-1995) of model variables stored for use in offline studies. Geostrophic eddy transfer is parameterized using the *Gent and McWilliams* [1990] scheme and the upper ocean mixed-layer is parameterized by convective adjustment. The MITgcm and offline model are discussed in more detail in *Dutkiewicz et al.* [2001].

The biogeochemical model is based on the cycles of phosphorus and oxygen in the ocean. The governing equations for phosphate, P, and oxygen, O_2 are

$$\frac{\partial P}{\partial t} = -\nabla \cdot (\mathbf{u}P) + \nabla \cdot (\kappa \nabla P) + C_P + S_b + S_r \tag{2.1}$$

$$\frac{\partial O_2}{\partial t} = -\nabla \cdot (\mathbf{u}O_2) + \nabla \cdot (\kappa \nabla O_2) + C_{O_2} + R_{O_2:P} \cdot (S_b + S_r) + E \tag{2.2}$$

where $\mathbf{u}$ is the transformed Eulerian mean velocity and $\nabla \cdot (\kappa \nabla P)$ is a tensorial representation of mixing along isentropic surfaces, with transfer coefficient $\kappa = 10^3$ m^2 s^{-1} as in the MITgcm [*Gent and McWilliams*, 1990]. Convective mixing (C) is achieved using statistics of convection in the MITgcm to govern the distribution and frequency of vertical mixing events [*Dutkiewicz et al.*, 2001], and acts on the local gradients of individual tracers. S_b is the loss of P due to formation of sinking particles, and S_r the source from remineralization.

We use a simplified, light and nutrient limited parameterization of particulate export: $S_b = -\epsilon(\partial\Phi/\partial z)(P/(P + P_{max}))$. Light limitation is implemented to ensure that the rate of export cannot exceed the photosynthetic energy supplied by the vertical flux divergence of photosynthetically radiation radiation, $\partial\Phi/\partial z$, assuming a photosynthetic efficiency, ϵ. This is an upper bound where all photosynthetically available photons are assumed used for new production. When light is limiting ($P \gg P_{max}$) the export rate asymptotes to $-\lambda_b \mathrm{P}_{max} = \epsilon(\partial\Phi/\partial z)$. Here P_{max} is the concentration of nutrients at which light becomes limiting to export production. The characteristic timescale for export of P, $1/\lambda_b$, is chosen such that when light is not limiting it is about 1 week. The monthly mean solar radiation

flux at the surface of the ocean (Φ(y,0,t)) is determined using the astronomical formula of *Paltridge and Platt* [1976] and a latitudinally varying albedo according to *North et al.* [1981]. The profile of light in the water column is assumed to follow $\Phi(z) = \Phi(0)e^{-k_w z}$, where k_w, the extinction coefficient, is an empirical function of latitude, based on Secchi depth observations [*Lewis et al.*, 1988; *Parsons et al.*, 1984]. Photosynthetic efficiency, ϵ, is assumed to have a value of 1.35×10^{-5} μmol P per Joule of surface incident radiation when vertically averaged over the euphotic zone, consistent with *Morel* [1978]. Export production is reduced by sea-ice, proportional to the fractional ice cover in each grid cell. The sinking particle flux at all depths is parameterized using an exponential profile with a scale height of 400m [*Dutkiewicz et al.*, 2001], the divergence of which provides the remineralization source of P.

Biological sources and sinks of O_2 are assumed to be in fixed proportion to those of P, where $R_{O_2:P} = -175 : 1$ [*Takahashi et al.*, 1985]. Air-sea gas exchange (E) of O_2 is parameterized as a function of wind speed, sea surface temperature and salinity [*Wanninkhof*, 1992] with solubility properties as determined by *Weiss* [1970]. Air-sea oxygen fluxes are reduced by sea-ice, proportional to the fractional ice cover in each grid cell. A constant atmospheric O_2 concentration of 21 pph is assumed.

At open boundaries, we restore to climatological P and O_2 [*Conkright et al.*, 1994; *Levitus and Boyer*, 1994] with a timescale of 2 months. Since we are primarily interested in upper ocean variability, we restore to P climatology, but not O_2, below 1200m on a 200 month timescale. Tracer fields are initialized from the climatology of *Conkright et al.* [1994] and *Levitus and Boyer* [1994] and the model is integrated over a repeating 9 year cycle for 10 cycles until an equilibrium solution, exhibiting interannual variability, is obtained.

2.3 Model Results

The model successfully captures the broad distribution of P and O_2 in the upper ocean and exhibits a strong surface seasonal cycle typical of the North Atlantic.

In Figure 2-1 we compare the 9 year mean modeled O_2 distribution on the mean $\sigma_\theta = 27.5$ isopycnal surface to the observed distribution [*Conkright et al.*, 1994; *Levitus and Boyer*, 1994]. Modeled dissolved O_2 decreases towards the interior of the subtropical

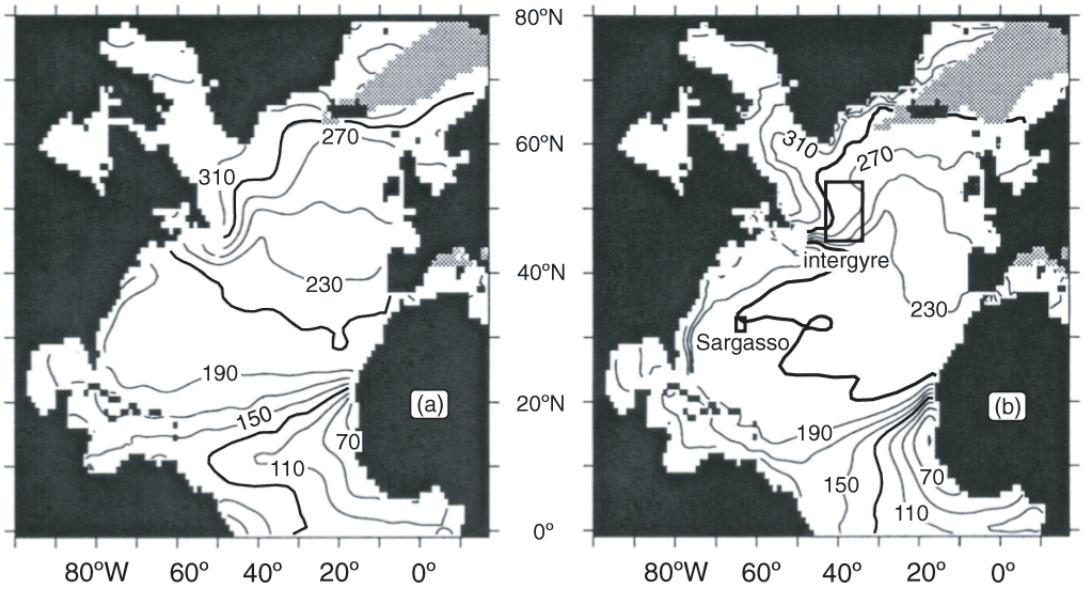

Figure 2-1: **(a)** Observed and **(b)** modeled climatological dissolved O_2 on $\sigma_\theta = 27.5$ density surface (μmol kg^{-1}). Gray areas are north of the isopycnal outcrop. The 130, 210 and 290 isolines are darkened for clarity.

gyre, indicative of respiration of exported organic matter, in a manner consistent with the broad features of the climatology. However, it overestimates the magnitude of the oxygen minimum zone on the eastern margin near Africa. In addition, high O_2 isolines extend too far south, suggesting that the model ventilates too quickly or does not export biological matter efficiently enough in other regions of the subtropics and tropics. Model isolines appear displaced to the north in the subpolar gyre in comparison to the data. This discrepancy may be due in part to summer bias in the data. Vertical displacement of the isopycnal in the physical model could also contribute to each of these discrepancies. In another comparison (not shown), we find that seasonal, surface ocean O_2 saturation levels are broadly consistent with the climatology of *Najjar and Keeling* [1997].

Over decadal and longer timescales, large scale circulation and surface heat fluxes lead to a net transfer of O_2 rich waters to the south at depth and a northward flux of warm, O_2 depleted waters near the surface. The model has a net transport of oxygen to the south, balanced by a net annual uptake from the atmosphere. At 24°N and 48° N, the modeled southwards O_2 transport is 2161 and 2057 kmol s^{-1} respectively, very close to the southward estimates of 2069±581 and 1748±475 kmol s^{-1}, respectively, deduced by *Ganachaud* [1999] from observed hydrographic and O_2 data.

Upper ocean convective mixing is particularly significant in determining nutrient supply to the surface ocean and air-sea fluxes of oxygen. The general circulation model captures the mean mixed-layer cycle and its interannual variability, as illustrated in Figure 2-2 where data from the Bermuda Atlantic Time-Series Station (BATS, 31°40"N, 64°10"W) are compared to area-averaged model results for a small region representative of the Sargasso Sea (marked on Figure 2-1b). We also find that modeled annual cycles of mixed layer depth, surface P and O_2 in the intergyre region (marked on Figure 2-1b) compare well (not shown) with observed data from Ocean Weather Ship "Charlie" (OWS C, 52°48"N, 35°30"W).

We compare observed and modeled surface O_2 at BATS and in the Sargasso region in Figure 2-3. The mean amplitude and phase of the surface annual cycle of O_2 in the Sargasso Sea compares well with the observed cycle (2-3a). The model, however, shows less variability than the observed data on sub-seasonal and interannual timescales (2-3b). The mean P cycle (not shown) in the model looks unlike the data, exhibiting a regular seasonal cycle that is not observed. Modeled P at BATS does not exhibit the intermittent

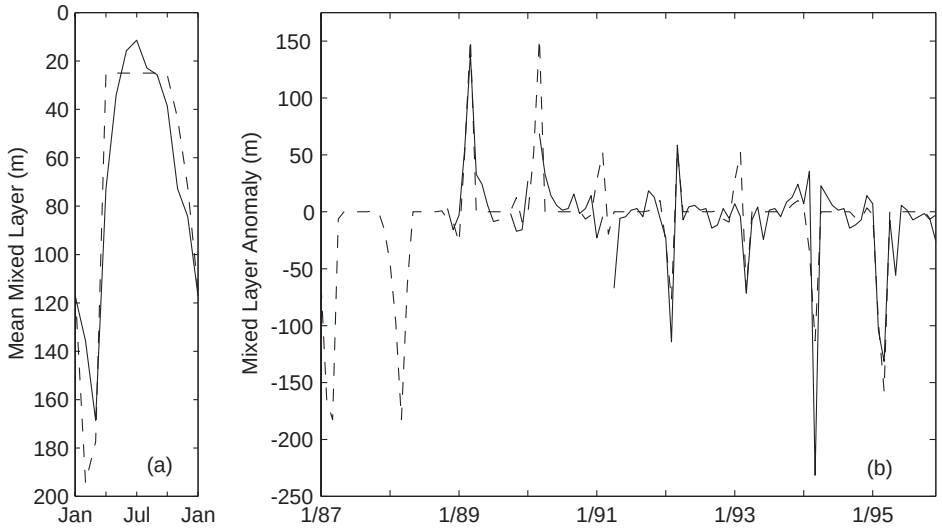

Figure 2-2: Observed (BATS, solid) and modeled (Sargasso region, dashed) mixed-layers. BATS observations began in October 1988. Mixed-layer depths are determined using a criteria of $\Delta T|_z = 0.5°C$. Both the modeled **(a)** mean annual cycle for 1989-95 and **(b)** variability with this cycle removed compare well with observations.

peaks in concentration that are seen in the data. The lack of sub-seasonal variations may be attributed to the low resolution of the model since mesoscale eddies are not explicitly resolved. Further, monthly mean model results should be less variable than instantaneous monthly observations.

In summary, the physical model works well in the North Atlantic, but the biological model is too simple to capture complex ecosystem dynamics at BATS. Despite this shortcoming, the model exhibits interannual variability in surface O_2 concentrations (and therefore, air-sea fluxes) that is comparable, although smaller in magnitude, to the data at BATS. We conclude that physical processes control surface O_2 concentrations and air-sea O_2 fluxes, and that the simplicity of the biological model is acceptable given the goals of our work.

What is the interannual variability in the integrated, basin-scale oxygen flux in the model? We find a substantial and significant interannual variability in the net air-sea exchange of O_2 over the North Atlantic basin (Figure 2-4a) which varies by as much as one-half of the mean flux from year to year. The standard deviation of the timeseries is 0.36 mol m^{-2}

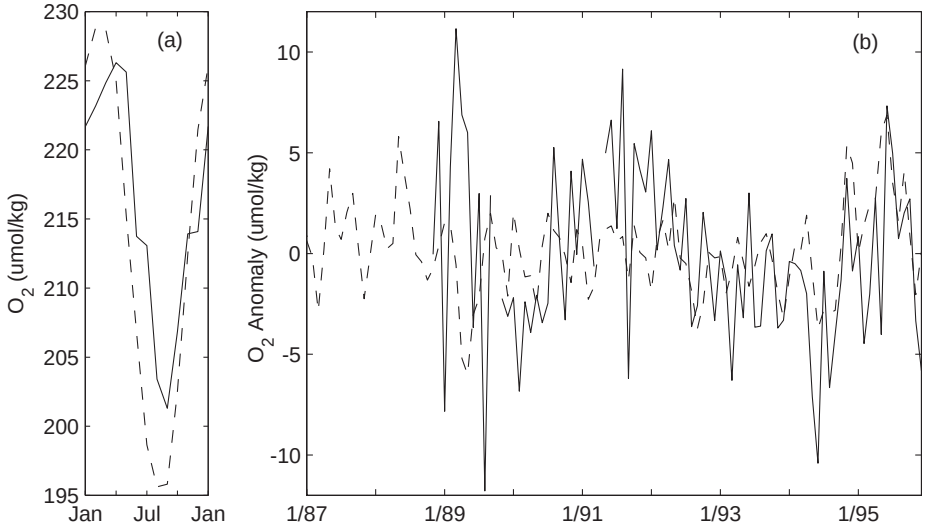

Figure 2-3: Surface O_2 at BATS / Sargasso: observed (solid) and modeled (dashed) **(a)** mean 1989-95 cycle and **(b)** variability with this cycle removed (μmol kg^{-1}).

y^{-1}, a large fraction of the mean flux into the North Atlantic (0.85 mol m^{-2} y^{-1}). Since the modeled surface O_2 exhibits weaker than observed variability on both short (month) or long (decadal) timescales, we expect that our estimate of variability in basin-averaged modeled air-sea fluxes represents a lower bound. Sensitivity experiments show similar variability over a range of values for the air-sea exchange and export parameterization coefficients.

What is the cause of this variability? The dominant balance on seasonal and interannual timescales in the North Atlantic is a vertical one; net O_2 supply to the surface ocean by wintertime air-sea exchange and net biological production is balanced by transfer of O_2 to the seasonal thermocline by convective overturning. Below, O_2 is consumed by remineralization of particles.

We illustrate the annual-average, basin-scale variations in the individual influences on the surface layer of the model in Figure 2-4b. Annual air-sea O_2 flux anomalies are largely driven by changes in convective mixing, primarily in the subpolar gyre, and the consequent transport of oxygen away from the surface waters. The dominant factor controlling changes in the air-sea flux is interannual change in entrainment of oxygen-depleted waters from the seasonal thermocline. Anomalies in biological production of oxygen tend to show the opposite influence, since enhanced entrainment also supplies more nutrients which may

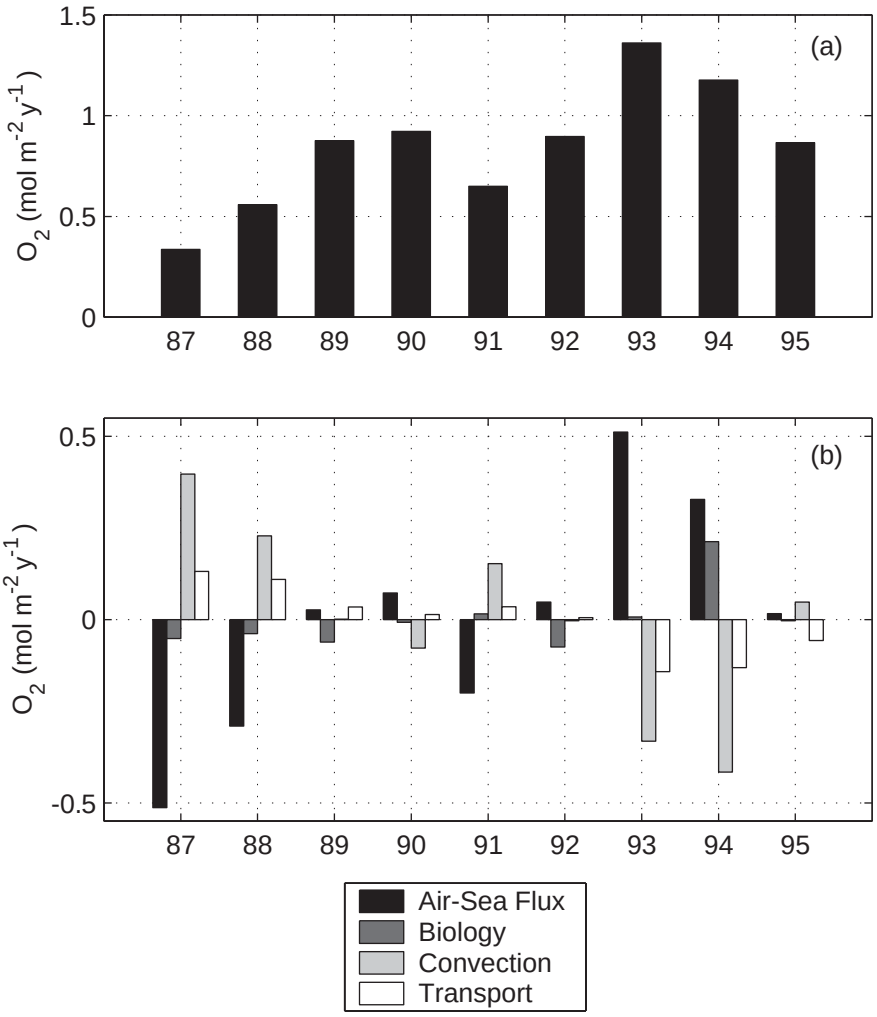

Figure 2-4: **(a)** Modeled sequence of North Atlantic annual and basin average, air-sea O_2 flux (mol m^{-2} y^{-1}). **(b)** Annual, basin-averaged, anomalies (relative to 9 year mean) of the air-sea flux and the dominant biological and physical influences driving the flux anomalies.

boost the biological production, but this process is generally of secondary importance to the air-sea O_2 flux anomaly. Advective transport anomalies in the model are generally small.

2.4 Conclusions

Using a biogeochemical model of the North Atlantic, we have shown that there may be significant interannual variability in the basin-wide air-sea flux of O_2. We find variations as much as one half of the mean uptake of O_2 by the North Atlantic. The variability, we believe, represents a lower bound, since modeled surface O_2 tends to be less variable than the observed ocean. This significant variability prompts further investigation. We are pursuing a global, multidecadal study which will provide an estimate of the annual global imbalance of air-sea O_2 fluxes.

Chapter 3

The Global Biogeochemical Model

Motivated by the finding of a significant interannual variability in O_2 fluxes in the North Atlantic, I develop an expanded offline biogeochemical model for the purpose of estimating the mechanisms and amplitudes of global air-sea fluxes of O_2. The variability of the ocean CO_2 sink is also estimated and its driving mechanisms evaluated with this model. In this chapter, the ocean general circulation model that provides the circulation and physical properties of the offline model is discussed. The mean properties and variability of the physical fields from this model are evaluated through comparisons to ocean observations. Next, the structure of the biogeochemical components of the offline model are specified. Finally, the calculation of a spatially varying export parameter that improves the climatological nutrient distribution of the model is explained in detail.

3.1 The Ocean General Circulation Model

The offline biogeochemical model is based upon the MITgcm [*Marshall et al.*, 1997b,a]. Physical model results were produced at the Jet Propulsion Laboratory, simulating the period 1980-1998 [*Lee et al.*, 2001]. Horizonal resolution is 1° in longitude, 1° in latitude at high latitudes and transitions smoothly between 26° and 10° from the equator to a 0.3° tropical resolution. There is a closed boundary at 79° N, and thus the Arctic circulation is neglected. The Mediterranean Sea is included in the model, connecting to the Atlantic over a 300m sill at Gibraltar. The online model has 47 vertical levels, with 10m resolution from the surface to 150m, transitioning to 100m resolution between 865 - 1265, and tran-

sitioning again to 400m resolution at depths greater than 3015m. To achieve a reasonable representation of mixed layers and eddy transfer processes, the Gent-McWilliams [*Gent and McWilliams*, 1990] for eddy parameterization and the KPP mixed layer [*Large et al.*, 1994] schemes are used.

The general circulation model was forced with 12 hourly reanalyzed wind stress, and heat and freshwater fluxes. These fields are a product of the National Center for Environmental Prediction (NCEP) variability of each quantity added to the Comprehensive Ocean-Atmosphere Data Set (COADS) long-term mean quantity. The COADS mean, instead of the NCEP mean, has been used because it was found that COADS mean winds corresponded better to observations at the TOGA/TAO moorings than do NCEP mean winds. Sea surface temperature (SST) is also relaxed to NCEP fields with a spatially varying relaxation constant that has a global average value of approximately 40 $W/m^2/K$. (D. Menemenlis, personal communication)

The physical model was initialized with *Conkright et al.* [1998] fields, and integrated for 10-years with climatological surface forcing fields that included the seasonal cycle prior to 19-year real-time integration. The model was largely spun-up at the point where the varying run began, but still exhibited some drift due to longer diffusive and advective time scales. A complete spin-up to depth would take many thousands of years. A salinity adjustment of relaxation to climatological sea surface salinity (SSS) with a timescale of 60 days is included in the real time 19-year run to address salinity drift. Drifts in other parameters are assumed to be small. (D. Menemenlis, personal communication)

Ten (10) day average output from the physical model is used to force the offline model. These parameters are $\mathbf{u}$, Gent-McWilliams tensors and background diffusion (K13, K23, KGM), the KPP mixing coefficients which determine all convective mixing in the model, temperature (T), and salinity (S). The salinity relaxation term, added to the freshwater forcing term, is applied to the surface of the offline model as a total freshwater flux. Model sea surface height (SSH) is also determined for diagnostic purposes.

Results for the evolution of an idealized passive tracer field in equatorial Pacific sector of the offline model have been compared to online calculations. Differences in the development in the offline tracer field from the online results are negligible when 10-day average fields are used to force the offline model. (Ichiro Fukumori, personal communication)

3.1.1 Model performance

The realism of the offline biogeochemical model estimates of O_2 and CO_2 fluxes depends to a large degree upon the quality of the physical model's representation of the global ocean, both in the mean and variability. Further, it has been illustrated in Chapter 2 and by *LeQuéré et al.* [2000] that physical variability is an important influence on O_2 and CO_2 air-sea flux variability. It is therefore important to understand how well the physical model represents the global ocean and its variability.

Mean temperature sections

Comparisons of SST in all months to the *Levitus and Boyer* [1994] climatology indicate that the model deviates from the climatology by at most 3°C in small regions, but typically deviates by less than 1°C (comparisons not shown).

Figure 3-1 illustrates that the model captures the basic shape and depth of the thermocline in the Atlantic. Comparisons in other regions of the ocean have a similar quality. In Figure 3-2 the difference of observed climatological temperatures from 19-year mean model temperatures are presented along meridional sections in both the Atlantic and Pacific, and some of the deviations of the model from the observations can be seen. In both basins, the model thermocline is too shallow in the subtropics and equatorial regions, creating low thermocline temperatures, or negative differences, in Figure 3-2. In the North Atlantic, the plume of anomalously warm water at approximately 55° acts as evidence that deep mixing occurs too vigorously in this region. Although the model deviates spatially from the observations, the broad structure of the thermocline in the model is consistent with the data.

Meridional overturning

The meridional overturning of the general circulation model is presented in Figure 3-3. The circulation reaches a maximum of 22 Sv at 1000m and 45°N in the Atlantic, reasonably consistent with the estimate by *Ganachaud* [1999] of 16 ± 2 Sv North Atlantic Deep Water formation north of 48°N. In the model, 15 Sv of Antarctic Bottom Water is formed the Southern Ocean, consistent with the 22 ± 8 Sv estimate by *Ganachaud* [1999]. Approximately 20 Sv of Antarctic Intermediate Water is formed from North Atlantic Deep

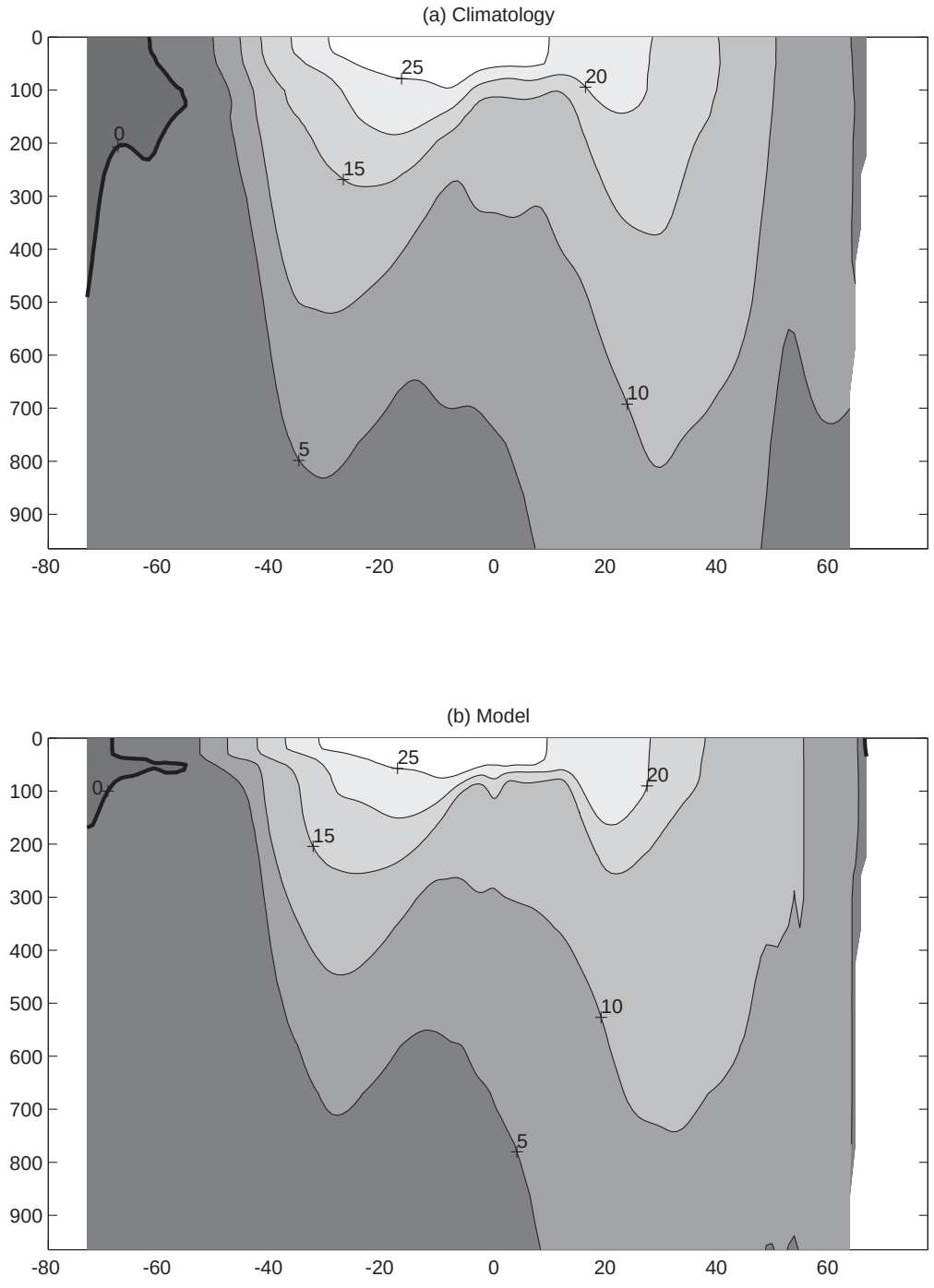

Figure 3-1: Thermocline temperature sections at 329°E in the Atlantic in (a) *Levitus and Boyer* [1994] climatology and (b) the 19-year model mean conditions for March.

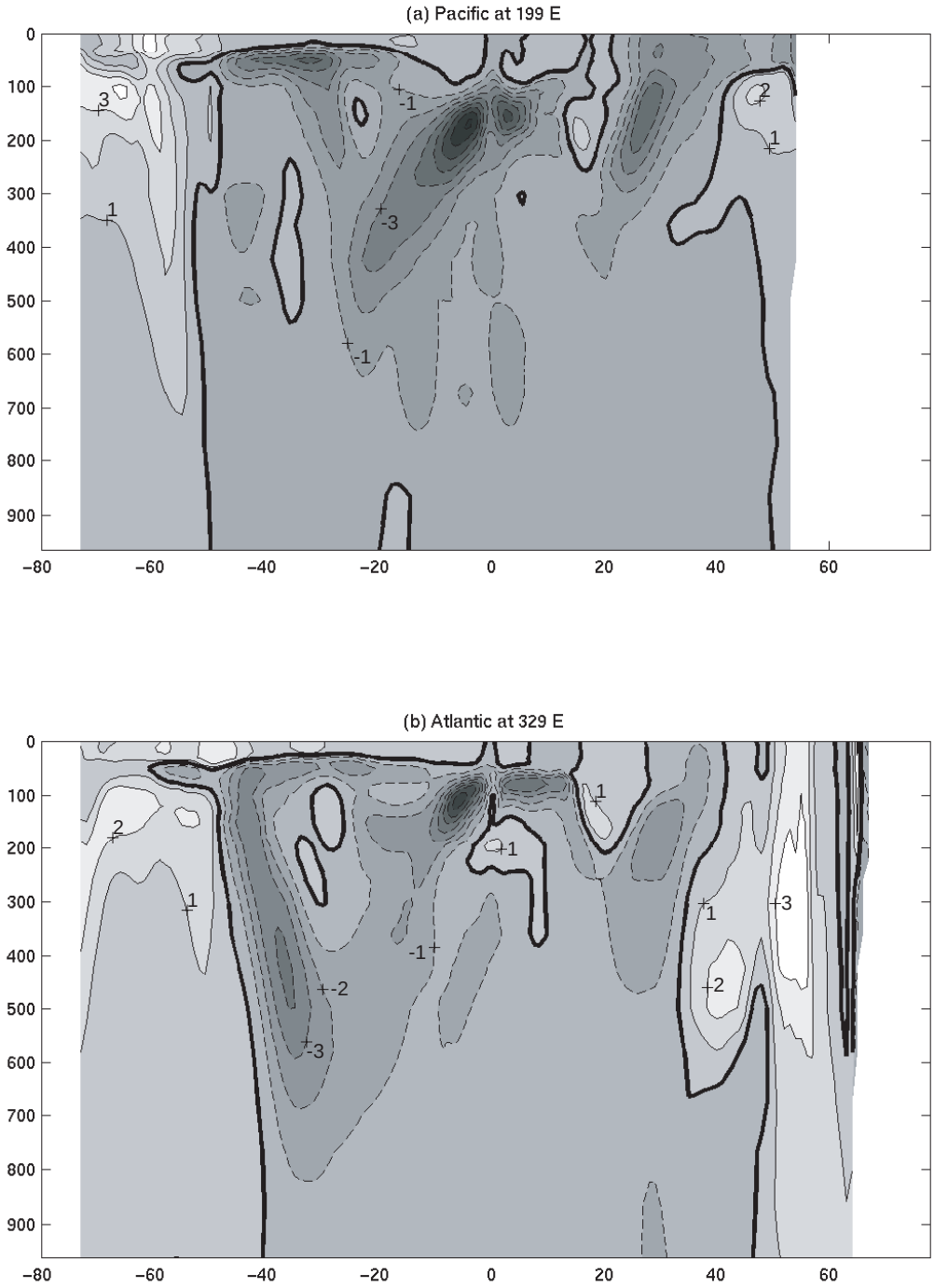

Figure 3-2: Temperature sections: difference of *Levitus and Boyer* [1994] from model in March at (a) 199°E in the Pacific and (b) 329°E in the Atlantic. Positive values indicate the model is warmer than the climatology. The thick contour indicates zero, and dashed contours indicate negative values.

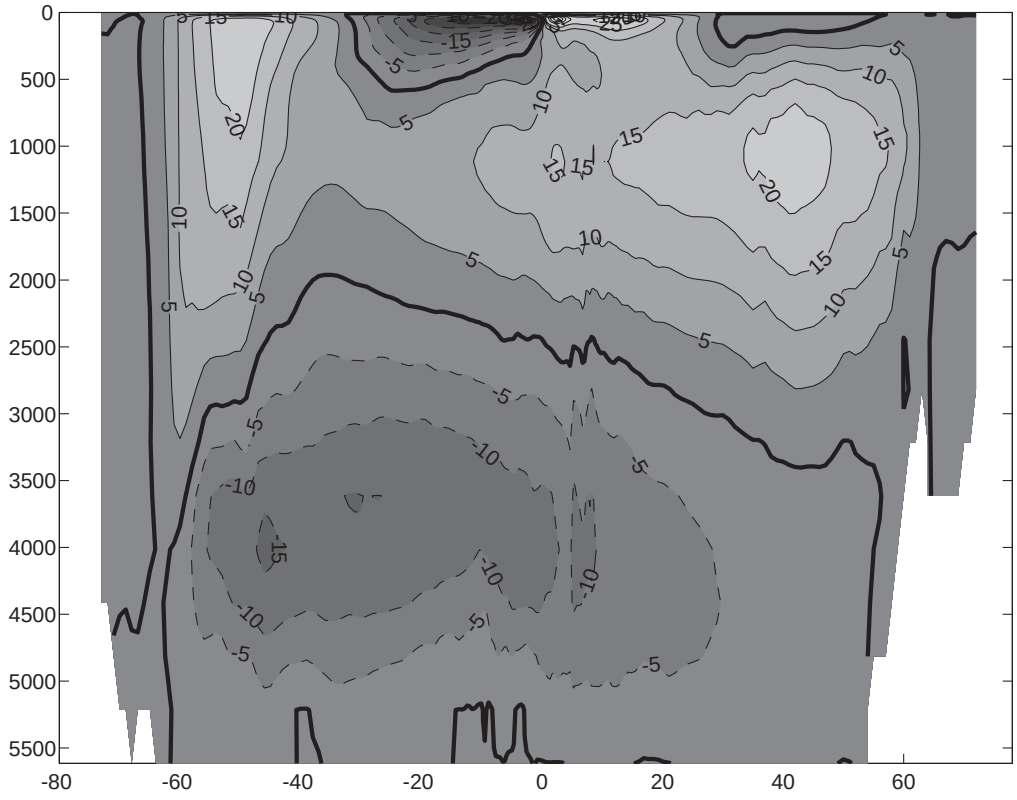

Figure 3-3: The zonal average meridional overturning circulation of the MITgcm (in 10^6 $\mathrm{m^3 s^{-1}}$ = Sv).

Table 3.1: Transport of major currents

Transport Comparisons in Sv			
location	model	observed	source
Gulf Stream at Cape Hatteras	42	70-100	*Tomczak and Godfrey* [1994]
Gulf Stream at 65°W	33	90-150	*Tomczak and Godfrey* [1994]
Gulf Stream at 40°W	36	37	*Worthington* [1976]
Kuroshio at Japan	29	40	*Pickard and Emery* [1990]
Kuroshio Extension at 152°E	33	57	*Tomczak and Godfrey* [1994]
Drake Passage	134	140 ± 6	*Ganachaud* [1999]

Water in the Southern Ocean, somewhat larger than the rather uncertain value of 6 ± 9 Sv from *Ganachaud* [1999]. Overall, the model is close to consistency with the observational estimates.

Transports of major currents

In Table 3.1, the model transport in major ocean currents is compared to published observational estimates. For all model estimates except the Drake Passage, the flow over a section 10° wide and 965m deep is integrated to calculate the transport. At the Drake Passage, the flow over the full width and depth of the channel is integrated. Model transports compare favorably with the observational estimates in the Drake Passage, the Gulf Stream at 40°W and in the Kuroshio off the coast of Japan. The underestimation of transport in the Gulf Stream at Cape Hatteras and at 65°W and in the Kuroshio system is due in large part to the model's lack of recirculation which would act to strengthen western boundary current transport.

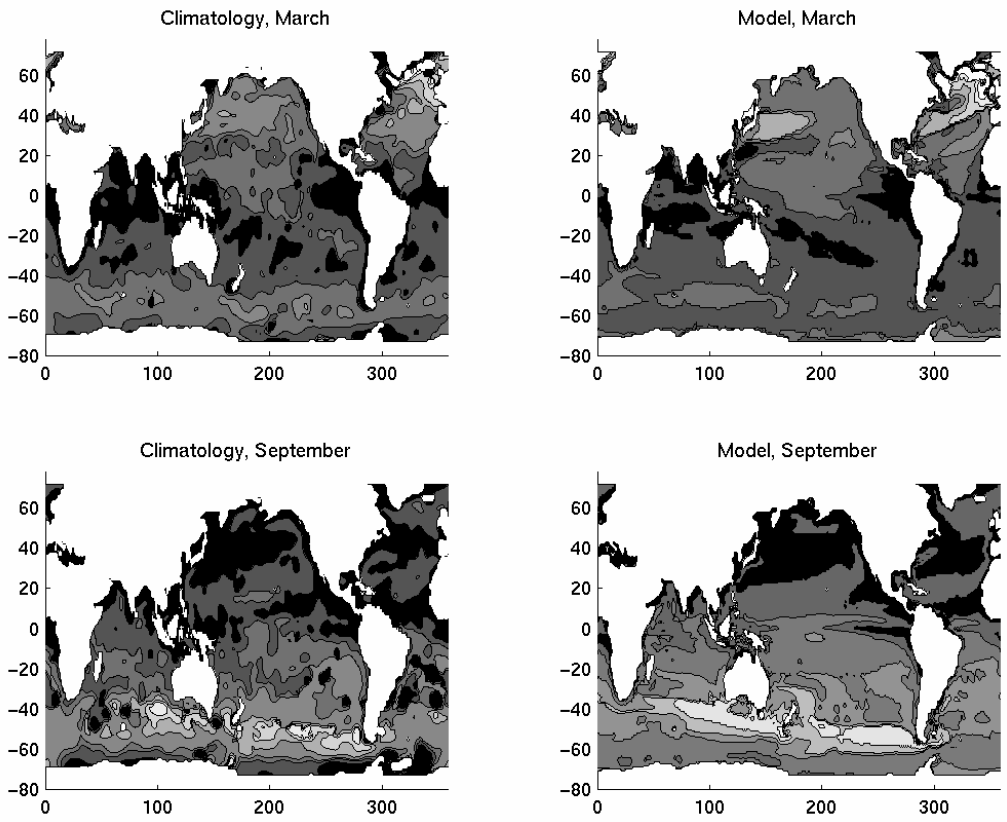

Figure 3-4: Mixed layer depth comparisons. *Levitus and Boyer* [1994] (left) compared to the 19-year model average (right) in March (top) and September (bottom). Contours are at 25, 50, 100, 250, 500, 750, 1000, and 3000m.

Mixed layer depths

In Chapter 2, it was shown that variability in high latitude mixing dominates O_2 air-sea flux variability in the North Atlantic. Thus, in addition to being an indicator of overall physical skill, mixed layer depths are likely to be important to global air-sea flux variability of O_2 and CO_2. Here, model monthly climatological mixed layer depths of the model are compared to the *Levitus and Boyer* [1994] observed climatology and to four timeseries stations. For consistency with *Levitus and Boyer* [1994], the mixed layer depth criterion in all comparisons is the depth at which the difference from the surface potential density equals or exceeds 0.125 kg m^{-3}.

In Figure 3-4, the global distribution of model and climatological [*Levitus and Boyer*, 1994] mixed layer depths in March and September are shown. The model exhibits a global

distribution, magnitude, and seasonality of deep mixing similar to the data. In the Tropics and mid-latitudes, model mixed layer depths compare well to the observations in both March and September.

In March, the deepest mixed layers occur in the subpolar North Atlantic and the northwest Pacific. Model mixed layers are approximately 150m too deep in a region to the east of Japan, and too shallow by 50m in the western subpolar North Pacific. In the subpolar North Atlantic, model mixed layers are significantly deeper than the observed estimate in the Labrador Sea where they extend beyond 3000m in areas where observations indicate depths of 1000m - 2000m. In the region of the Gulf Stream, mixed layers are deeper than observed by 150-250m. Model mixed layers are too shallow by 25-75m across much of the Southern Ocean in March.

In September, the deepest mixing occurs in the Southern Ocean. The model demonstrates less small scale variation in mixed layer depths than the observations but still captures the broad scale extent of the mixing regions and their depths. The model does not capture the deepest mixing, below 750m, that is indicated in a few localized regions of the observational climatology.

In Figure 3-5(a-d), timeseries of model mixed layers are compared to ocean timeseries data from Bermuda-Atlantic Timeseries Station (BATS, 31°40"N, 64°10"W,[*Bates*, 2001]), Ocean Weather Station "Charlie" (OWS C, 22°45"N, 158°W, [http://www.ices.dk/ocean/]), the Hawaii Ocean Timeseries Station (HOT, 52°48"N, 35°30"W, [*Karl and Lukas*, 1996]), and at the Kerguelen islands (KERFIX, 50°41"S, 68°25"E, [*Jeandel et al.*, 1998]).

At BATS, the timing of mixing in the model is quite close to that of the data, although the model is often overly deep at its deepest point. The overestimation of winter mixed layer depths at BATS is consistent with the comparison of mean model mixed layers to the climatology in March (Figure 3-4). This comparison of indicates that, on the mean, the mixing region associated with the Gulf Stream is overly broad and deep in the model. BATS lies near the edge of this mixing region, and thus horizontal displacement of the region from year to year is likely responsible for overly deep model mixed layers in some years.

At OWS C, observed mixed layer cycles starting in 1975 are compared to the nineteen years of the model. The model is quite close to the data in the summer, spring, and fall, but it is likely deeper than reality in winter, consistent with the broadscale patterns illustrated

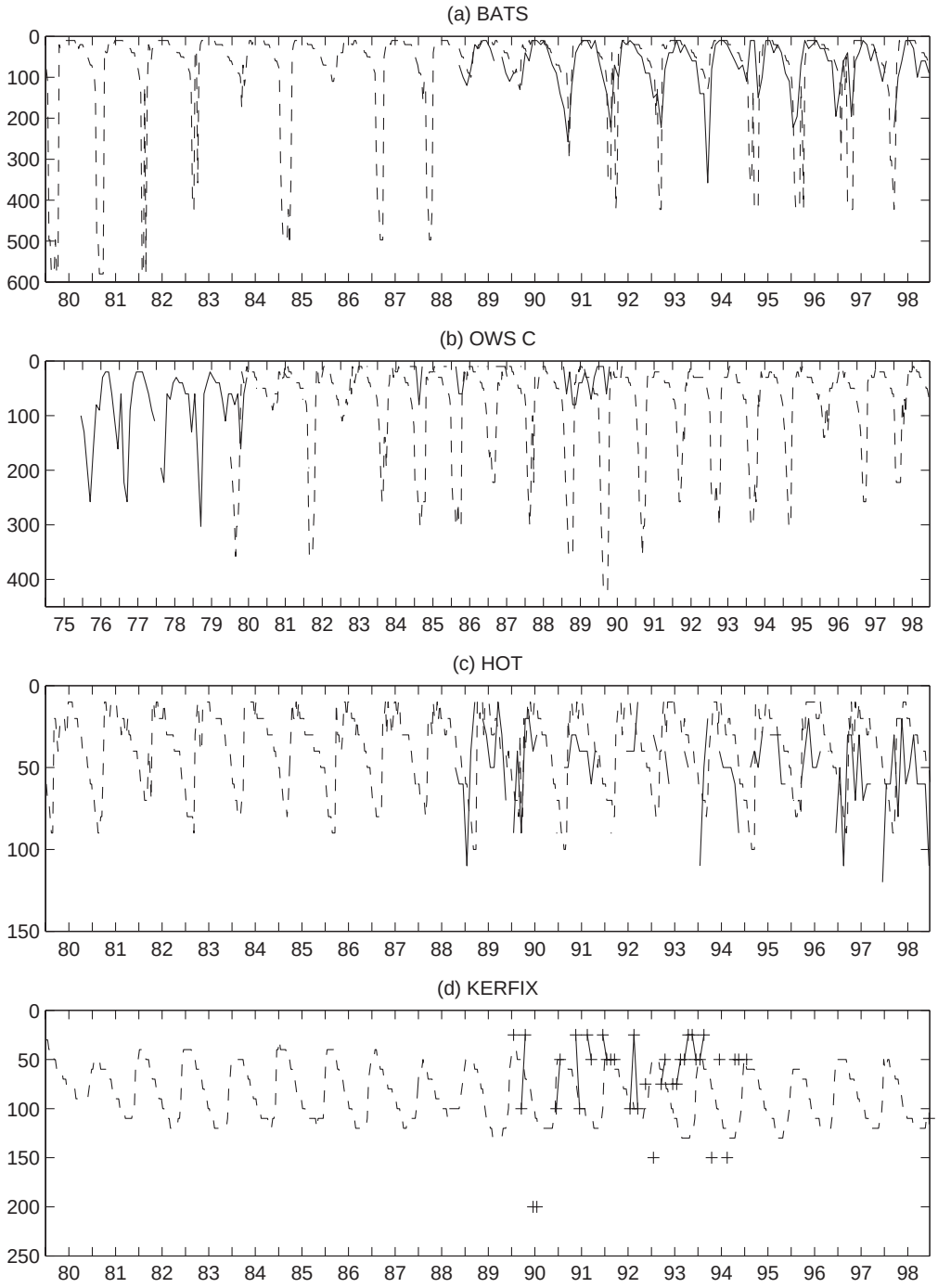

Figure 3-5: Mixed layer depth comparisons at four ocean timeseries stations. Averages over local regions in the model (dash and crosses) are used to compare to the in-situ data (solid): (a) BATS (model area: 30-32° N, 297-299° E) (b) OWS C (model area: 45-55° N, 318-328° E), (c) HOT (model area: 22-24° N, 156-158° E) and (d) KERFIX (model area: 50-52° S, 67-70° E)

in Figure 3-4 in March. At HOT, the model captures the depth and timing of the mixing in a manner generally consistent with the observations. At KERFIX, data are scarce, but the indication is that model mixed layers are 50-100 meters deeper and less variable than in the real ocean. Similar to the situation at BATS, relatively small displacement of the location of the Antarctic Polar Front in the model could be responsible for the mixed layer depth discrepancies at KERFIX.

Sea surface temperature variability

Modeled SST variability is compared to the *Reynolds and Smith* [1994] weekly analyzed fields in this section. *Reynolds and Smith* [1994] SSTs are interpolated from the weekly analyzed product to daily values, and then reaveraged to 10 days before the following analyses are performed.

When considering these comparisons, it is crucial to remember that modeled SST is relaxed toward NCEP fields that are, in large part, based the analysis of *Reynolds and Smith* [1994]. The relaxation constant for model SST varies in space and time. Its approximate global average is 40 $W/m^2/K$ in the model, which implies that it typically takes 1.7 weeks for a model - data temperature difference of 1K in the upper 10m to be eliminated. Where surface forcing creates deep mixed layers, it will take significantly longer for model - data SST differences to be removed. Nevertheless, approximately one-half of the model heat flux can be attributed to the SST relaxation (D. Menemenlis, personal communication). As such, a good model - data agreement in SST may not necessarily indicate that ocean subsurface processes have skill. Despite the complication of SST relaxation, I choose to present this comparison because SST has been shown to be a central driver of the seasonal cycles of O_2 and CO_2 fluxes over much of the ocean [*Najjar and Keeling*, 2000; *Takahashi et al.*, 1993; *Keeling et al.*, 1993], and may be an important driver of interannual variability.

SST comparisons in four representative ocean regions are shown in Figure 3-6. In the subpolar North Atlantic (Figure 3-6(a)), modeled SST exhibits a larger seasonal cycle than the data in most years, with significantly lower SSTs in the winter months than observed. These lower SSTs are most likely due to model mixed layers being too deep in this region. Interannual variations in maximum annual SSTs are well captured by the model. In the subtropical North Atlantic (Figure 3-6(b)), mean SSTs and their interannual variability are

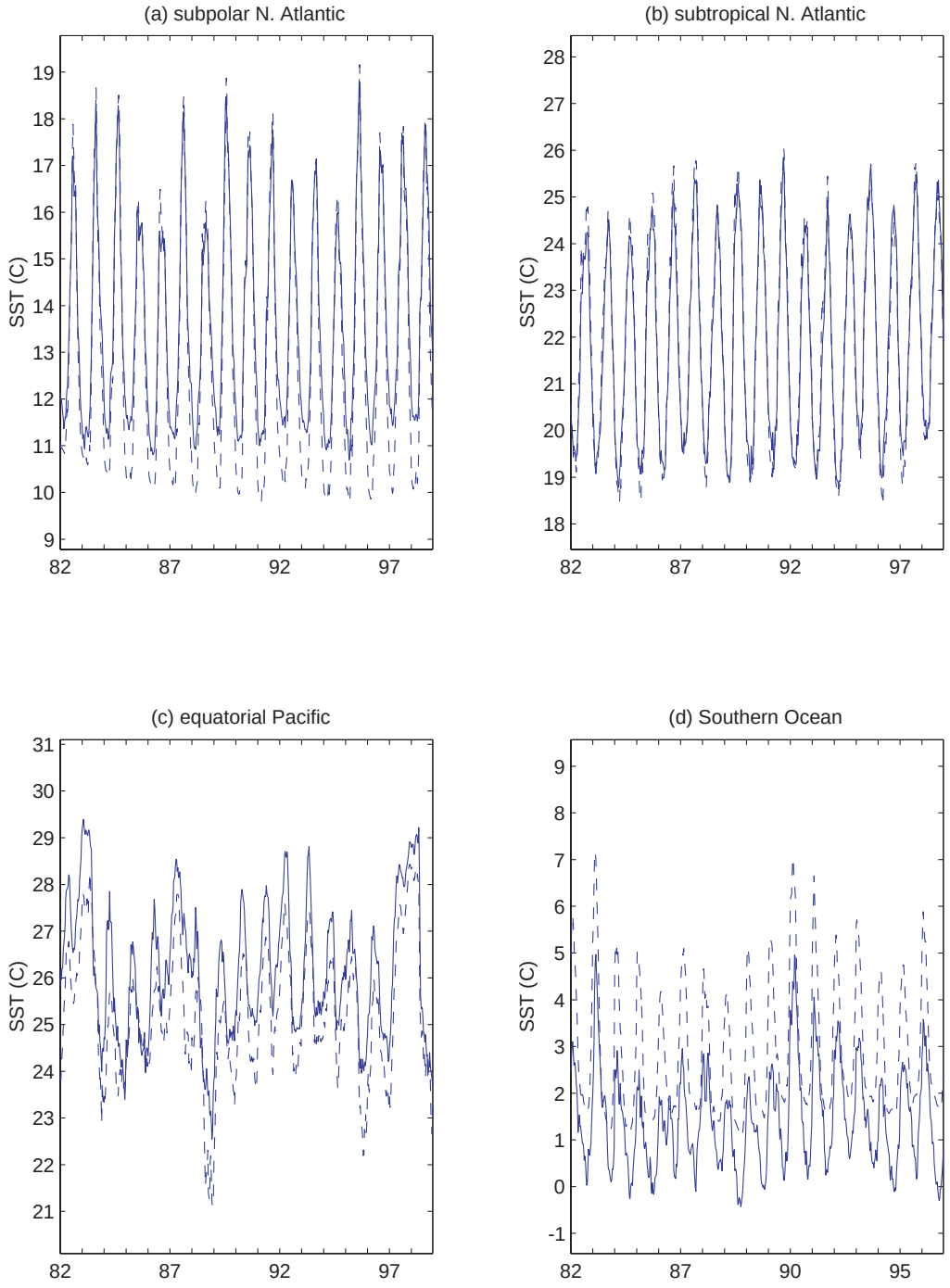

Figure 3-6: SST in four representative ocean regions: model (dashed) compared to *Reynolds and Smith* [1994] (solid). (a) Subpolar North Atlantic at 45-55°N, 340-350°E, (b) Subtropical North Atlantic at 25-35°N, 330-340°E, (c) Equatorial Pacific at 5°S - 5°N, 220-250°E, and (d) Southern Ocean at 55-65°S, 215-225°E.

well captured. In the equatorial Pacific (Figure 3-6(c)), modeled SSTs are too low on the mean by 1°C. Yet, interannual and shorter timescale variability is well represented. The high SST characteristic of El Niño events is clearly seen in 1982-1983 and 1997-1998. In the Southern Ocean (Figure 3-6(d)), the model mean SST is too high by 1.5°C, perhaps due excessive stratification in this region. Nevertheless, much of the interannual variability of SST is captured.

In Figure 3-7, the zonal average SST variance is presented for each basin. These comparisons indicate that the model either correctly estimates or slightly overestimates the observed variance in SST in most regions. In the Atlantic from 40-60° N, however, the model significantly overestimates SST variance. Excessive winter mixing in this region may be responsible for this overestimate.

In summary, while the model underrepresents local features of the annual SST cycle and variability, it successfully captures SST variance on the large scale in most regions. Model relaxation to NCEP SSTs, providing approximately one-half the total heat flux, is a significant contributor to the good agreement shown here.

Sea surface height

Sea surface height (SSH) has been observed by the TOPEX/POSEIDON satellite since late 1992. Here, model SSH variability is compared to the TOPEX/POSEIDON observations in order to estimate the model's skill at capturing variability in the circulation of the upper ocean on a global scale. This comparison follows the methodology of *Stammer et al.* [1996].

For these comparisons, the MIT altimetric data set, with 10 day temporal resolution and 2°x2° spatial resolution is used [*King et al.*, 1994]. Model SSH is regridded to 2°x2° for these comparisons. After mean seasonal cycles of both the observations and the model are removed, comparisons are made for the period 1993-1998.

The global variance of SSH is compared to TOPEX/POSEIDON in Figure 3-8. While the model captures the basic features of the upper ocean circulation, such as the western boundary currents, it significantly underestimates the magnitude of the variability. This underestimation can also be seen in Figure 3-9 where the SSH variance averaged zonally across the center of each basin is compared between the model and the observations. Again, the model captures the basic features, but only 35% of the observed variance. When the

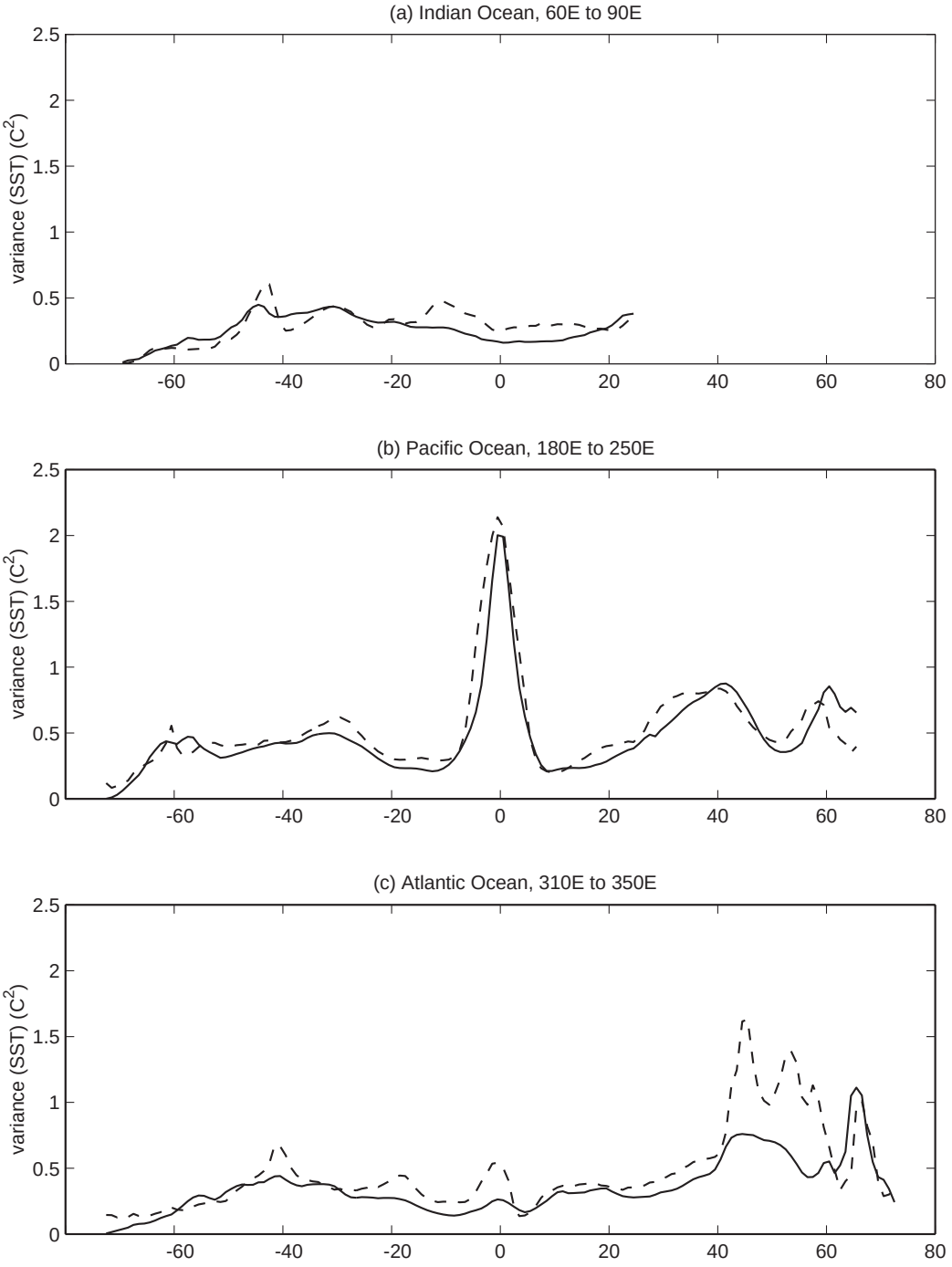

Figure 3-7: Zonal averages of SST variance in the major ocean basins: model (dash) compared to *Reynolds and Smith* [1994] (solid). (a) Indian from 60-90°E, (b) Pacific from 180-250°E, and (c) Atlantic from 310-350°E. The seasonal cycle of both the observations and the model is removed before the variance is calculated.

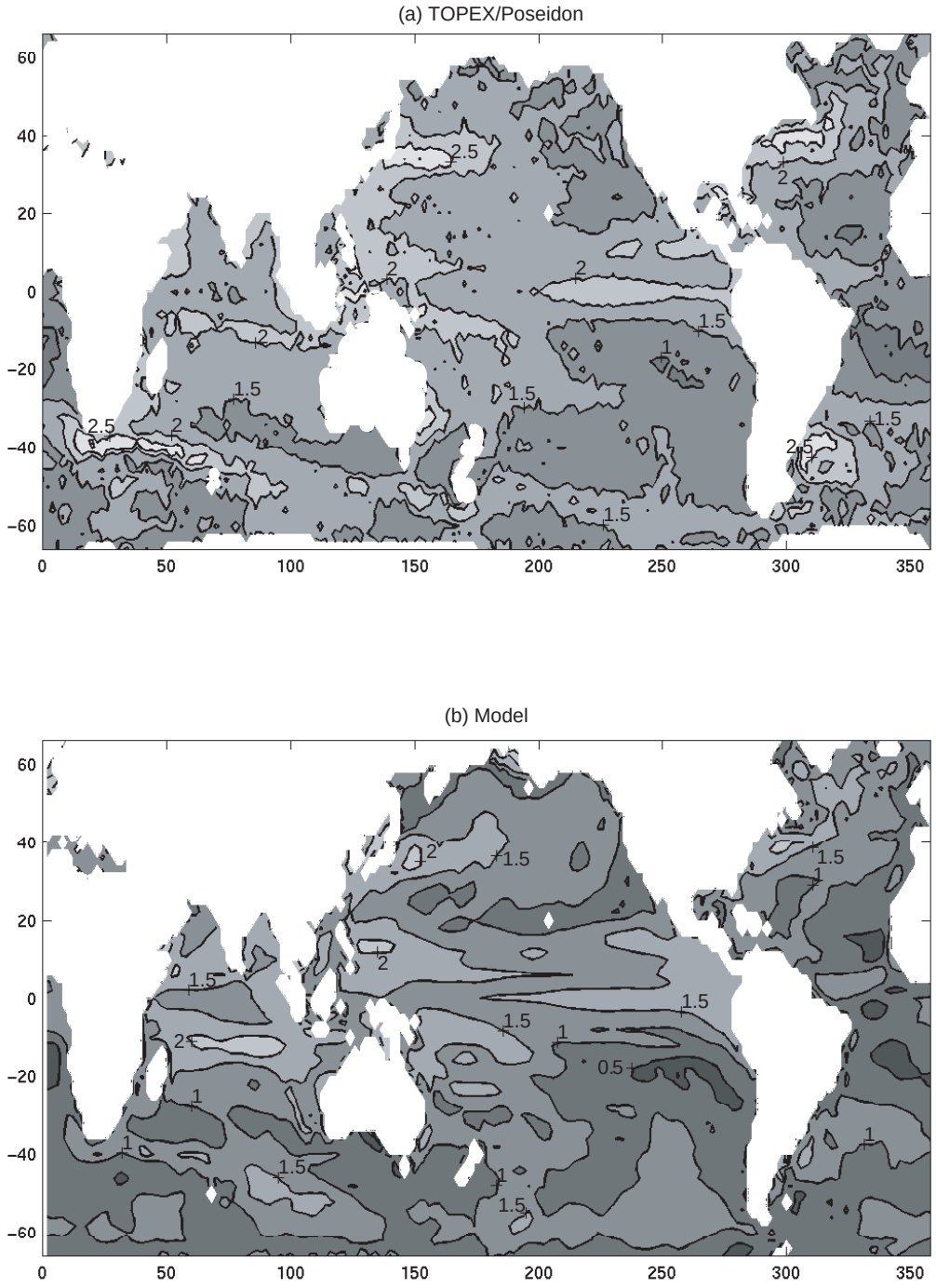

Figure 3-8: Global SSH variance comparison (log10(cm^2)) (a) TOPEX/POSEIDON, and (b) model.

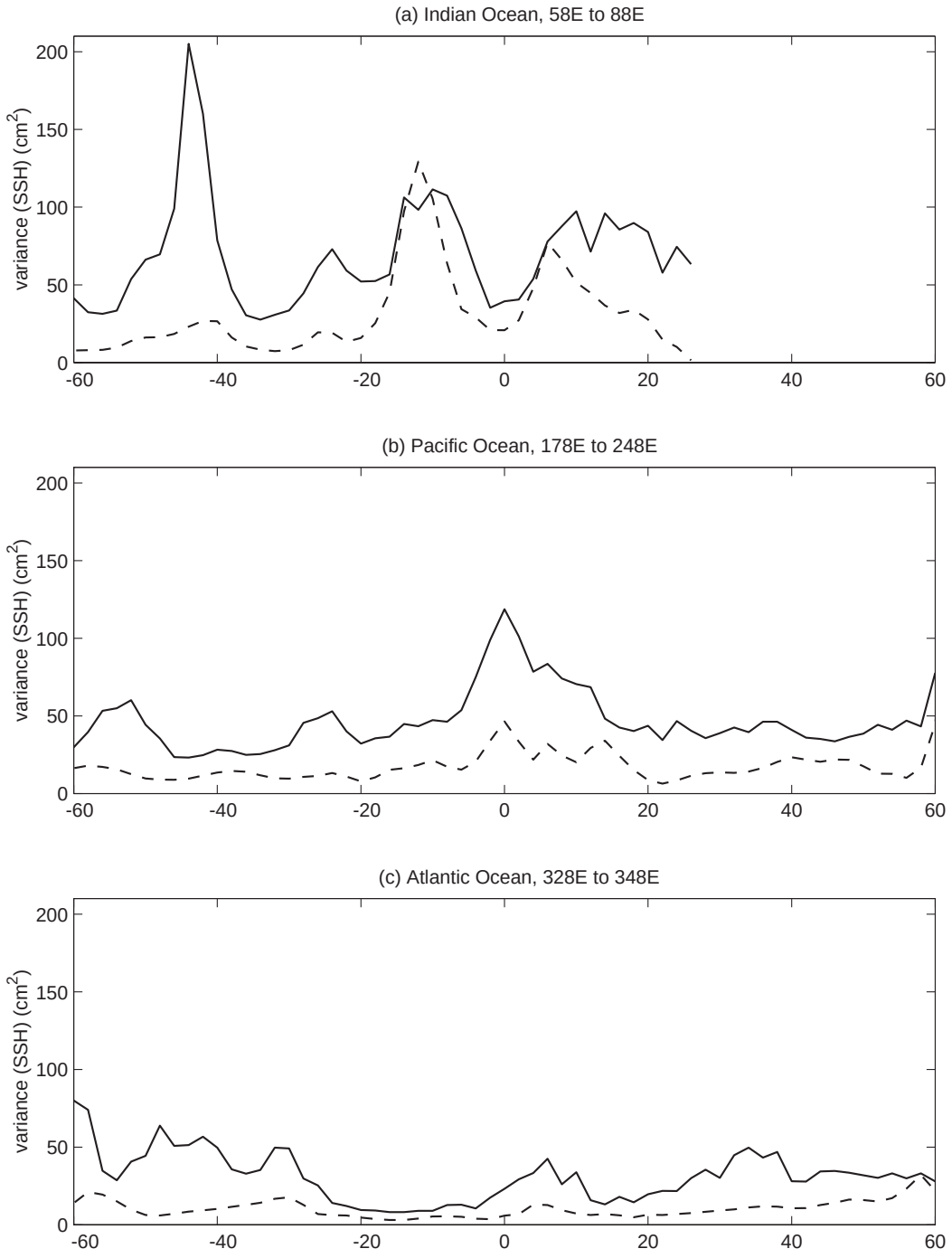

Figure 3-9: Zonal averages of SSH variance in the major ocean basins: model (dash) compared to TOPEX/POSEIDON (solid). (a) Indian, 58-88°E, (b) Pacific, 178-248°E, and (c) Atlantic, 328-348°E.

comparison shown in Figure 3-9 is repeated with both the model and observations averaged to 10°x10°, the model still only captures approximately 35% of the observed variance, indicating that the model does not fare better at larger spatial scales. Similar to the finding of *Stammer et al.* [1996], the model significantly underrepresents upper ocean variability at all spatial scales. The use of boundary conditions that damp small scale variability and the lack of mesoscale eddies, with high-frequency energy that may cascade upscale, are likely contributors to the model's underrepresentation [*Stammer et al.*, 1996].

Summary of physical comparisons

Overall, the physical model captures the major features of the observed temperature and density structures of the global oceans. The model captures SST variance on the global scale, but locally deviates from *Reynolds and Smith* [1994] observations. SSH comparisons indicate that the model significantly underestimates the physical variability of the upper ocean.

Bearing in mind that significant deviations from the observations do occur in the model, I believe that the model is still useful for estimating the magnitude and mechanisms of interannual variability in air-sea fluxes of O_2 and CO_2 because it captures the major features of the upper ocean circulation and its variability. However, caution is required when interpreting air-sea gas flux results, and the underrepresentation of physical variability indicates that the gas flux variability results are likely to be lower bounds.

3.2 Offline Biogeochemical Model

The offline biogeochemical model that is forced by the MITgcm is an expanded and updated version of the offline biogeochemical model used in the North Atlantic to estimate O_2 fluxes. Carbon cycle biogeochemistry is added for the purpose of estimating CO_2 flux variability. The biological export parameterization is modified in order to account for the heterogeneity of global biogenic export efficiency. Freshwater forcing and interannually varying wind speeds for gas exchange estimation are also included.

3.2.1 Governing equations

The governing equations for phosphorus (P, O_2, and Dissolved Inorganic Carbon (DIC)) in the offline biogeochemical model are:

$$\frac{\partial P}{\partial t} = -\nabla \cdot (\mathbf{u}P) + \nabla \cdot (K\nabla P) + S_b + FW_P \tag{3.1}$$

$$\frac{\partial O_2}{\partial t} = -\nabla \cdot (\mathbf{u}O_2) + \nabla \cdot (K\nabla O_2) + R_{O_2:P} * S_b + FW_{O_2} + E_{O_2} \tag{3.2}$$

$$\frac{\partial DIC}{\partial t} = -\nabla \cdot (\mathbf{u}DIC) + \nabla \cdot (K\nabla DIC) + R_{C:P} * S_b + FW_{DIC} + E_{DIC} \tag{3.3}$$

where DIC is the summation of the concentrations of aqueous CO_2, the bicarbonate ion, and the carbonate ion:

$$DIC = CO_2^* + HCO_3^- + CO_3^= \tag{3.4}$$

$$CO_2^* = CO_2(aq) + H_2CO_3 \tag{3.5}$$

In Equations 3.1, 3.2, and 3.3, $\mathbf{u}$ is the transformed Eulerian mean velocity, $\nabla \cdot (K\nabla X)$ is a tensorial representation of mixing along isentropic surfaces as in the MITgcm [*Gent and McWilliams*, 1990] and the boundary layer mixing scheme of *Large et al.* [1994]. The physical model that provides these components is described in Section 3.1. A third-order upwind, flux corrected advection scheme is used in the offline model for tracers in the model [*Dutkiewicz et al.*, 2001].

As described in detail below, S_b represents both the loss of P due to the biological formation of sinking particles and a source of P from remineralization. Biological changes to O_2 and DIC occur proportionally to changes to P based on the Redfield ratios: $R_{O_2:P}$ = -170:1, $R_{C:P}$ = 117:1 [*Anderson and Sarmiento*, 1994]. FW is the change in surface tracer concentrations due to of precipitation and evaporation of freshwater, and E is the air-sea gas exchange of O_2 and CO_2. The neglect of the impact of the $CaCO_3$ cycle on DIC is likely to reduce surface DIC gradients and damp variability in DIC concentrations (Ray Najjar, personal communication).

3.2.2 Biological transformations

Chapter 2 and the work of *LeQuéré et al.* [2000, 2001] indicate that upper ocean mixing and advective processes dominate CO_2 and O_2 air-sea flux interannual variability. However, it has been shown that export production is important to the annual cycle of air-sea fluxes of O_2 [*Jenkins and Goldman*, 1985; *Keeling et al.*, 1993; *Najjar and Keeling*, 1997, 2000], and that the annual cycle of pCO_2 in the North Atlantic (north of 40°N) is dominated by DIC cycling associated with export production [*Takahashi et al.*, 1993]. Therefore, a parameterization of export that captures the broad features of biogeochemical processes affecting export in the global ocean is needed. Although in the North Atlantic I find that a range of export timescales in a simple production and remineralization scheme only minimally affects O_2 air-sea flux variability, the global ocean is far more heterogeneous in its export characteristics. The model must account for the wide variety of biogeochemical conditions in the global ocean, from the High Nutrient / Low Chlorophyll (HNLC) conditions in the Southern Ocean, eastern equatorial Pacific and north-east Pacific to the rapid export of the North Atlantic.

One way to address in heterogeneity of ocean biogeochemistry would be to use a multi-compartment ecosystem model in which heterotrophs, autotrophs, and nutrient compartments are resolved. This would require a significant effort to get a plausible result due to the sensitivity of these models to parameterization and parameter value choices. Although these models have been made to work on the local or basin scale, multi-compartment models are only very recently becoming successful on the global scale [*Moore et al.*, 2002; *Gregg*, 2002]. As the goal of this thesis is to study interannual variability in gas fluxes, the implementation of a multi-compartment ecosystem is not a feasible choice.

Another possibility would be to restore the surface nutrient field to observations and calculate export production based on the magnitude of the restoration [*Najjar et al.*, 1992]. However, existing observed surface nutrient distributions are multi-year composites and do not capture interannual variability. Forcing the model toward the long-term average should undesirably damp the variability imparted to the model by the varying physical fields.

For this global biogeochemical model, a prognostic export parameterization based on light and nutrient limitation, the most fundamental controls on export is used. All other controls are lumped into a tunable export factor, α. For each layer z in the model's euphotic

zone (0-140m), export is:

$$B(z) = -\alpha(x,y) \cdot \left(\frac{I(z)}{I(z)+Io}\right) \cdot \left(\frac{P(z)}{P(z)+Po}\right) \qquad h(z) \leq 140m \tag{3.6}$$

Here, the factor α incorporates all processes either not represented or incompletely represented in the terms for nutrient and light limitation. The flux of photosynthetically active radiation (PAR) at the surface of the ocean (I(y,0,t)) is determined using the astronomical formula of *Paltridge and Platt* [1976], a conversion factor of 0.42 for total radiation to PAR [*Morel*, 1978], and a latitudinally varying albedo according to *North et al.* [1981]. The profile of light in the water column is assumed to follow I(z) = I(0) $e^{-k_w h(z)}$, where k_w, the extinction coefficient, is an empirical function of latitude, based on Secchi depth observations [*Lewis et al.*, 1988; *Simonot and LeTreut*, 1986]. The half-saturation constant for light (Io) is 30 W m^{-2} in PAR, and for phosphate (Po) is 0.01 μmol kg^{-1} [*Dutkiewicz et al.*, 2001].

This form for the export parameterization is motivated by analytically reducing a more realistic, although still highly simplified, Nutrient - Phytoplankton - Zooplankton (NPZ) model to this form in Appendix A. We show that the factor α can be expressed as a function of the input parameters required for the NPZ model. In other words, α may be seen as an expression of the multitude of unknowns in an multi-compartment model. Using this derivation, it is estimated that α has a plausible range of 4x10^{-9} to 1x10^{-5} μmol P kg^{-1} s^{-1} over the top 140 meters of the ocean.

The sinking particle flux at all depths is parameterized by using an exponential profile with a scale height (z^*) of 400m [*Dutkiewicz et al.*, 2001]. The instantaneous remineralization source of P into each layer z is calculated as the divergence of the export from each layer above that is within the euphotic zone:

$$F(z) = \sum_{h_o=10m}^{h(z-1)} B(h_o) \left(e^{(h_o - h(z))/z^*} - e^{(h_o - h(z+1))/z^*}\right) \qquad h(z) \leq 140m \tag{3.7}$$

$$F(z) = \sum_{h_o=10m}^{140m} B(h_o) \left(e^{(h_o - h(z))/z^*} - e^{(h_o - h(z+1))/z^*}\right) \qquad h(z) > 140m \tag{3.8}$$

where h(z) is the total depth of the layer z.

The total biological change (S_b) of each layer within the euphotic zone is the sum of export removal of nutrients and remineralization:

$$S_b(z) = B(z) + F(z) \qquad h(z) \leq 140m \tag{3.9}$$

Below the euphotic zone, only remineralization is active, such that:

$$S_b(z) = F(z) \qquad h(z) > 140m \tag{3.10}$$

Using Redfield ratios, this P source is translated into an instantaneous sink of O_2 and source of DIC (Figure 3.2 and 3.3). Anoxic respiration of exported particles, wherein the source of P and DIC are active without an O_2 sink, occurs in the model when the O_2 concentration falls below 4 μmol/kg [*Orr et al.*, 2000].

Similar particle export parameterizations have been used with constant parameter values in the North Atlantic [*McKinley et al.*, 2000; *Williams and Follows*, 1998], and for a global study of anoxia in the Permian deep ocean [*Zhang et al.*, 2001]. When combined with various representations of light limitation, the resulting fallout timescales are a week in the summer to many years in the high latitude winter. These models have been able to capture the major features and annual cycles of nutrients in the North Atlantic. *Maier-Reimer* [1993] uses such a model with a constant export factor to calculate production in the HAMMOC3 global ocean model and finds reasonable agreement with surface nutrient observations in most of the ocean, but significantly overestimates new production and underestimates CO_2 partial pressure in the eastern equatorial Pacific. In order to avoid these effects, it is necessary that this global model have a spatially inhomogeneous α. Building on the simplified prognostic form representing export production in Equation 3.6, a novel approach to imparting spatial heterogeneity to the parameterization will be introduced in Section 3.3.

3.2.3 Freshwater forcing

Freshwater forcing on tracer concentrations was not included in the offline model used in the North Atlantic study presented in Chapter 2. This element is added to the global offline model. To compute the impact of freshwater fluxes on the tracers in the offline model, a combination of forcing fields used for the physical model and the diagnosed relaxation of the physical model to climatological SSS is used. The forcing fields used for the physical

model are the NCEP 12 hourly freshwater fluxes, minus the NCEP long-term mean, plus the COADS long-term mean. This field is then adjusted to conserve mass over the 19 year run (T. Lee, personal communication). However, the physical model still drifts in surface salinity. Thus, a term for relaxation to climatological SSS [*Levitus and Boyer*, 1994] was included in the online physical model run. The 10 day mean of the relaxation term is diagnosed from the physical model and is added to the 10 day average of the forcing field to arrive at the total freshwater forcing to the physical model (EP in m/s) over each 10 day interval.

The impact of total freshwater forcing on the tracers is to either dilute or concentrate them in the surface layer. This impact is calculated following the specifications of the Ocean Carbon-Cycle Model Intercomparison Project (OCMIP) [*Orr et al.*, 2000].

$$FW_X = EP \cdot X^* \cdot \frac{1}{dz_1} \tag{3.11}$$

Freshwater forcing in the surface layer of the global model is applied for each tracer (X = P, O_2, or DIC) as in Equation 3.11. X^* is the global mean tracer concentration, calculated each 10 days, and dz_1 is the depth of the surface layer of the model (dz_1 = 10m).

3.2.4 Gas exchange

For the global model, interannual variability in the gas exchange forced by wind speed variability is included. This variability was not present in the North Atlantic study where a monthly climatology of wind speed was used.

The method of *Wanninkhof* [1992] is used to parameterize gas exchange of O_2 and CO_2 as a function of a gas-transfer velocity and surface layer excursion from the saturation concentration for O_2 or as an excursion from equilibrium with the atmospheric partial pressure of CO_2 ($pCO_2{}^{atm}$). Fluxes are positive to the ocean. The solubility of CO_2, L, is is also required for the CO_2 gas exchange calculation [*Weiss*, 1974].

$$E_{O_2} = \frac{1}{dz_1}\left(k * (O_2^{sat} - O_2)\right) \tag{3.12}$$

$$E_{CO_2} = \frac{1}{dz_1}\left(k * L * (pCO_2^{atm} - pCO_2)\right) \tag{3.13}$$

In Equations 3.12 and 3.13, k is the gas transfer coefficient, calculated as a function of wind speed (u), a constant exchange coefficient calibrated with ^{14}C invasion data (a), and the Schmidt number (Sc), in turn a function of temperature and salinity for each gas. After *Wanninkhof* [1992],

$$k = a \cdot u^2 \cdot (\frac{Sc}{660})^{-\frac{1}{2}} \tag{3.14}$$

O_2 saturation (O_2^{sat}) is determined following *Weiss* [1970] as a function of sea surface temperature and salinity. The partial pressure of carbon (pCO_2) in the surface ocean is calculated a function of DIC concentration, alkalinity, temperature, salinity, and borate concentration as in *Follows et al.* [1996]. Alkalinity is assumed to be a linear function of salinity based on GEOSECS data after *Campbell* [1983]. The carbonate equilibrium coefficients of Merbach are used, following *Dickson and Millero* [1987]. Water dissociation is calculated according to *Hoffert et al.* [1979]. Borate equilibrium is based on GEOSECS data following *Takahashi et al.* [1981], with a globally constant dissolved inorganic boron concentration of 409 μmol/kg.

The pCO_2 of seawater is a function of $CO_2{}^*$ ($CO_2(aq) + H_2CO_3$) which, due to carbonate chemistry, is only approximately 0.5% the total DIC concentration. Thus, when air-sea gas fluxes occur to address a disequilibrium of atmospheric and oceanic pCO_2, 20 times more carbon than that which ends up in the $CO_2{}^*$ form must be exchanged. This means that the equilibration time for CO_2 is approximately 20 times longer than for O_2, a gas that does not react with seawater.

Wind speeds

As previously described, NCEP 12 hour reanalysis wind stress variability for 1980-1998 added to COADS mean wind stress were used to force the physical model. Thus, for the offline biogeochemical model to have consistency with the physical fields, NCEP vector wind components are adjusted by removing the NCEP mean and adding the COADS mean at 12 hour resolution. The scalar wind speed at 12 hour resolution is then computed from the two components.

Ideally, these high temporal resolution wind magnitudes could be used directly to calculate gas exchange. However, with a 10 day resolution in all other fields, it would be

inappropriate to impose this rapid variability on the model when all other physics, particularly convective mixing, change at lower temporal resolution. At the same time, it is desirable to capture the high gas exchange imparted by transient high wind events.

As illustrated by *Boutin and Etcheto* [1995] and implemented in OCMIP, this dilemma can be resolved by adding the second moment about the 10 day mean of the 12 hour wind magnitude to the square of the 10 day mean wind. The 10 day average of the solution to Equation 3.14 using the 12 hour wind magnitude in Equation 3.14 is:

$$k = a \cdot (\overline{u_{12}} + u'_{12})^2 \cdot (\frac{Sc}{660})^{-\frac{1}{2}} \tag{3.15}$$

Equivalent to:

$$k = a \cdot (\overline{u_{12}}^2 + 2\overline{u_{12}}u'_{12} + (u'_{12})^2) \cdot (\frac{Sc}{660})^{-\frac{1}{2}} \tag{3.16}$$

Averaging over 10 days results in the cancellation of $2\overline{u_{12}}u'_{12}$ in Equation 3.16. Thus, Equation 3.14 can be revised to:

$$\overline{k}^{10d} = a \cdot (\overline{u_{12}}^2 + \overline{(u'_{12})^2}^{10d}) \cdot (\frac{Sc}{660})^{-\frac{1}{2}} \tag{3.17}$$

The term $\overline{(u'_{12})^2}^{10d}$ in Equation 3.17 is the second moment about the mean of the 12 hourly wind speed data set. This is calculated and added to the mean of the square of the 12 hourly wind, resulting in a 10 day average wind magnitude product that includes the impact of high wind events on gas exchange that is associated with wind variability at 12 hour resolution.

Calibration of gas exchange with ^{14}C invasion data

An appropriate exchange coefficient, a, is needed to calibrate the wind fields to ^{14}C invasion data. Following *Wanninkhof* [1992], the probability distribution, P(u), of the 12 hour wind magnitude fields is estimated by forming a histogram of all wind magnitude data points. The global mean Schmidt number is estimated to be 660, appropriate for CO_2 and global average SST of 20°C. The appropriate value for a is then:

$$a = \frac{k_{av}}{\sum[P(u) \cdot u^2]} \tag{3.18}$$

where k_{av} is the natural and bomb ^{14}C invasion rates, 21.2 cm/hr and 21.9 cm/hr, respectively. An average a from the two calculations is taken to be our constant, a = 0.39 (cm/hr)/(m^2/s^2). This coefficient is the same as that arrived at by *Wanninkhof* [1992] for long-term averaged winds, and is greater than his a = 0.31 for instantaneously observed winds. This comparison indicates that, as expected, the 12 hourly winds from NCEP plus the COADS mean are less intense than in-situ observed winds, and therefore necessitate a larger exchange coefficient in order to agree with the ^{14}C invasion data.

3.2.5 Sea ice

Gas exchange and export production are reduced by the percent of the ocean surface covered with sea ice in the monthly climatology of the Ocean Carbon-Cycle Model Intercomparison Project [*Orr et al.*, 2000].

3.2.6 Boundary conditions

Due to computational constraints, the offline biogeochemical model is run only in the upper ocean (0 - 1265m) and relaxation to the climatological P, O_2 and DIC fields over the bottom three layers (965-1265m) is imposed. In the bottom-most layer, relaxation to climatological tracers is instantaneous to prevent unrealistic fluxes across the bottom boundary; and in the second-to-bottom and third-to-bottom layers, relaxation occurs with timescales of 16 days and 128 days, respectively.

A annual climatology of the 19 years (1980-1998) of model physical fields is used to force the model during spinup and for the work on adjusting the export parameterization which is explained in the following section.

The recently published DIC climatology of *Goyet et al.* [2000] is used to both to initialize model DIC and for restoration at the base of the model domain. For P and O_2 the climatological values from *Conkright et al.* [1998] are used. A constant atmospheric O_2 concentration of 20.946 pph [*Weiss*, 1970], and a CO_2 concentration of 354 ppm, a mean value for 1990 from the Mauna Loa measurements [*Keeling and Whorf*, 2000], are used as the atmospheric boundary conditions. We choose 1990 as a reference year as this is approximately the temporal midpoint of our variable physical fields.

3.3 Export Parameterization

Here, I describe in detail a novel approach to impart spatial heterogeneity to the export parameterization introduced in Section 3.2.2. In Section 3.3.1, it is shown that when such a model is run forward with spatially constant parameter values, significant deviation from the climatological nutrient field occurs. The pattern of the deviation has distinct spatial coherence and can be related to known or hypothesized controls on export production in the various ocean regions, e.g. iron limitation in the HNLC regions. In Section 3.3.2, a method to include spatial variability in the tunable export parameter is derived, and in Section 3.3.4, it is illustrated that there is improvement in the modeled upper ocean nutrient distribution and global mean air-sea O_2 fluxes when this spatial variability is included.

3.3.1 A constant export parameter

A spatially homogeneous export constant, $\alpha_o = 2.3\text{x}10^{-8}$ μmol kg^{-1} s^{-1} (derived from a 9 month estimated global average fallout timescale and a global average surface PO_4 from World Ocean Atlas 1998 (WOA98) [*Conkright et al.*, 1998] of 0.5 μmol kg^{-1}) is chosen; the model is initialized with the WOA98 winter climatology on January 1 and integrated forward. The model becomes adequately equilibrated in terms of surface phosphorus after a 15 year model run. At this point, the model global volume weighted average change of the annual average nutrient field is under 1% per year, due to adjustment toward initial and boundary conditions. The volume weighted average change for the surface is $\pm$1.1% per year. The spatial pattern of the change is distributed relatively evenly across the globe, with local maxima / minima not exceeding $\pm$5% from year-to-year, except for a few small regions of large change (up $\pm$20%) around the north and east margins of the Pacific. Although it would be desirable to further reduce the magnitudes of these drifts by integrating the model for additional years, the computational expense of the model makes this impractical.

The resulting nutrient climatology for the final year of this run is compared to the annual climatology in Figure 3-10.

Large-scale patterns of deviation in the mean phosphorus field (averaged 0-140m) from the climatological distribution are found (Figure 3-11a). This comparison is also made over 14 large-scale ocean regions (defined in Table 3.2) in Figure 3-11b. In both figures,

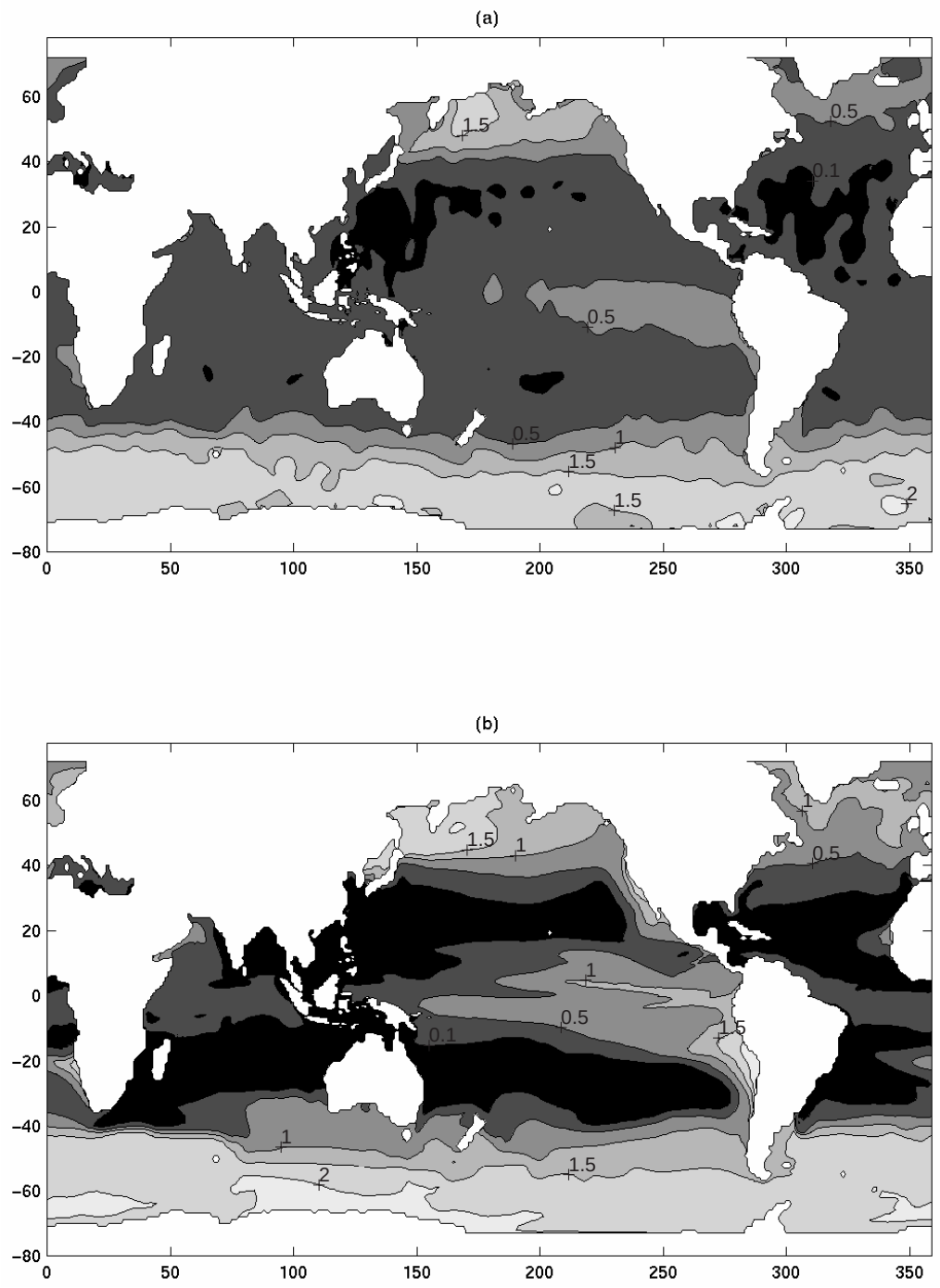

Figure 3-10: Euphotic zone (0-140m average) nutrient distribution comparison. *Conkright et al.* [1998] climatology of phosphate (top), and model phosphorus after 15 years run with constant α(bottom).

it can be seen that the subtropical regions and the Atlantic and Indian equatorial sectors are phosphorus-depleted, while the subpolar North Atlantic, Subantarctic and Southern Ocean regions have too much phosphorus. This result is similar to that of *Maier-Reimer* [1993] because a spatially constant export parameter that does not account for the global heterogeneity of export is in use. The model drift from the climatology is due to missing processes such as iron limitation, community structure, nitrogen fixation or eddy nutrient supply that are not resolved in our parameterization. In the next sections, some of the effect of these processes is absorbed into a spatially variable α.

3.3.2 Solution for a spatially inhomogeneous export parameter

The α(x,y) that, given model flow fields, will produce a model annual mean phosphorous distribution consistent with climatological observations is sought. The result is a spatially varying α(x,y) into which all the unknowns of the biological system are incorporated. *Marshall and Molteni* [1993] used a similar method to determine spatially varying potential vorticity flux forcings for a quasigeostropic model of the atmosphere, and found a significant improvement in the streamfunction climatology of their model.

An α^*(x,y) is defined as the spatial distribution of the export parameter that makes the long-term mean of the global model nutrient field equal to the initial climatology; in other words, the drift of the model is exactly zero. Following Equation 3.1 and assuming negligible freshwater impacts, this can be written as:

$$\overline{\frac{\partial P}{\partial t}}^t = -\overline{\nabla \cdot (uP)}^t - \overline{\nabla \cdot (K \nabla P)}^t - \alpha^* \overline{\Gamma}^t = 0 \tag{3.19}$$

where $\Gamma = \left(\frac{I}{I+Io}\right) \cdot \left(\frac{P}{P+Po}\right)$.

The field α^*(x,y) is the spatial distribution of export factor values that we seek. To begin with, we have only α_o, a guess at α^*(x,y). The error in our guess is $\Delta\alpha$(x,y).

$$\alpha_o = \alpha^*(x, y) + \Delta\alpha(x, y) \tag{3.20}$$

By running the model for multiple iterations, successive values of $\Delta\alpha$(x,y) are found that allow α to be updated and to approach α^*(x,y) .

Specifically, the model is integrated forward for 15 years with α_o and it is found:

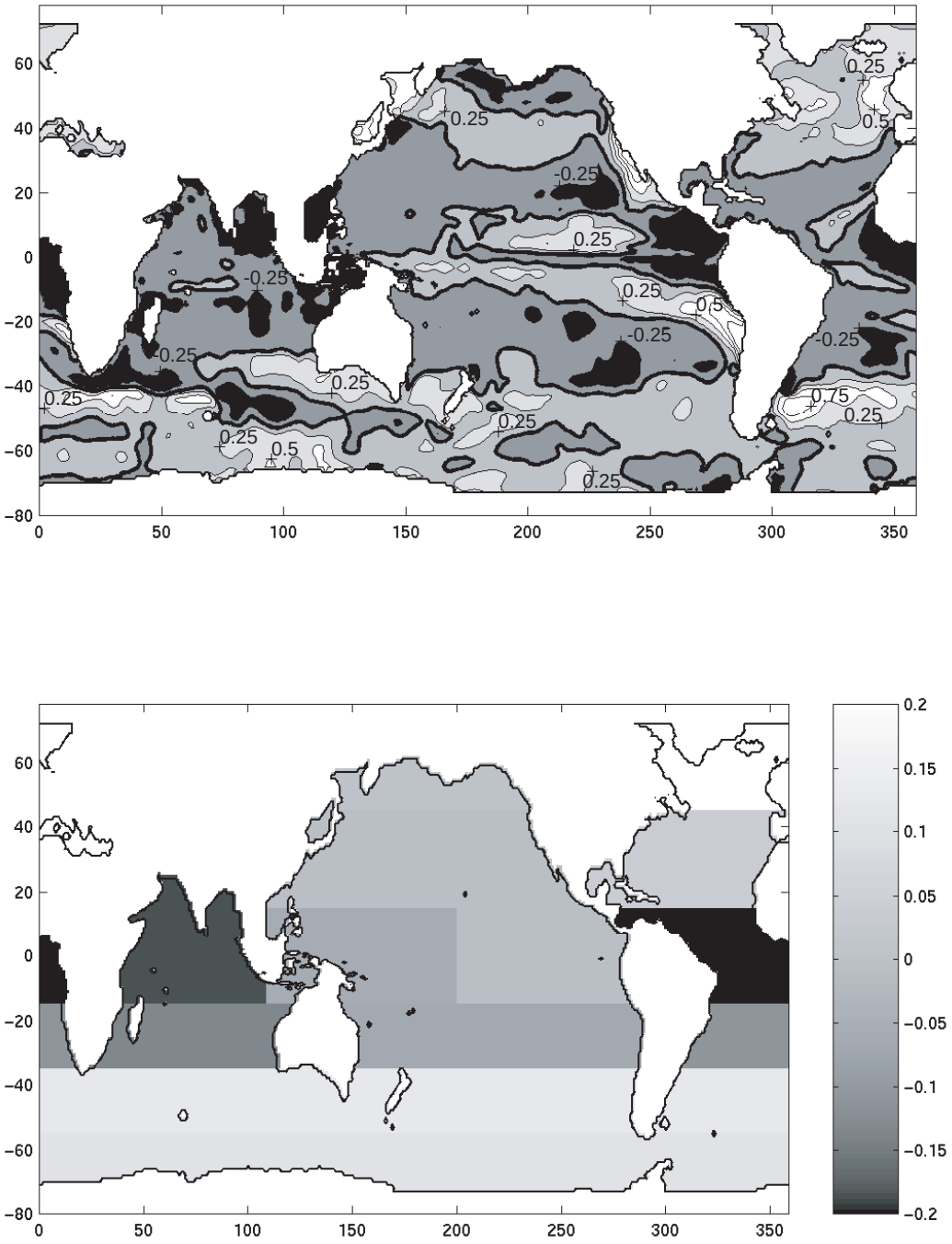

Figure 3-11: Difference of the observed nutrient distribution [*Conkright et al.*, 1998] from the model, averaged over the euphotic zone (0-140m) (top); same result, spatially averaged over the 14 ocean regions defined in Table 3.2
(bottom).

$$\overline{\frac{\partial P}{\partial t}}^t = -\overline{\nabla \cdot (uP)}^t - \overline{\nabla \cdot (K \nabla P)}^t - \alpha_o \overline{\Gamma}^t \neq 0 \tag{3.21}$$

Substitution of equation 3.20 into 3.21 gives:

$$\overline{\frac{\partial P}{\partial t}}^t = -\overline{\nabla \cdot (uP)}^t - \overline{\nabla \cdot (K \nabla P)}^t - \alpha^* \overline{\Gamma}^t - \Delta\alpha(\overline{\Gamma}^t) \tag{3.22}$$

The first three terms on the right-hand side of 3.22 are zero by definition (Equation 3.19), leaving:

$$\overline{\frac{\partial P}{\partial t}}^t = -\Delta\alpha(\overline{\Gamma}^t) \tag{3.23}$$

which allows solution for the error in the initial guess.

$$\Delta\alpha(x,y) = -\frac{1}{\overline{\Gamma}^t} \overline{\frac{\partial P}{\partial t}}^t \tag{3.24}$$

Due to the model's non-linearity, iterative solutions are used to approach α^*(x,y).

The optimal spatial structure of α for the 14 regions defined in Table 3.2 is that which is solved for here. These regions are used so that an α^*(x,y) consistent with ocean biogeochemical regimes defined at the broadest possible scale can be found. Our evaluation of the physical model (Section 3.1) indicates that while the model captures the broad features of the ocean circulation, mixed layers and transports locally deviate from observations. The climatological nutrient field is also not accurate on the small scale due to data sparsity and smoothing, but it is reasonable to expect that it captures the major features of the large scale distribution of phosphate. As this method requires a consistency of the model circulation and climatological nutrient fields, α is adjusted only on the large scale where that consistency is possible.

This approach attributes all drift in the model to missing biogeochemical processes, while deficiencies in the physical model may contribute to the drift. With this approach, we do not have a direct way to distinguish between missing biogeochemistry and missing physics.

Table 3.2: Ocean regions for export parameter solution

Region	Abbreviation	Boundaries
Southern Ocean	SO	80°S to 55°S
Subantarctic	SAnt	55°S to 35°S
South Indian	SInd	35°S to 15°S, 22°E to 140°E
North Indian	NInd	15°S to 26°N, 38°E to 108°E
Subtropical South Pacific	STSP	35°S to 15°S, 145°E to 295°E
Subtropical South Atlantic	STSA	35°S to 15°S, 295°E to 22°E
Eastern Equatorial Pacific	EEP	15°S to 15°N, 200°E to 283°E
Western Equatorial Pacific	WEP	15°S to 15°N, 109°E to 200°E
Equatorial Atlantic	EqAt	15°S to 15°N, 284°E to 25°E
Subtropical North Pacific	STNP	15°N to 44°N, 105°E to 267°E
Subtropical North Atlantic	STNA	15°N to 44°N, 267°E to 354°E
Subpolar North Pacific	SPNP	45°N to 79°N, 115°E to 240°E
Subpolar North Atlantic	SPNA	45°N to 79°N, 266°E to 20°E
Mediterranean	Med	30°N to 44°N, 355°E to 38°E

3.3.3 Finding α^*(x,y)

The 15 year run where α_o is globally applied is used to calculate $\overline{\frac{\partial P}{\partial t}}^t$ and $\overline{\Gamma}^t$ (with t=15 years) and $\Delta\alpha(x, y)$ is found via Equation 3.24 for each of the 14 regions, and the new field $\alpha(x, y)$ field is α_1. Two further iterations are similarly done, an extrapolation to speed convergence of the α solution is undertaken, and then two final iterations are performed.

Extrapolation to Speed Convergence

Three 15-year iterations require a significant computational effort to complete. Although substantial progress has been made towards improving the final year nutrient concentration with respect to the climatology by adjusting α in this way, the α^*(x,y) solution has not yet converged. In order to speed convergence, the terms of Equation 3.24 from iterations 1 through 3 are used to extrapolate $\alpha(x, y)$ toward α^*(x,y) in each region. In most regions, a quadratic fit is used, but when a quadratic solution results only in imaginary solutions (in SPNP, SPNA, Med), a linear fit is used.

The extrapolated α result for the Subtropical North Atlantic is rejected because lateral transport of nutrient from the equatorial Atlantic in successive iterations causes nutrient concentrations to increase in the Subtropical North Atlantic even though α is increasing here (see Figure 3-14 and Table 3.3). As α is reduced in the equatorial Atlantic, phosphorus is retained at the surface and some is transported along the Gulf Stream pathway into the Subtropical North Atlantic. Due to this forcing, the increasing α (increasing export) is not physically linked to increased nutrient retention in the Subtropical North Atlantic, motivating the rejection of the extrapolation that simply correlates these processes. The α of the third iteration is retained for the fourth iteration in the Subtropical North Atlantic.

Results from the extrapolation (giving α_3) are used in a fourth iteration and then a fifth iteration (using α_4) is done to ensure convergence of the model. This final iteration allows an additional solution (for α_f) for input to the model with which interannual variability of CO_2 and O_2 air-sea fluxes is estimated. The α results in most regions do not change after the extrapolation (see Table 3.3), indicating this approach successfully achieves convergence in most regions. Only in the South Indian does α change significantly after the extrapolation.

In Figure 3-12, the drift of Southern Ocean mean nutrient away from the annual climatology through each iteration is presented to illustrate the impact of the changing α on

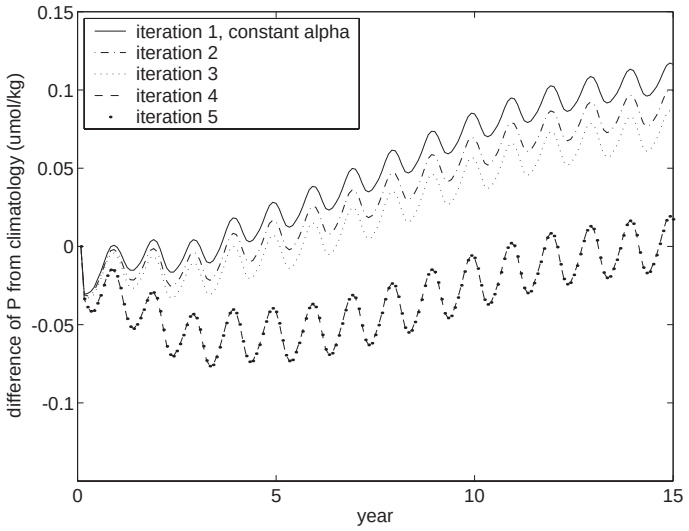

Figure 3-12: Adjustment trajectories for the Southern Ocean: timeseries of regional mean phosphorus concentration minus regional mean climatology, averaged 0-140m. Results for iteration 4 and 5 are indistinguishable.

regional nutrient concentration. With the spatially constant α_o, the model quickly diverges from the initialization climatology. After the first adjustment to α, the trajectory is qualitatively the same as the original, but the final value of global mean total P is closer to the WOA98 climatology. The third iteration reduces the difference from the climatology at year 15 yet again. A shift occurs with the extrapolation before iteration four, and there is no distinguishable change between the fourth and fifth iterations as there has been no change to α. The difference of the mean nutrient concentration from the climatology at the end of iterations 4 and 5 is quite close to zero, as theoretically predicted (see also Figure 3-14).

Note on computational expense

Important to note is that an iterative method of this sort is computationally expensive. With this global model at 1°x 0.3-1° resolution with 32 vertical levels, a single iteration on a dedicated 8 processor machine takes approximately 2 weeks to complete. Thus, improvements in the model - data nutrient climatology agreement must be viewed in light of the expense required to achieve them.

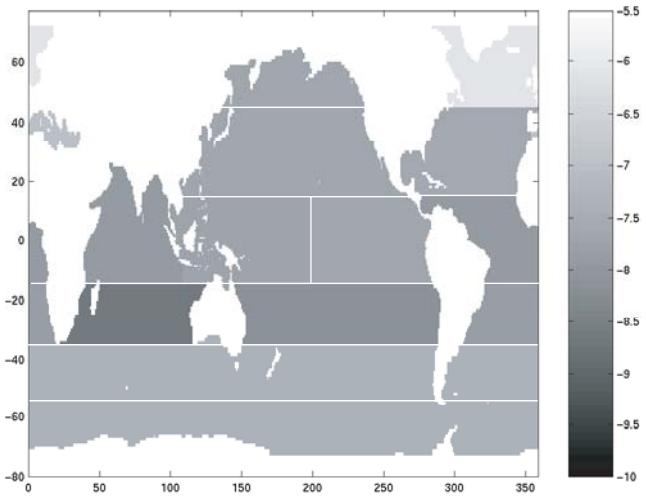

Figure 3-13: Final solution to α (α_f in μmol/kg/s, log scale). White lines delineate region boundaries.

3.3.4 Results

The α_f is plotted in Figure 3-13 and all α values are summarized in Table 3.3. Export timescales are calculated with Equation 3.25 using area average WOA98 annual mean phosphate concentrations (P_{woa}) [*Conkright et al.*, 1998] and are presented in Table 3.4.

$$\tau(x,y) = \frac{P_{woa}(x,y)}{\alpha(x,y)} \tag{3.25}$$

The α values found after the final adjustment range from an order of magnitude smaller to more than an order of magnitude larger than α_o (2.3x10^{-8} μmol kg^{-1} s^{-1}) and are within the range estimated (excepting the South Indian region) from typical input parameters to a multi-compartment ecosystem model (see Appendix A). Timescales are reduced by almost two orders of magnitude in the subpolar North Atlantic, increased by an order of magnitude in the South Indian region, and changed by varying degrees in other regions.

Changes to the export timescales are broadly consistent with known controls on export in the global ocean. The shortest timescales are found in the northern subtropical gyres and in the subpolar North Atlantic. This is consistent with the results of *Takahashi et al.* [1993] who find that it is only in the North Atlantic where the winter maximum nutrient concentration is approximately equivalent to the total photosynthetic drawdown in the

Table 3.3: Iterative solutions for α (x10^8 μmol/kg/s)

Region	α_o	α_1	α_2	α_3	α_4	α_f
SO	2.3	2.7	3.0	4.6	4.6	4.6
SAnt	2.3	2.5	2.7	4.3	4.3	4.3
SInd	2.3	2.0	1.8	0.13	0.20	0.25
NInd	2.3	2.1	1.9	1.2	1.2	1.2
STSP	2.3	2.2	2.1	0.76	0.76	0.76
STSA	2.3	2.1	2.0	1.4	1.4	1.4
WEP	2.3	2.2	2.1	1.8	1.8	1.8
EEP	2.3	2.3	2.3	2.3	2.3	2.3
EqAt	2.3	2.1	1.9	1.1	1.1	1.1
STNP	2.3	2.3	2.3	2.2	2.2	2.2
STNA	2.3	2.4	2.4	2.4	2.5	2.6
SPNP	2.3	2.3	2.3	2.5	2.5	2.4
SPNA	2.3	3.0	3.7	76.5	76.9	77.2
Med	2.3	2.7	3.1	9.5	9.9	10.3

Table 3.4: Export timescale (τ in yrs) and mean WOA98 phosphate

Region	τ_o	τ_1	τ_2	τ_3	τ_4	τ_f	$P_{woa}(\mu mol/kg)$
SO	2.6	2.2	2.0	1.3	1.3	1.3	1.9
SAnt	1.4	1.3	1.2	0.73	0.73	0.73	0.98
SInd	0.35	0.40	0.46	6.3	4.1	3.2	0.25
NInd	1.0	1.0	1.1	1.9	1.8	1.8	0.68
STSP	0.41	0.44	0.46	1.3	1.2	1.2	0.29
STSA	0.52	0.56	0.60	0.85	0.86	0.86	0.37
WEP	0.52	0.53	0.55	0.66	0.65	0.65	0.37
EEP	1.4	1.4	1.4	1.4	1.4	1.4	0.97
EqAt	0.79	0.88	1.0	1.6	1.6	1.6	0.57
STNP	0.52	0.52	0.52	0.54	0.54	0.54	0.37
STNA	0.26	0.26	0.25	0.25	0.24	0.23	0.19
SPNP	2.2	2.2	2.2	2.0	2.1	2.1	1.6
SPNA	0.94	0.71	0.58	0.03	0.03	0.03	0.67
Med	0.18	0.16	0.14	0.04	0.04	0.04	0.13

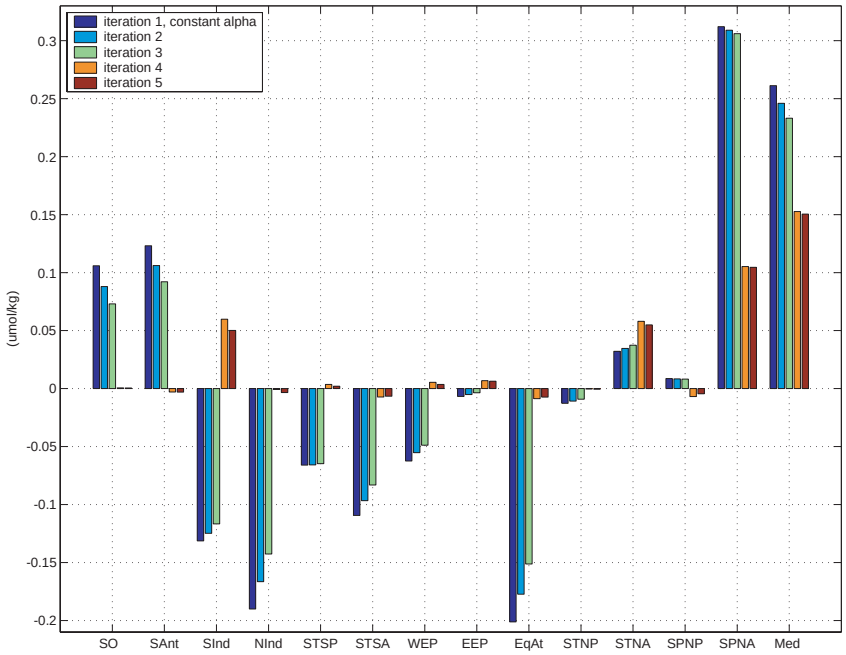

Figure 3-14: Difference of year 15 phosphorus and climatological phosphate for each iteration.

spring and summer. The complete use of nutrients indicates the North Atlantic ecosystem is unique in its limitation by only macro nutrients and light availability. The solution for very short export timescales (large α_f) in the North Atlantic means that export can be very rapid when nutrients and light are in abundant supply (see Equation 3.6). In contrast, the long export timescales in the Southern Ocean, the Eastern Equatorial Pacific, and the Subpolar North Pacific are consistent with known HNLC regions. It is likely that the long export timescale, which acts to restrict export in HNLC regions, is implicitly accounting for iron limitation in the real ocean [*Martin*, 1990; *Moore et al.*, 2002]. In summary, the substantial heterogeneity of the final α_f solution allows for the basic patterns of observed export variability to be captured by the model.

Figure 3-14 illustrates the difference of the year 15 annual mean nutrient concentration from the climatology in the 14 ocean regions for each of the 5 iterations. In all regions except the subtropical North Atlantic, there is substantial improvement in agreement with the nutrient climatology by the end of the fifth iteration, as is expected with more realistic export timescales. The extrapolation after iteration 3 clearly speeds this improvement.

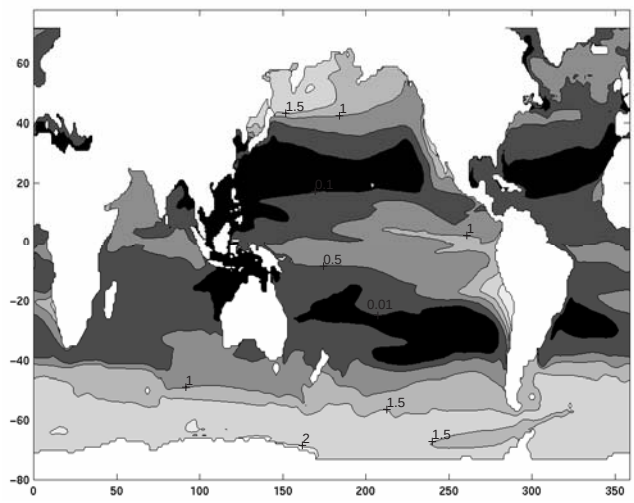

Figure 3-15: Annual mean nutrient distribution, averaged over the euphotic zone (0-140m) in year 15 of the fifth iteration.

Also notable is the overshoot of the α extrapolation in the South Indian that is partially compensated for with the solution for α_4 that is input to iteration 5.

The nutrient climatology at the end of the fifth iteration is shown in Figure 3-15. In comparison to Figure 3-10, the improvement in the model annual mean nutrient field is most evident in the Southern Ocean, the Indian Ocean, the South Atlantic, and the subpolar North Atlantic.

Figure 3-16 compares the annual cycle of the fifteenth year of the fifth run to the annual cycle fifteenth year of the run with α_o, and also to the WOA98 seasonal phosphate climatology in a selection of six open ocean regions. There is an improved agreement with the mean WOA98 climatology with the spatially variable α_4 (iteration 5) over the spatially constant α_o (iteration 1). Adjustments to α do not generally affect the shape of the seasonal nutrient cycle, affecting only the mean, as expected from the analytical solution in Section 3.3.2. However, in the Subpolar North Atlantic, the seasonal cycle is significantly improved by the adjustment to α because the fallout timescale changes from 11 months (0.94 year) with α_o to 1.6 weeks (0.03 year) with $\alpha_4(x, y)$. The rapid timescale with $\alpha_4(x, y)$ allows export to respond quickly to changes in surface nutrient concentration and light availability in the spring, allowing a rapid seasonal drawdown of nutrients and the pronounced improvement seasonal cycle. In Section 4.3.1, this improvement in the seasonal

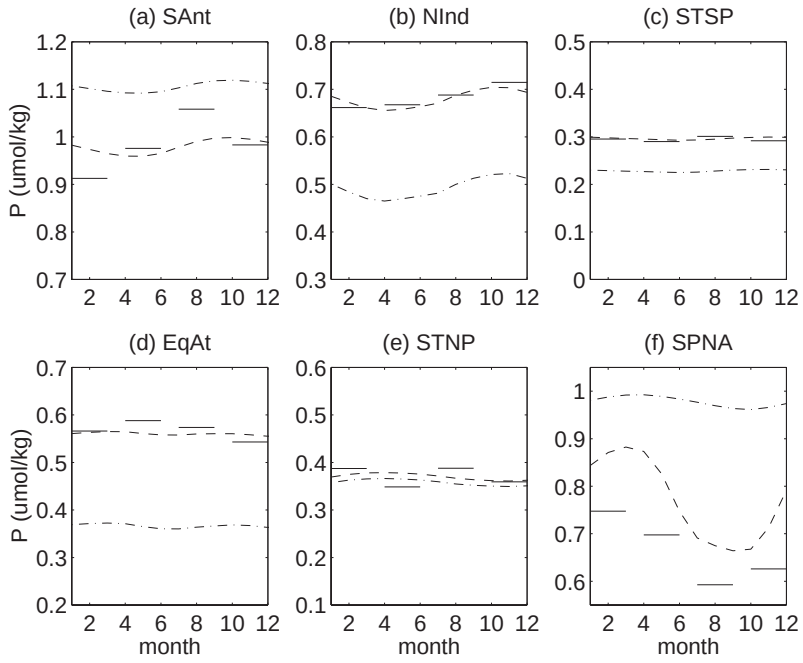

Figure 3-16: Comparison of seasonal cycles in α adjustment regions. WOA98 seasonal (solid), iteration 1, year 15 (dash-dot), iteration 5, year 15 (dash). Both model and data are averaged over the euphotic zone (0-140m).

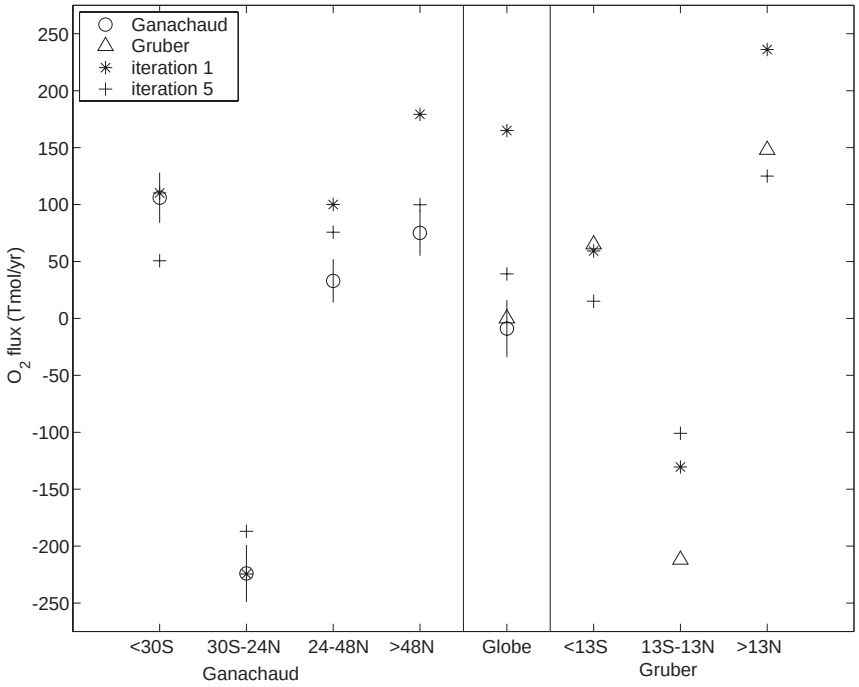

Figure 3-17: Annual mean O_2 fluxes at end of iteration 1 and iteration 5 compared to data studies of *Ganachaud* [1999] and *Gruber et al.* [2001].

cycle of nutrients is found to be significant to estimates of the interannual variability of O_2 air-sea fluxes.

Impact of export adjustment on air-sea O_2 fluxes

Here, the effect of adjustments to α on the mean O_2 fluxes is considered. In the central panel of Figure 3-17, it can be seen that the global net air-sea O_2 flux is drawn toward consistency with the data studies of *Ganachaud* [1999] and *Gruber et al.* [2001] due to the adjustment of α between iteration 1 and iteration 5.

On a regional basis, agreement with the data studies is most improved in latitudes north of 13°N. This is due in part to the large increase in spring and summer nutrient export in the subpolar North Atlantic that increases net O_2 release to the atmosphere. Agreement with the data studies worsens slightly in the tropics the southern latitudes from iteration 1 to iteration 5. Low O_2 influx into the high southern latitudes may be due to sluggish mixing in the Southern Ocean. Improved agreement with nutrient climatology by adjustment to α

cannot correct for all deficiencies in the physical model, and thus it is not unexpected that the improved agreement with the nutrient climatology (see Figure 3-14) does not necessarily lead to an improved air-sea O_2 flux estimate in the high southern latitudes as it does in the high northern latitudes.

3.3.5 Conclusions

Model drift from the climatological nutrient field is reduced by spatially adjusting the nutrient export parameter over large-scale ocean regions. Resulting export timescales are understandable in terms of known or hypothesized controls on ocean export production. Export extremes are captured - from the slow export in HNLC regions that is consistent with iron limitation; to the rapid export in the North Atlantic associated with the dominance of nutrient and light limitation.

Global net air-sea O_2 fluxes are improved in comparison to data studies by the spatial adjustment of the nutrient export parameter. Regionally, significant improvement in this comparison is found in the mid and high latitudes of the Northern Hemisphere.

Suggested improvements

While the solution for a spatially inhomogeneous export parameter is successful in improving model agreement with the nutrient climatology, there are improvements to the method that could be made. First, ocean regions could be redefined based on broad biogeochemical and physical regimes instead of latitude circles. Winter mixed layers depths or mean surface nutrient concentration could be considered as parameters upon which regional definitions could be made. Second, the transitions between α regions could be smoothed. The lack of smoothing in this implementation of the method creates unnaturally sharp transitions in nutrient concentrations and air-sea gas fluxes between some regions.

3.4 Timestep and spin up of the offline model

Once the global α(x,y) is determined, the model is re-initialized with all three tracers: DIC from *Goyet et al.* [2000] and P and O_2 from *Conkright et al.* [1998]. It is run forward with an annual climatology of the 19-year variable physical fields for model spin-up at a four

hour timestep for 20 years. Then, model year 1980 is run once for initial adjustment in year 21, and then 1980 is repeated for the output run which then continues from year 22 to year 40. The 19-year run with interannually varying physical fields uses a two hour timestep.

Model results are presented in the following chapter.

Chapter 4

Global Air-Sea Fluxes of Carbon Dioxide and Oxygen

The model developed in Chapter 3 is integrated forward for the years 1980-1998. The mean and variability of tracer concentrations and air-sea fluxes are presented in this Chapter. First, model mean tracer concentrations are compared to climatological and timeseries data. Next, the 19 year mean CO_2 and O_2 fluxes and flux seasonal cycles are presented and compared to data estimates where available. Then, model estimated interannual variability in the air-sea fluxes of CO_2 and O_2 and the driving mechanisms of this variability are discussed.

4.1 Tracer Concentrations Compared to Data

In Figure 4-1, mean tracer concentrations are compared to climatological estimates. The model captures the broad pattern of the observed phosphate distribution. Model nutrients are too high off the west coast of South America, suggesting of overly strong upwelling in this region. The model underestimates P concentration in the subpolar North Atlantic and in some regions of the Southern Ocean. Differences between the model surface P shown here and that in Figure 3-15 are due to the fact that the model has been run on from the 15 year period for which α was derived. Although the model approached equilibrium after these 15 years, mean surface nutrients continue to change as the model is spun up for an additional 6 years (21 years total), and then run for another 19 years with the varying physical forcing.

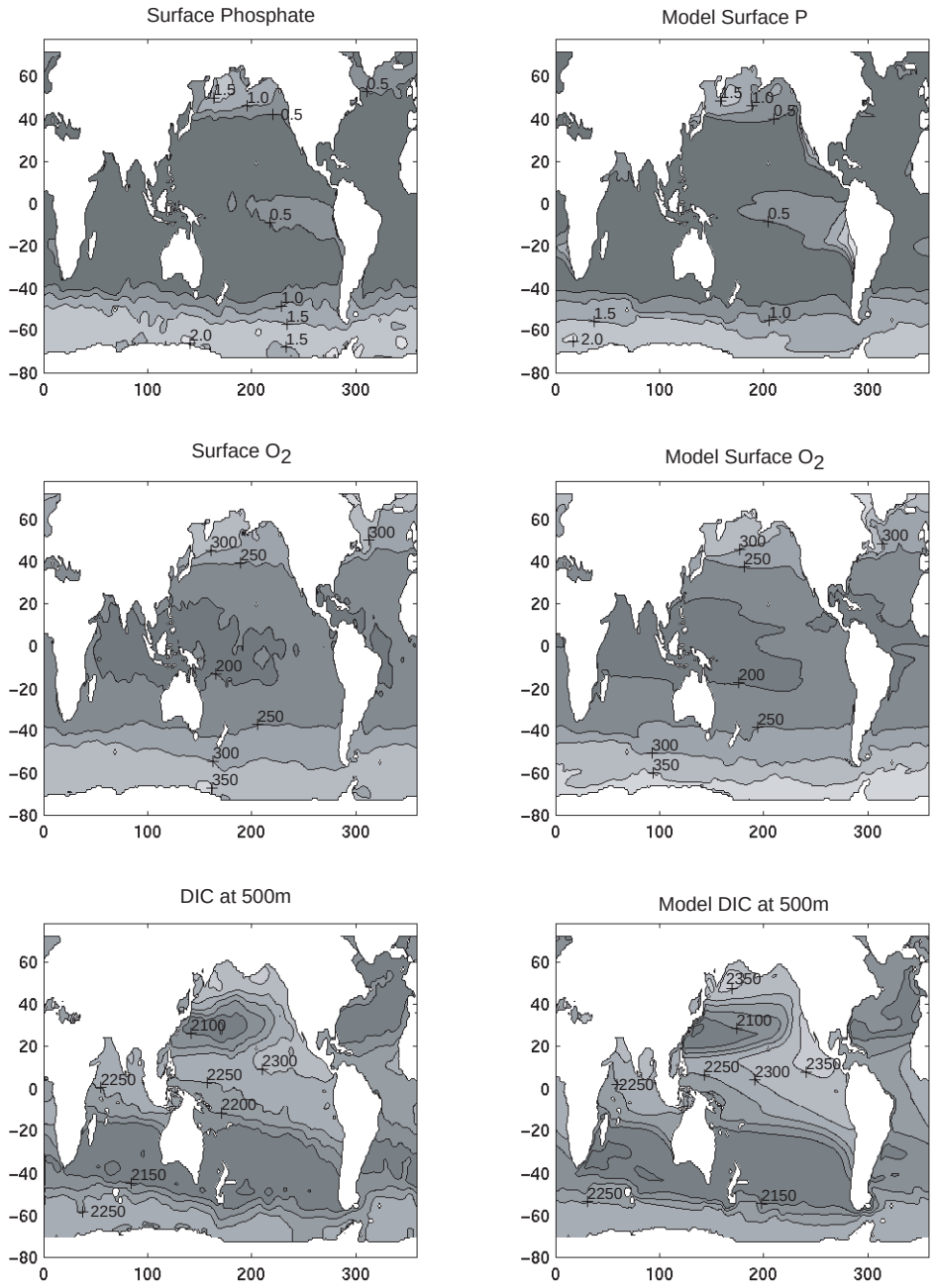

Figure 4-1: Comparison of climatological tracer concentrations (left) to model 19-year mean results (right). Climatological estimates are from *Conkright et al.* [1998] for phosphate and O_2, and from *Goyet et al.* [2000] for DIC. DIC results are compared at 500m as this is the first layer of the climatology presented by the authors. It is only below the winter mixed layer where the DIC climatology is considered reliable according to *Goyet et al.* [2000].

Although model agreement with the climatology is not as good as that shown in Figure 3-15, the comparison shown in Figure 4-1 is still improved over the comparison in Figure 3-10 from before α was spatially adjusted.

The surface O_2 concentration compares well to the observed climatology. Rapid air-sea exchange of O_2 means that there is a high correlation of SST with surface O_2 concentration. Therefore, the model's faithful representation of observed SST, due in part to restoration, aids this comparison. The region of most significant model difference from the climatology is in the high southern latitudes at the coast of Antarctica. This is likely due to the fact that model mean surface concentration includes periods in which sea ice blocks air-sea exchange and maintains high surface O_2 concentrations. Climatological data is also likely to be summer biased in this region and to not include much, if any, below-ice data.

Model DIC at 500m compares well to the climatology over most of the ocean. In the eastern equatorial Pacific, model DIC is about 50 μmol/kg too high from about 200°E to the coast. High nutrient concentrations against the coast of South America, likely due to overestimation of the strength of coastal upwelling, drive excess export of particulate carbon to depth. *Aumont et al.* [1999] indicate that the prediction of nutrient and carbon concentrations in the equatorial Pacific is quite sensitive to the model circulation. The model's constant remineralization length scale, and the lack of an explicit dissolved organic carbon (DOC) pool may also contribute to this model / data discrepancy [*Buesseler*, 1998; *Aumont et al.*, 1999]. Consistent with low surface nutrient concentrations in the northern North Atlantic, model DIC at 500m is higher than the observations by approximately 50 μmol/kg .

In Figure 4-2, model surface phosphorus is compared to observed phosphate at four ocean timeseries stations. At OWS C, the mean nutrient concentration is too low, consistent with Figure 4-1. The amplitude of the mean cycle of nutrients is somewhat underestimated in the model because the mean nutrient concentration in summer approaches zero. The variability at OWS C cannot be directly compared to the data because this data were primarily collected between 1975-1979. Nevertheless, the amplitude of the interannual variability in model nutrient concentration is consistent with the observations.

At BATS / Hydrostation S, the model exhibits a larger seasonal cycle than the observations, and model variability is too large. At HOT, the model underestimates the mean P

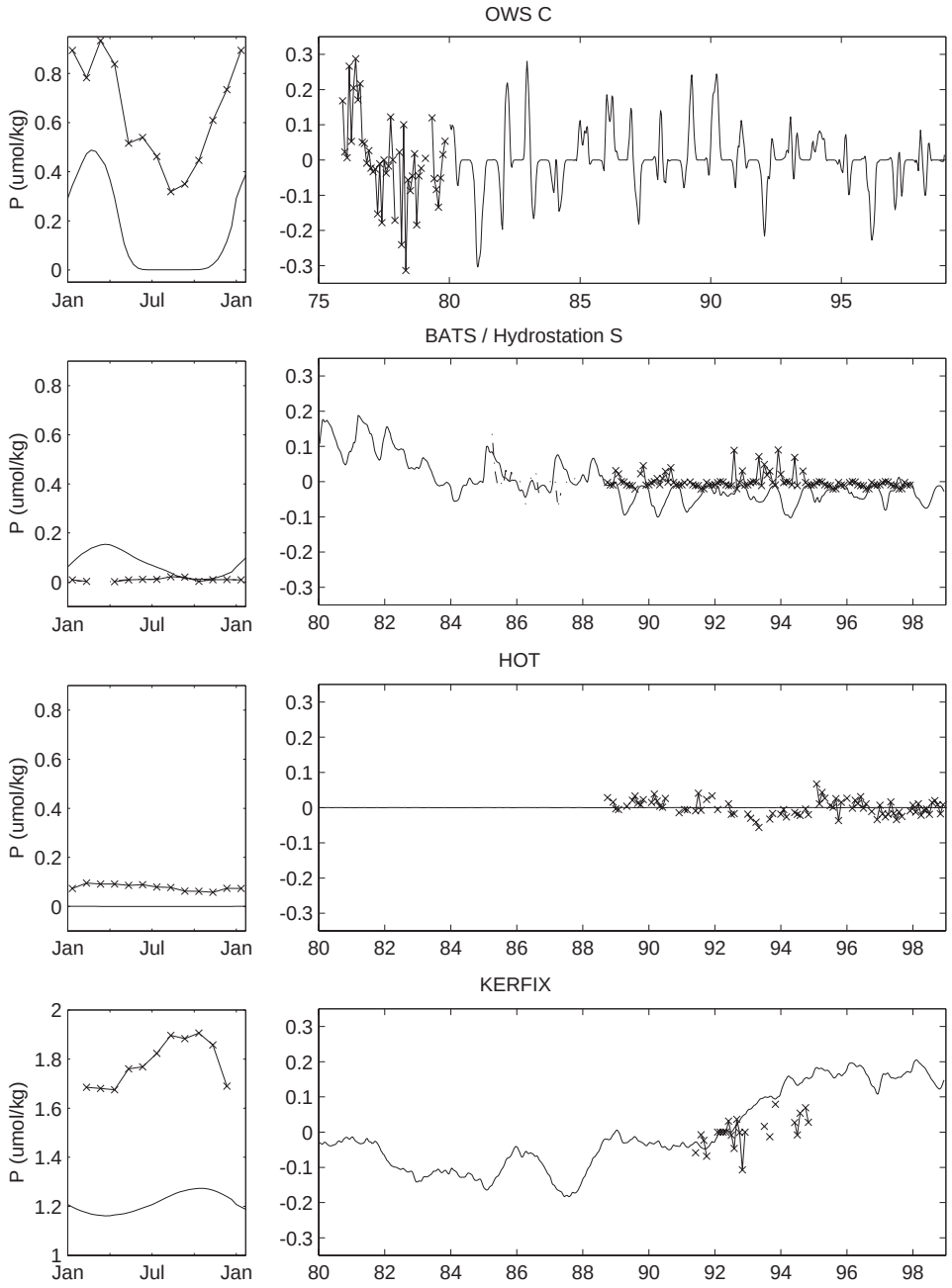

Figure 4-2: Comparison of model surface P (solid line) to observed phosphate at timeseries stations (crosses): OWS C, BATS (crosses) / Hydrostation S (dash-dot), HOT, and KERFIX. The same model areas described in Figure 3-5 are used for these comparisons. The mean seasonal cycle is shown to the left and the interannual variability around the mean cycle is shown at right. The mean cycle and variability are plotted on different scales, both in μmol/kg.

concentration and has too little variability. At HOTS and BATS, the export parameterization used in the model is clearly too simple to capture the intricacies of ecosystem dynamics at these subtropical locations. Nitrogen fixation [*Karl et al.*, 1997] and eddy nutrient supply [*McGillicuddy et al.*, 1998; *Oschlies and Garçon*, 1998] are two of the missing processes that are likely important to determining nutrient cycles at these locations. As discussed in Section 3.1.1, spatial offsets in mixing regions associated with the Gulf Stream is also likely to contribute to high mean nutrient concentrations at BATS.

At KERFIX, the model has too low mean P, but captures the amplitude of the seasonal cycle. Due to limited data, it is difficult to compare the nutrient variability to the data at KERFIX. Relatively minor offsets in the location of the Polar Front zone could be responsible for the mean P difference at KERFIX. At all stations, the model exhibits less high frequency variability than the data, due likely to the model's lack of explicitly resolved eddies or boundary conditions resolving high frequency storm events.

In Figure 4-3, model surface O_2 is compared to observed surface O_2 at the same four ocean timeseries stations. At OWS C, O_2 is low in the mean, and the amplitude of the seasonal cycle is somewhat larger than in the data. The variability of surface O_2 compares well in amplitude to the data. Low O_2 in the mean here is likely related to the overly deep mixed layers in this region (see Figures 3-4 and 3-5).

At BATS / Hydrostation S, the model captures the mean and seasonal cycle of O_2 extremely well. The model exhibits less variability in surface O_2, especially in comparison to Hydrostation S. The lack of explicitly resolved eddies is at least partially responsible for this limited high frequency variability. The difference of high frequency variability between Hydrostation S and BATS may be due to the fact that Hydrostation S is more than twice as close to the island of Bermuda than is BATS, and physical conditions of the two sites are likely to be impacted differently by the island's topography. BATS is should be better representative of the open ocean conditions for which the model is intended to have greater skill.

At HOT, model O_2 is somewhat low and the amplitude of the mean cycle is overrepresented in the model, and variability is well captured in its amplitude and some of its features. At KERFIX, the mean is well captured in the model, but the amplitude of the seasonal cycle is sightly too large. Model variability seems to be too small, although there

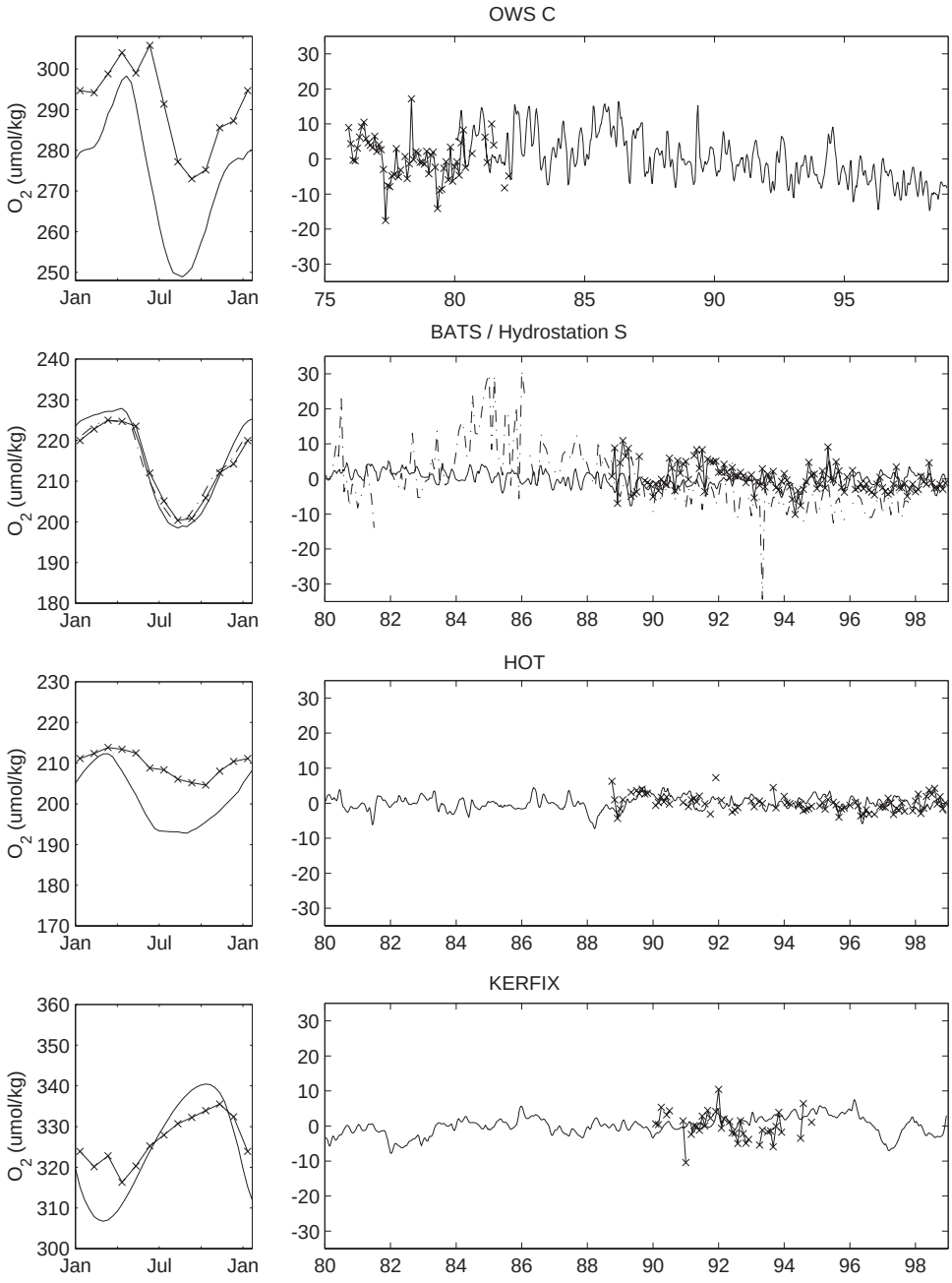

Figure 4-3: Same as Figure 4-2 for the comparison of model surface oxygen to observations at timeseries stations.

is limited data with which to make this comparison.

Model overestimation of mean DIC in the low latitudes and underrepresentation of mean DIC in the high Southern latitudes is illustrated in Figure 4-4. Normalization by salinity changes these comparisons minimally, indicating that a freshwater offset in the model is not responsible for the mean offsets seen here. The linear relationship of salinity to alkalinity, which tends to overestimate alkalinity in the warm waters of the subtropics and underestimate alkalinity in the cold waters of the high latitudes [*Millero et al.*, 1998], is likely to contribute to these deviations. In the subtropics, high alkalinity would drive the ocean pCO_2 to be too low, and this would cause an accumulation of excess DIC. At high latitudes, low alkalinity would create high oceanic pCO_2 and promote a loss of DIC. At KERFIX, both low DIC and low nutrient indicate that mean export may be overestimated. Similarly, high DIC and high nutrient concentrations at BATS are consistent with a low mean export.

The magnitude of the seasonal cycle in DIC at BATS compares well to the data, although this may be fortuitous when the overestimation of the annual cycle of P is also considered. Variability at BATS is underrepresented at the high frequency, but the model does capture longer timescale variability that appears to occur between the early and late 1990's. At HOT, the model overestimates the amplitude of the mean DIC cycle. Longer timescale variability in the early 1990's at HOT is captured to some degree in the model, but this comparison breaks down after 1994. At KERFIX, the shape of the mean cycle is well represented by the model, and there is too little data to make a reasonable comparison on the variability.

In summary, model tracer concentrations compare reasonably well to climatological estimates and timeseries observations. Significant offsets in mean concentrations for P in the high latitudes and DIC at all latitudes do exist in the model. Low frequency variability tends to be well captured in the model, but high frequency changes are underrepresented. High frequencies are damped due to multiple model limitations including the lack of explicitly resolved eddies, the simplified export parameterization, and the use of boundary conditions which damp small scale variability. Yet, for the purpose of studying interannual anomalies of air-sea fluxes of O_2 and CO_2, the model is a reasonable tool because it does capture many features of the long-term variability in the observations.

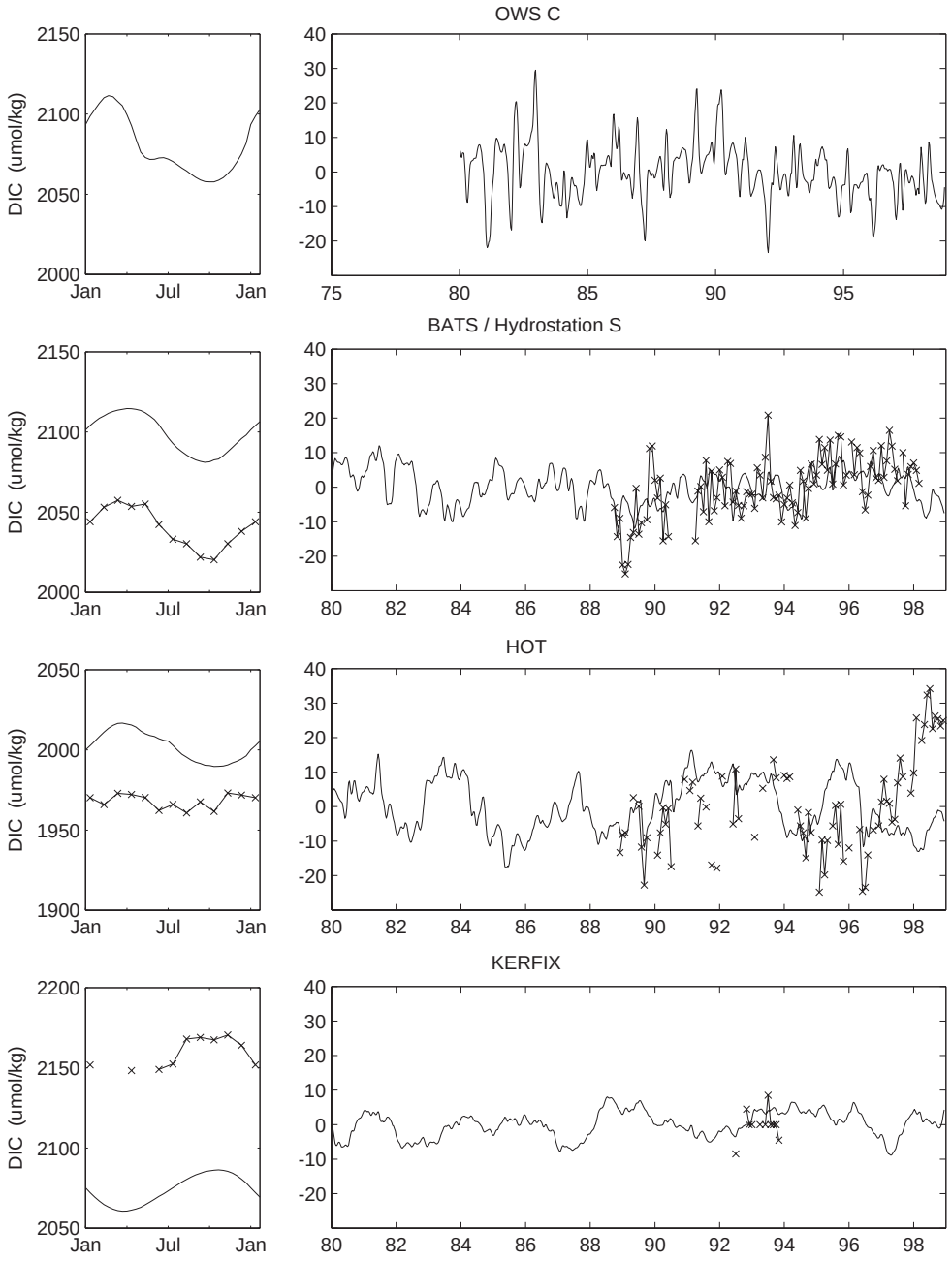

Figure 4-4: Same as Figure 4-2 for the comparison of model surface DIC to observations at timeseries stations. No DIC data was collected at Ocean Weather Station C (OWS C) or Hydrostation S. Model DIC results are presented at OWS C for consistency with the previous two figures.

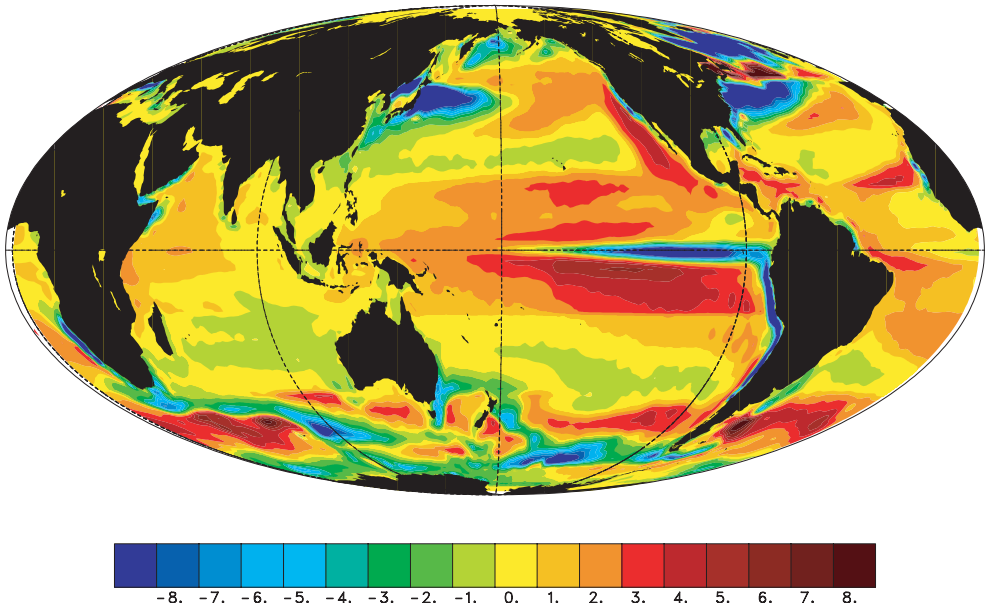

Figure 4-5: Model mean O_2 flux in mol/m^2/yr . Positive flux is to the atmosphere.

4.2 Mean and Seasonal Air-Sea Fluxes

4.2.1 Mean fluxes

Oxygen

The model mean air-sea O_2 flux is presented in Figure 4-5. O_2 is outgassed at the cold tongue in the eastern equatorial Pacific, and taken up into the ocean over the remainder of the tropics. In the subtropical gyres, O_2 is outgassed except in the western boundary current regions where rapid cooling and deeper mixing occurs. In the subpolar North Atlantic, O_2 is outgassed, associated with significant heat loss and deep mixing. In the Southern Ocean, O_2 is outgassed where deep mixed layers occur. The occasional sharp meridional gradients in the O_2 flux are due to the choice of distinct regional values for α(x,y). Values of α(x,y) may change significantly between areas, thereby altering the mean biogenic export and the mean O_2 flux. While these sudden changes are unrealistic at the local scale, they allow the model to capture large scale regional variations in biological productivity as shown in Section 3.3. The elimination of these locally sharp gradients could be achieved by smoothing

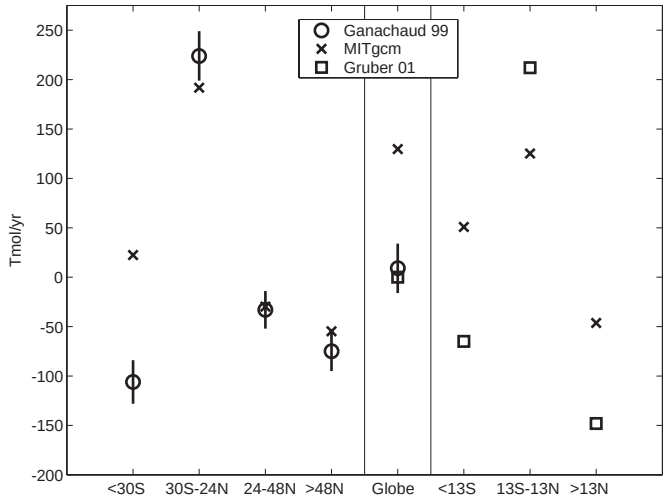

Figure 4-6: Model mean O_2 fluxes compared to the zonal mean estimates of *Ganachaud* [1999] and *Gruber et al.* [2001] in Tmol/yr. The error bars *Ganachaud* [1999] are indicated. Fluxes are positive to the atmosphere.

the α(x,y) field before applying it to the model.

In the Northern Hemisphere, the model compares well to the mean O_2 flux estimates of *Ganachaud* [1999] who used World Ocean Circulation Experiment (WOCE) data and an inverse model to estimate both the mean ocean circulation and O_2 fluxes, and from this inferred mean air-sea O_2 fluxes over the period 1985-1996. The comparison of the mean O_2 flux is also close to consistency in the tropics from 30°S to 24°N. However, this comparison is not good in the Southern Ocean where the model estimates a small O_2 outgassing and *Ganachaud* [1999] estimates a large ingassing. This discrepancy in the Southern Ocean is partly responsible for the global air-sea flux estimate (shown in the middle panel) being significantly different from the global mean estimate of *Ganachaud* [1999] which is indistinguishable from zero.

The study of *Gruber et al.* [2001] used a tracer inverse method related to that of *Ganachaud* [1999] with an ocean general circulation model to estimate the global circulation. *Gruber et al.* [2001] find significantly larger mean fluxes than this model estimates. The relatively coarse resolution OGCM used by *Gruber et al.* [2001] may in part be responsible for the discrepancy between it, the study of *Ganachaud* [1999], and estimates from this study. The inverse estimate of *Gruber et al.* [2001] was constrained to have a global

net zero mean O_2 flux.

This model has a mean efflux of -130 Tmol/yr. The magnitude of this efflux is not supported by the data estimate of *Ganachaud* [1999]. However, several coupled ocean-atmosphere modeling studies forced with increasing greenhouse gas emissions over the industrial period indicate a net O_2 outgassing from the ocean [*Plattner et al.*, 2001; *Matear et al.*, 2000; *Sarmiento et al.*, 1998]. Modeling studies find that O_2 outgassing and O_2 concentration decreases are primarily due to changes in ocean stratification. The Southern Ocean is a region where the change is predicted to to be most significant. *Keeling and Garcia* [2002] create an O_2 flux / ocean heating relationship and apply it to recent observational estimates of surface ocean warming to estimate the magnitude of the net O_2 flux in the 1990's. They find a 40 Tmol/yr outgassing, significantly smaller than estimated by this model. *Plattner et al.* [2001] estimate a net efflux of 42 Tmol/yr in the 1990's. Observational evidence of decreasing in-situ O_2 concentrations exists in support of these estimates in the North Pacific [*Keller et al.*, 2002; *Emerson et al.*, 2001].

In this model, approximately sixty-five percent (65%) of the mean O_2 efflux is due to a net loss of O_2 due to model adjustment, particularly in the Southern Ocean; and thirty-five (35%) is due to an exaggerated net biological production at depth in the tropics.

The net change of the surface to 1265m integrated concentration of O_2 in the model over the course of the 19 year model run indicates the regions responsible for this net outgassing of the model. This analysis is performed over the regions defined by *Ganachaud* [1999]. It is found that half of the net O_2 loss occurs in the Southern Ocean ($<30°$S). The remaining loss is shared equally between the tropics and the two Northern Hemisphere regions.

The net biological production of O_2 in the Tropics (30°S - 24°N) is due to excessively large areas of anoxic respiration that act as an effective O_2 source. The primary area of high anoxic respiration is between 300 to 800 m in the eastern equatorial Pacific, and a less intense region exists at the same depths in the Arabian Sea. Climatological analysis [*Conkright et al.*, 1998] indicates O_2 concentrations of $<4\mu$mol/kg, the limit below which oxygen-independent respiration occurs in the model, in similar regions, but their spatial extent is many times larger in the model than in the climatology. The creation of anoxia is a sensitive balance of biogeochemical and physical processes which is clearly imperfectly captured in the model. The high surface nutrient concentrations and high DIC at 500m off the coast of

western South America (Figure 4-1) indicates that high nutrient supply is driving excessive nutrient export and contributing to the excessive anoxic respiration at depth. Further improving model physics, refining the representation of particulate remineralization, and explicitly resolving the dissolved organic pool may reduce the extent of these anoxic regions [*Aumont et al.*, 1999; *Buesseler*, 1998; *Najjar et al.*, 1992].

In the Southern Ocean, the net outgassing of O_2 in the model may be due to excessive stratification in this region. The typically shallow model mixed layer depths in this region (Figure 3-4) and somewhat low nutrient concentrations (Figure 4-1 and Figure 4-2) are consistent with a reduced connection between surface and deep waters in the Southern Ocean. There is evidence [*Orr*, 2001] that the Gent-McWilliams eddy parameterization scheme in such models may lead to excessive stratification in the Southern Ocean, limiting the connection of deeper waters to the surface, and therefore preventing net O_2 uptake in this model and promoting the net O_2 loss over the region. In addition, O_2 efflux in the Southern Ocean may be due to an overestimation of particle export in the model which is consistent with low surface phosphate concentrations (Figure 4-1).

Unfortunately, it is not possible to directly separate model drift, possible parameterization deficiencies and the anoxic respiration O_2 source from potential credible changes in the ocean O_2 budget and O_2 air-sea flux that would allow comparisons to be made to the observed and postulated changes in the ocean's O_2 budget and O_2 flux [*Keller et al.*, 2002; *Emerson et al.*, 2001; *Plattner et al.*, 2001; *Keeling and Garcia*, 2002; *Matear et al.*, 2000; *Sarmiento et al.*, 1998]. Therefore, for this study I consider the model mean O_2 efflux to be a model artifact and focus on examining model estimates of interannual variability in air-sea O_2 fluxes.

Carbon Dioxide

In Figure 4-7, the observed mean CO_2 flux [*Takahashi et al.*, 1997] is compared to the model mean flux. The model does a good job of capturing the broad features and magnitudes of the mean CO_2 flux as estimated by *Takahashi et al.* [1997]. Net outgassing of CO_2 to the atmosphere occurs across the equatorial Pacific due to wind driven divergence and upwelling. CO_2 is taken up in the high Northern latitudes, particularly in the subpolar North Atlantic. In the Southern Ocean, the model captures the CO_2 ingassing due to the

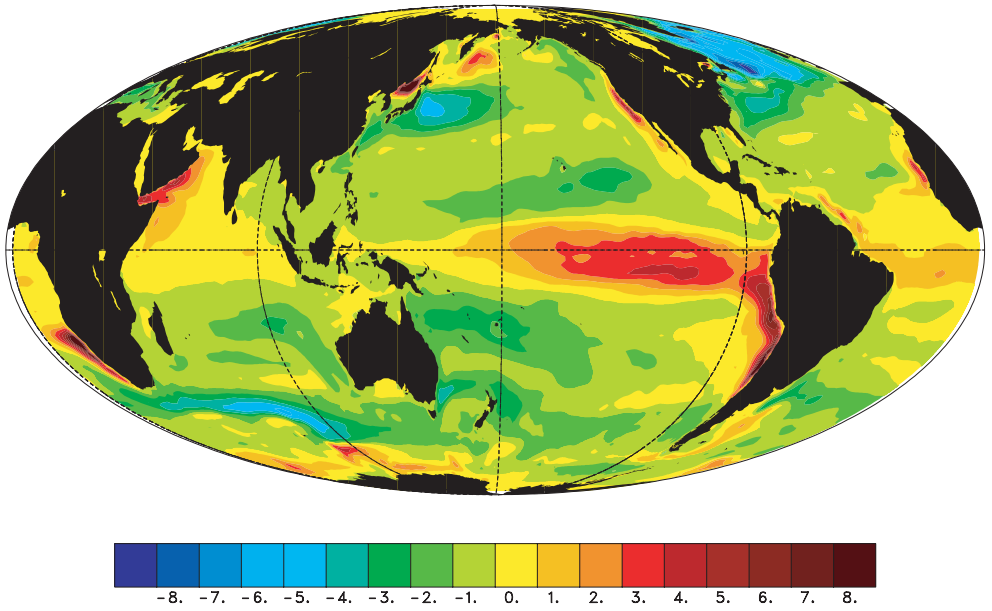

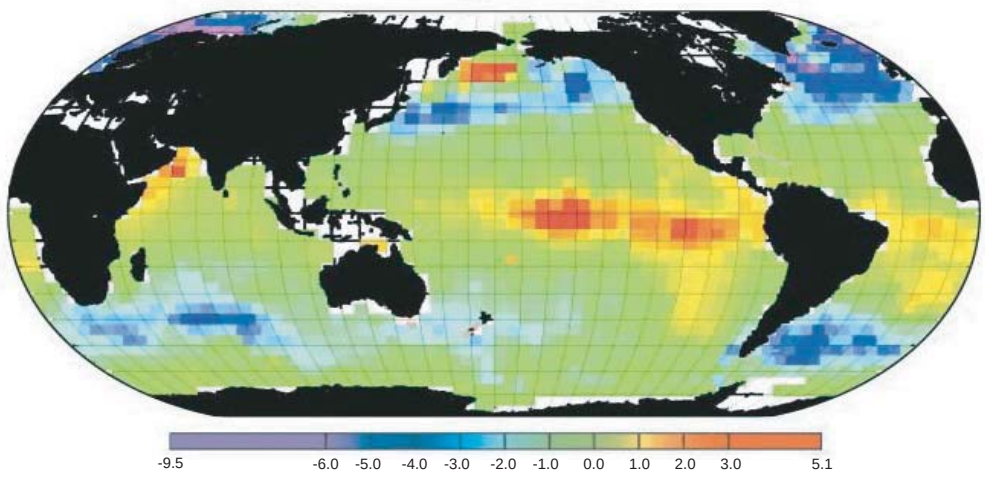

Figure 4-7: Model mean CO_2 flux (top) compared to the 1990 mean flux estimate from *Takahashi et al.* [1997] (bottom) in mol/m^2/yr . Positive flux is to the atmosphere.

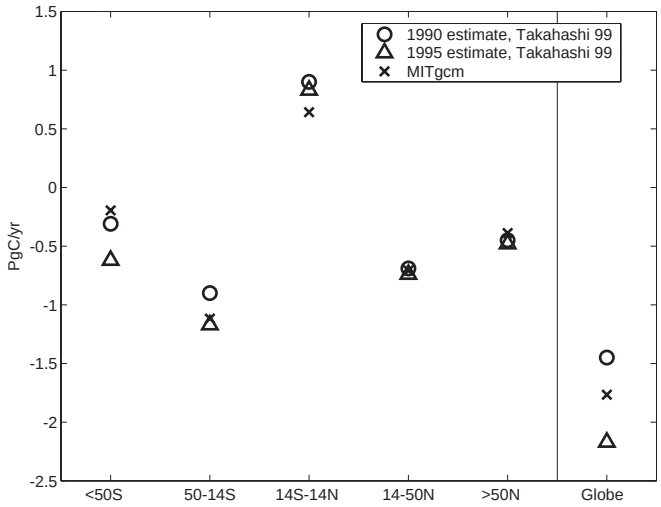

Figure 4-8: Zonal average model mean CO_2 flux compared to *Takahashi et al.* [1999] in PgC/yr . The 1990 estimate updated from *Takahashi et al.* [1997] and an estimate for 1995 are presented. Positive flux is to the atmosphere.

cooling of the pole-ward flowing Agulhas current at the southern tip of Africa, but does not capture the magnitude of the net ingassing due to a similar cooling of the Brazil current off South America. Coastal upwelling regions are stronger sources of CO_2 to the atmosphere in the model than in the data estimate, perhaps due to overly strong upwelling in the model as indicated by nutrients in Figure 4-1. The discrepancies in upwelling regions are further complicated by poor resolution of the climatology in coastal areas.

In Figure 4-8, zonally averaged mean CO_2 fluxes are compared to *Takahashi et al.* [1999], a study updating *Takahashi et al.* [1997]. Zonal average mean model fluxes compare very well to the data estimates in all regions. Net outgassing occurs in the tropics and net ingassing occurs in the middle and high latitudes. The global mean CO_2 flux of the model is 1.79 PgC/yr into the ocean. As will be discussed in Section 4.2.3, the model exhibits a significant trend in the global mean flux over the 19-year run that can be attributed to the Southern Hemisphere from 50-14°S. This trend makes it difficult to interpret the 19-year mean CO_2 flux from the model, and clearly adds significant uncertainty to the estimate.

Although mean DIC offsets have been found at timeseries stations (see Figure 4-4), mean fluxes compare extremely well to the global data compilation. This may indicate that the timeseries station DIC comparisons are not indicative of mean DIC offsets over large

ocean regions, or that the magnitude of the local DIC differences are not significant to the global CO_2 flux.

Eighty-nine percent (89%) of the 19-year net air-sea influx (34 PgC) of CO_2 is balanced by inventory gain in the model domain from 0-1265m. The remaining eleven percent (11%) of net air-sea flux is lost through the bottom boundary to the deep ocean.

4.2.2 Seasonal cycles of the hemispheric and regional O_2 and CO_2 flux

Over most of the ocean, the seasonal air-sea flux cycles of O_2 and CO_2 are comprised of large fluxes to the ocean in winter and from the ocean in summer. These fluxes are thermally, biologically, and/or dynamically driven. The interannual variability of net air to sea fluxes of O_2 and CO_2 are small residuals of these gross seasonal fluxes, and therefore it is important to understand the seasonal cycles of the fluxes and their driving mechanisms.

Oxygen

The O_2 anomaly in the surface water is the difference of the the O_2 saturation concentration from the in-situ O_2 concentration ($O_2 - O_2^{sat}$), and along with wind speed, drives air-sea O_2 exchange (see Equation 3.12). In Figure 4-9, the seasonal cycle of the O_2 anomaly in the model is compared to the data studies of *Najjar and Keeling* [1997] and *Garcia and Keeling* [2001] over fourteen basin-scale regions (high latitudes, middle latitudes and tropics of each major ocean basin). *Garcia and Keeling* [2001] show that their estimate of air-sea O_2 fluxes (based upon their O_2 anomaly and *Wanninkhof* [1992], and then transported through an atmospheric model) compares significantly better to observed seasonal cycles of atmospheric O_2/N_2 than do O_2 air-sea fluxes calculated from the *Najjar and Keeling* [1997] climatology by *Stephens et al.* [1998] (and identically transported through an atmospheric model).

In general, model O_2 anomaly results compare more favorably to the results of *Garcia and Keeling* [2001] than to those of *Najjar and Keeling* [1997]. This is particularly true in the tropical Pacific and tropical Atlantic. At high latitudes, the model faithfully represents the shape and timing of the mean seasonal cycle of the O_2 anomalies, but underestimates its magnitude in comparison to *Garcia and Keeling* [2001]. It will be shown shortly that this underestimation is best explained in most regions by a damped seasonal cycle of surface nutrients. In the Southern Ocean, excessive stratification could contribute to the model's

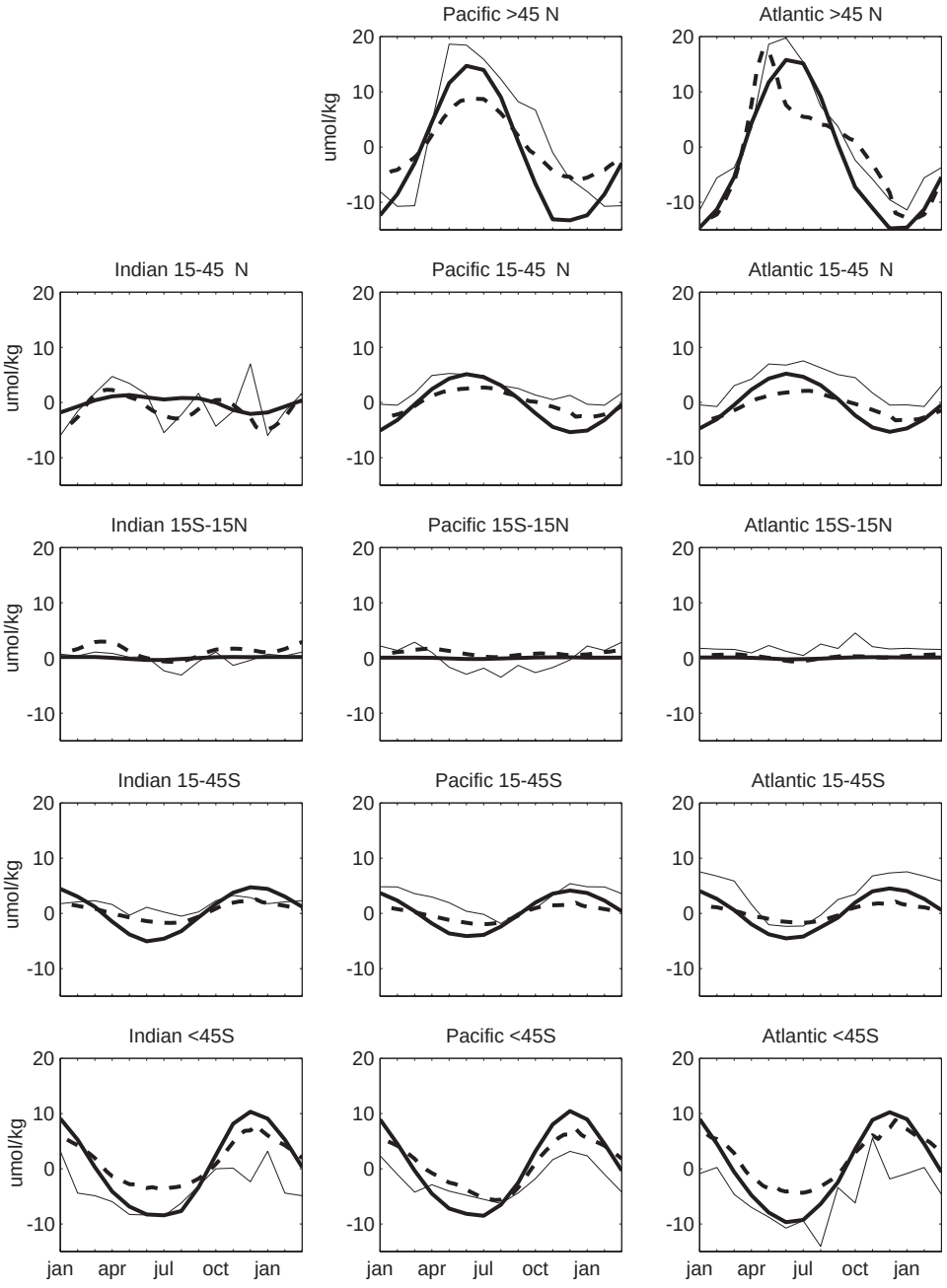

Figure 4-9: Regionally averaged seasonal cycle of the modeled O_2 anomaly compared to observational estimates: *Garcia and Keeling* [2001] (bold solid), *Najjar and Keeling* [1997] (solid), and modeled (bold dash). A positive O_2 anomaly indicates oversaturation and implies an O_2 efflux from the surface ocean. Model and *Najjar and Keeling* [1997] seasonal O_2 anomalies occurring under model sea ice are omitted for consistency with *Garcia and Keeling* [2001] who do not report values under ice.

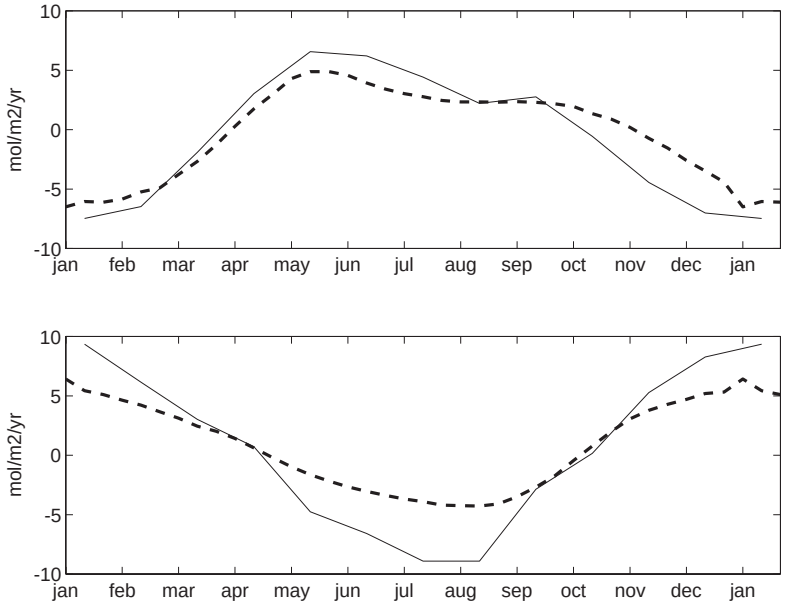

Figure 4-10: Northern (top) and Southern (bottom) hemisphere mean seasonal cycle of the air-sea flux of O_2 (bold dash) compared to the data-based estimate of *Najjar and Keeling* [2000] (solid). Fluxes are positive to the atmosphere.

damped seasonal cycle. Overall, this comparison indicates that while the model captures the basic features of the seasonal O_2 anomaly cycle, it underrepresents the cycle magnitude outside of the tropics. Consistent with conclusions regarding the physical variability of the model, the finding of a damped seasonal cycle of the O_2 anomaly indicates that the interannual variability of the O_2 anomaly, and thus of the O_2 air-sea flux, is likely to be a lower bound estimate.

In Figure 4-10, hemispheric-averaged model mean seasonal cycles of O_2 are compared to the estimate of *Najjar and Keeling* [2000], based on the O_2 anomaly results of *Najjar and Keeling* [1997]. The model result compares well to *Najjar and Keeling* [2000] in the Northern Hemisphere, but the seasonal cycle has a smaller amplitude in the Southern Hemisphere, consistent with the comparisons to *Najjar and Keeling* [1997] presented in Figure 4-9.

The model components that drive the mean cycle of O_2 fluxes are presented for nine ocean regions (extratropics and tropics, for each major ocean basin) in Figure 4-11. Here, the change in the integrated O_2 concentration (dashed line) is almost entirely due to seasonal heat fluxes that alter O_2 solubility and drive net fluxes, also known as the "thermal flux"

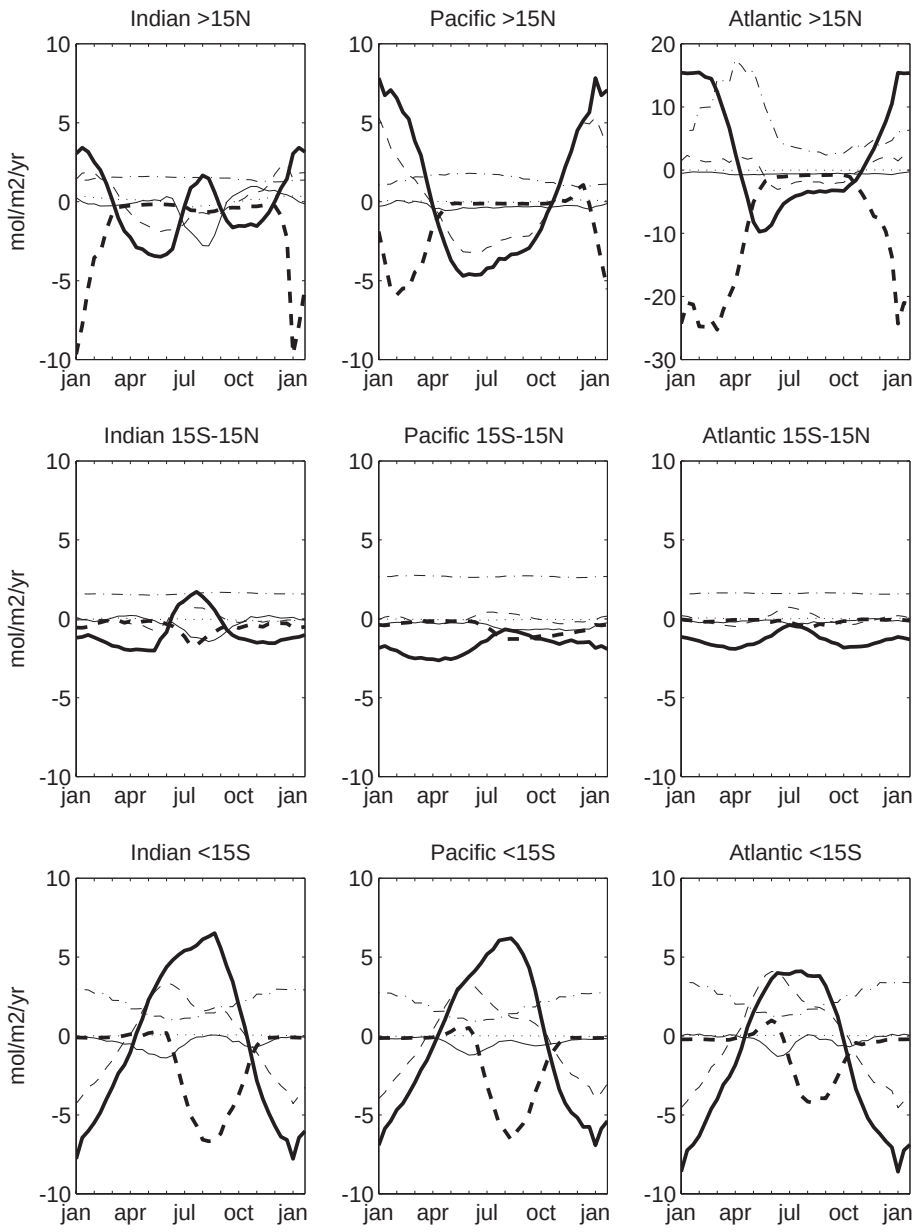

Figure 4-11: Components of the mean seasonal cycle of surface O_2 fluxes in nine ocean regions. Plotted are the impacts on the O_2 concentration in the top 50m of the ocean by advection (solid), convection (bold dash), biology (dash-dot), internal change or dO_2/dt (dash), freshwater (dotted), and air-sea flux (bold solid). Model fluxes are averaged over regions bounded by 15°S and 15°N and the major land masses. Note that the Atlantic north of 15°N is plotted on a different scale. Air-sea fluxes are positive to the ocean.

[*Keeling et al.*, 1993; *Najjar and Keeling*, 2000]. Tropical regions exhibit a far smaller seasonal cycle in air-sea fluxes than do the high latitudes, and are driven primarily by thermal forcing and dynamical (convective and advective) changes. In the small region of the Indian Ocean north of 15°N, monsoon forcing is clearly active, with convective changes driving the air-sea flux during the winter monsoon and advective change responsible during the summer monsoon. There is also a thermal cycle of importance to the seasonal fluxes. In the Pacific north of 15°N, convective and thermal changes drive the air-sea flux seasonal cycle. In the Atlantic north of 15°N, biology is more important than thermal changes to the air-sea flux. Biology can respond here and have a significant impact on the O_2 flux seasonal cycle because of the very short export timescale (τ) in the subpolar North Atlantic. In the three regions of the Southern Ocean, the seasonal cycle is primarily thermally and convectively controlled. There is also a relatively small biological cycle due to changes in light availability.

Especially in the Atlantic north of 15°N, the local balance mechanism [*Bender et al.*, 1996; *Keeling et al.*, 1993] for O_2 can be seen to be in operation over the seasonal cycle in the middle and high latitudes in the model. Mean O_2 ingassing occurs when convective mixing brings up low O_2 waters to the surface from the deep. The nutrients supplied with this mixing combined with seasonal light availability provides for a biological O_2 production in the surface layer and a net outgassing. The thermal cycle reinforces this cycle to a small degree in the North Atlantic and to a much larger degree in the North Pacific and the Southern Ocean.

Carbon Dioxide

The relationship of CO_2 fluxes to surface DIC concentration is less straightforward than with O_2 because of the reaction of CO_2 with seawater. The partial pressure of CO_2 in water (pCO_2) is determined by DIC concentration, temperature, alkalinity and salinity. Atmosphere - ocean CO_2 exchange (see Equation 3.13) is driven by the difference of the atmospheric pCO_2 from the surface ocean pCO_2 ($\Delta pCO_2 = (pCO_2 - pCO_2^{atm})$).

In Figure 4-12, the seasonal cycle of the modeled ΔpCO_2 is compared to the observational climatology of *Takahashi et al.* [1997]. Here, the comparison is presented over 14 basin scale regions in order to separate regions of substantially different surface pCO_2

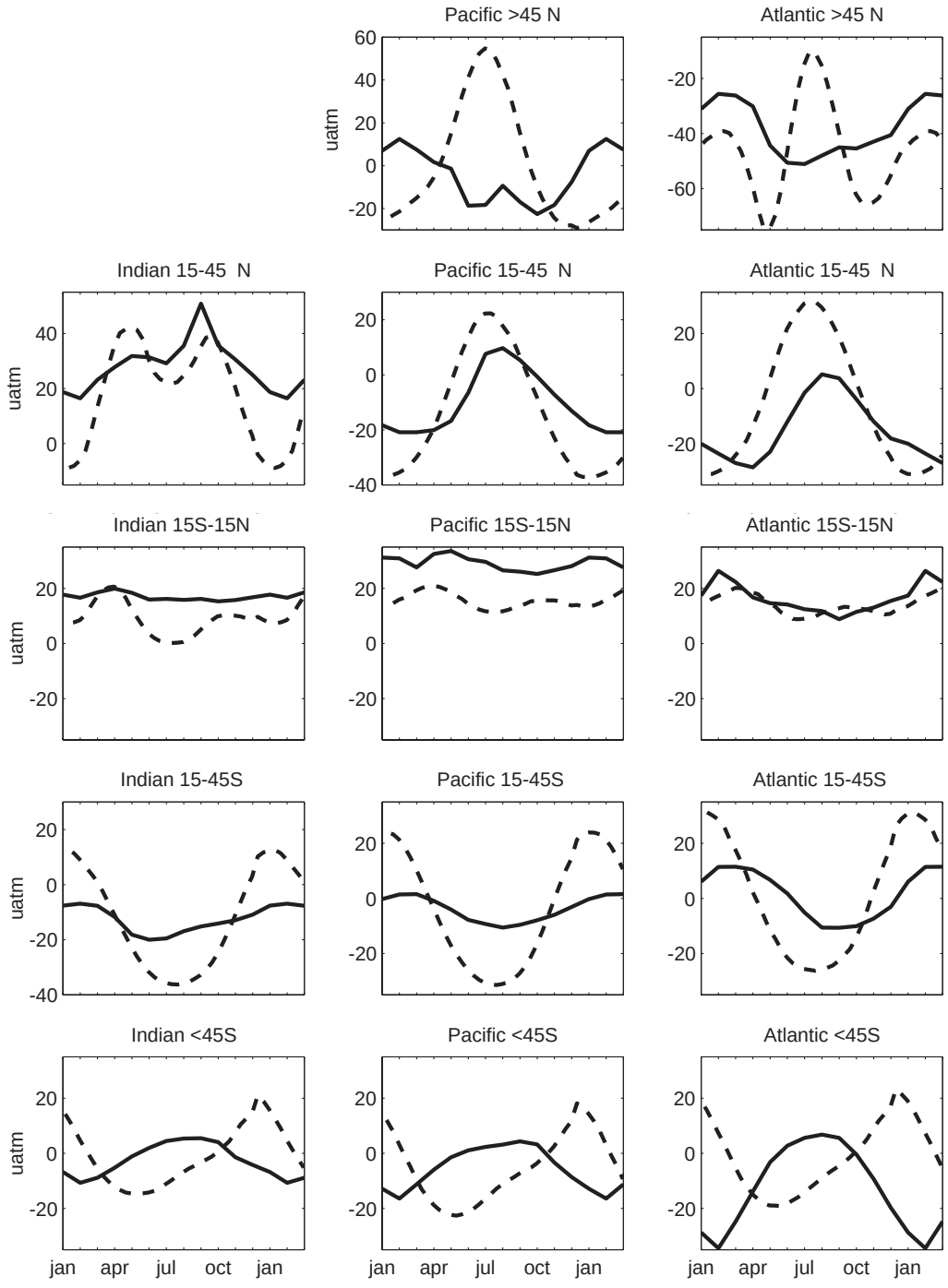

Figure 4-12: Regionally averaged seasonal cycle of modeled ΔpCO_2 (bold dash) compared to the observational estimate of *Takahashi et al.* [1997] (bold solid).

control as indicated by *Takahashi et al.* [1993].

In the high latitudes, the model ΔpCO_2 cycle is out of phase with the observational climatology. *Takahashi et al.* [1993] indicates that the pCO_2 of the high latitude ocean is primarily controlled by DIC concentration. As will be shown in Figure 4-13, the model indicates primary control by temperature of the pCO_2 seasonal cycle at all latitudes. Only in the Atlantic north of 45°N does the model illustrate a pCO_2 response to DIC supply by deep winter mixing, although the temperature peak clearly still remains. In the subtropics, *Takahashi et al.* [1993] finds temperature control of the seasonal cycle of pCO_2, and the model has a similar control. The model cycle is too large, however, particularly in the Southern subtropics. In the tropics, there is little seasonal cycle of ΔpCO_2 in either the model or the observations. The low mean ΔpCO_2 in the equatorial Pacific is consistent with the SST in this region being too low by 1°C (see Figure 3-6).

The overestimation of the model ΔpCO_2 cycle in the middle and high latitudes, as well as the underestimation of the O_2 anomaly cycle, can be partially explained by an underestimation of the seasonal nutrient cycle in regions outside the North Atlantic. This underestimation is evidenced in the nutrient cycle comparisons at KERFIX and HOT in Figure 4-2. The particle export parameterization developed for this model is intended to, as accurately as possible, represent mean export. It does not capture rapid nutrient and DIC drawdown, and O_2 production, associated with the spring bloom. This lack of DIC drawdown and O_2 production which would reduce the ΔpCO_2 cycle and increase the O_2 anomaly cycle certainly contributes to model deviations from the observations.

In the subpolar North Atlantic, comparisons to mean nutrient and O_2 cycles at OWS C, as well as comparison to the *Conkright et al.* [1998] seasonal nutrient climatology (Figure 3-16), indicate that the nutrient cycle is reasonably captured in this region. This is because of the rapid export timescale in this region that allows a spring bloom response to nutrient and light availability. Yet, the mean export is overestimated in the subpolar North Atlantic, as can been seen with the mean offset in nutrient concentration at OWS C. Nutrient concentrations become so low during the summer months that biological production becomes nutrient limited such that DIC drawdown and O_2 production are significantly reduced. Lacking the continued removal of DIC, the ΔpCO_2 increases under the control of temperature. In addition, O_2 production in summer is reduced such that the O_2 anomaly

drops far faster in the model than in the observations (Figure 4-9). Thus, I conclude that excessive mean export in the subpolar North Atlantic overdepletes surface nutrient and slows summer export production. This allows temperature to have a dominant role in the seasonal cycle of ΔpCO_2, which is inconsistent with the observations of *Takahashi et al.* [1993]. The low mean ΔpCO_2 in the subpolar North Atlantic in winter can be explained by low winter SSTs (Figure 3-6).

In the subtropical North Atlantic, comparisons to the mean nutrient cycle at BATS (Figure 4-2) indicate that the model's cycle is too large. Yet, it is found that seasonal DIC drawdown and O_2 production is too low. This discrepancy is consistent with findings of export at BATS that has carbon to nutrient ratios that are substantially higher than the Redfield ratios [*Ono et al.*, 2001]. At BATS, substantial amounts of DIC may be removed from the surface and O_2 may be produced by ecosystems that efficiently recycle scarce nutrients at the surface. The model, with a simple particle export scheme and the assumption of Redfield ratios, cannot capture these dynamics.

The apparent overestimation of the ΔpCO_2 seasonal cycle by the model is due in large part to deficiencies in the biogenic export scheme, but may also be impacted by the sparsity of data in the observational climatology of *Takahashi et al.* [1997]. This is particularly true in the Southern Hemisphere where data is quite sparse. Data density is increased at all latitudes in the seasonal ΔpCO_2 climatology of *Takahashi et al.* [1999], and the comparisons presented here may be notably different if that data estimate were used.

Following *Takahashi et al.* [1993], the effects on pCO_2 of surface DIC concentration, temperature, alkalinity and salinity may be written as:

$$\frac{dpCO_2}{dt} = \frac{\delta pCO_2}{\delta DIC}\frac{dDIC}{dt} + \frac{\delta pCO_2}{\delta T}\frac{dT}{dt} + \frac{\delta pCO_2}{\delta ALK}\frac{dALK}{dt} + \frac{\delta pCO_2}{\delta S}\frac{dS}{dt} \tag{4.1}$$

In Figure 4-13, the components driving the seasonal cycle of surface pCO_2 in nine ocean regions are shown. As previously discussed, the seasonal cycle of total change in pCO_2 is primarily thermally driven over all regions. The surface DIC concentration damps the thermally driven pCO_2 cycle, but the comparisons in Figure 4-12 indicate that this process is not sufficiently strong in the high latitudes of the model. In the North Atlantic, it can be seen that if there were a continued DIC drawdown in the summer months, the temperature forcing would be strongly opposed and the pCO_2 maximum in summer would

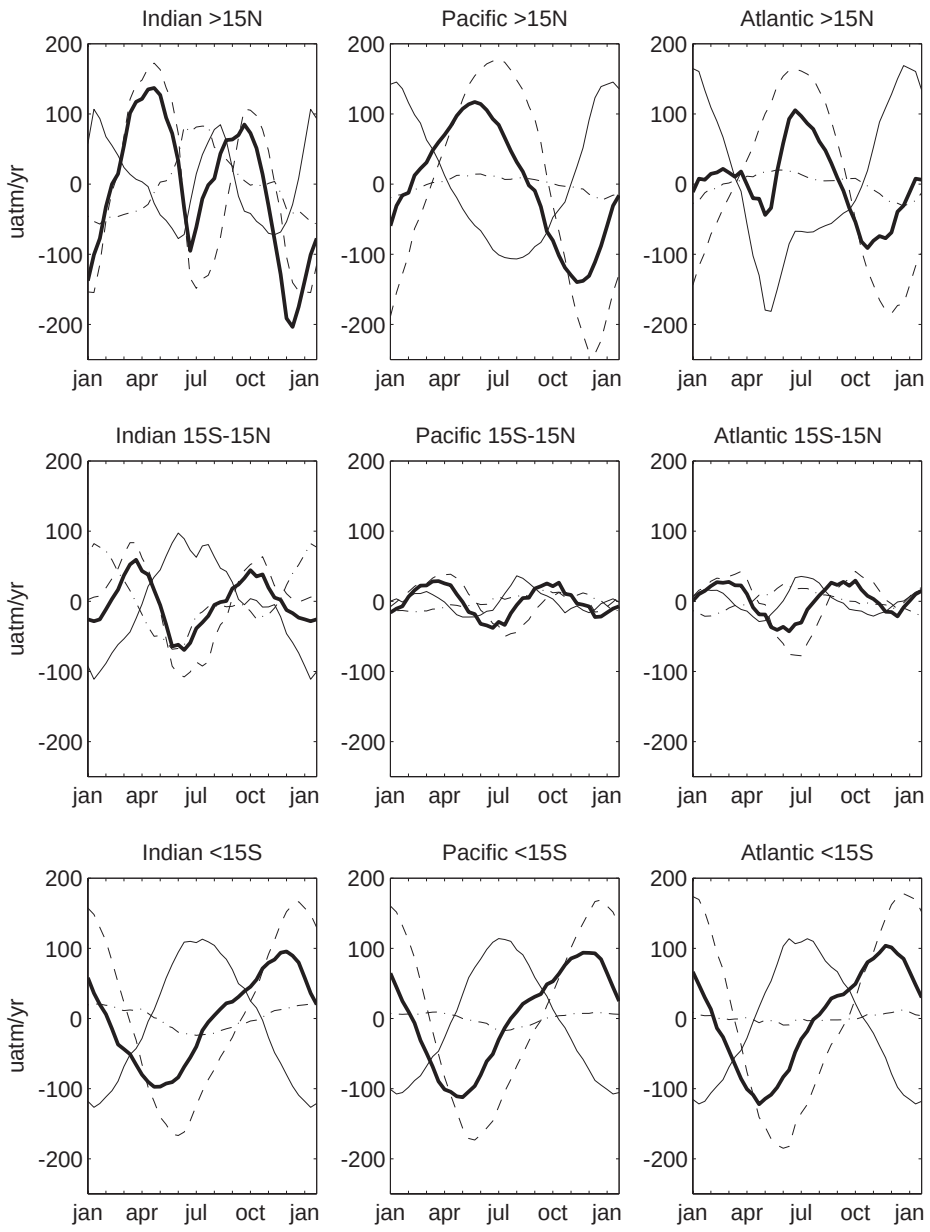

Figure 4-13: Components of the mean seasonal cycle of ocean pCO_2 in nine ocean regions. Plotted are the impacts on the pCO_2 in the surface 50m of the ocean by $(\delta pCO_2/\delta DIC)(dDIC/dt)$ (solid), $(\delta pCO_2/\delta T)(dT/dt)$ (dash), $(\delta pCO_2/\delta ALK)(dALK/dt)$ (dash-dot), and $dpCO_2/dt$ (bold solid). Model pCO_2 is averaged over regions bounded by 15°S and 15°N and the major land masses. The impact of salinity on the pCO_2 seasonal cycle is negligible and is not presented.

be substantially damped. If this were the case, the model cycle of ΔpCO_2 would be far more similar to that of *Takahashi et al.* [1997]. Alkalinity changes are only significantly important in the tropical and northern Indian Ocean, where they tend to cancel the impact of DIC changes. Overall, the model's seasonal cycle of the air-sea CO_2 flux is primarily thermally forced.

Changes in model pCO_2 drive the cycle of CO_2 air-sea flux with a lag due to the buffering of CO_2 by reaction with seawater. In Figure 4-14, the balance for the surface DIC concentration is shown, including the impact of the air-sea flux. In general, the seasonal cycle of surface DIC concentration is determined by a combination of the thermally-driven air-sea CO_2 flux and convection. In some regions, advection, biology, and/or freshwater fluxes are also significant. The limitation on summertime biological DIC drawdown in the extratropical North Atlantic is clear in this figure. In all regions, the seasonal cycle of surface DIC concentration acts to damp the primarily thermally driven pCO_2 seasonal cycle (Figure 4-13). As previously discussed, DIC damping is too weak in the North Atlantic because of excessive mean export that results in summertime nutrient limitation, and in other extratropical regions, the DIC component of the pCO_2 cycle is too weak because of weak seasonal nutrient cycling.

4.2.3 Calculation of interannual flux anomalies

The seasonal cycle of the air-sea fluxes is removed from the 19 year flux timeseries so that the interannual variability can be considered. This is accomplished by subtracting from each 10-day flux distribution the 19-year mean flux for the respective 10 day interval. However, before considering flux interannual variability, the model trend must be addressed.

In Figure 4-15, the global air-sea flux anomalies are presented. Both the O_2 and CO_2 flux have non-negligible trends. As will be explained below, the trend is due in large part to model drift. Evidence for real long-term trends in the O_2 and CO_2 fluxes does exist, but for this it is not possible to distinguish any real trends from model-induced trends.

Oxygen

The trend of the undetrended model results toward a weaker O_2 outgassing over the 19-year period is due both to a net cooling of the physical model and to continuing model

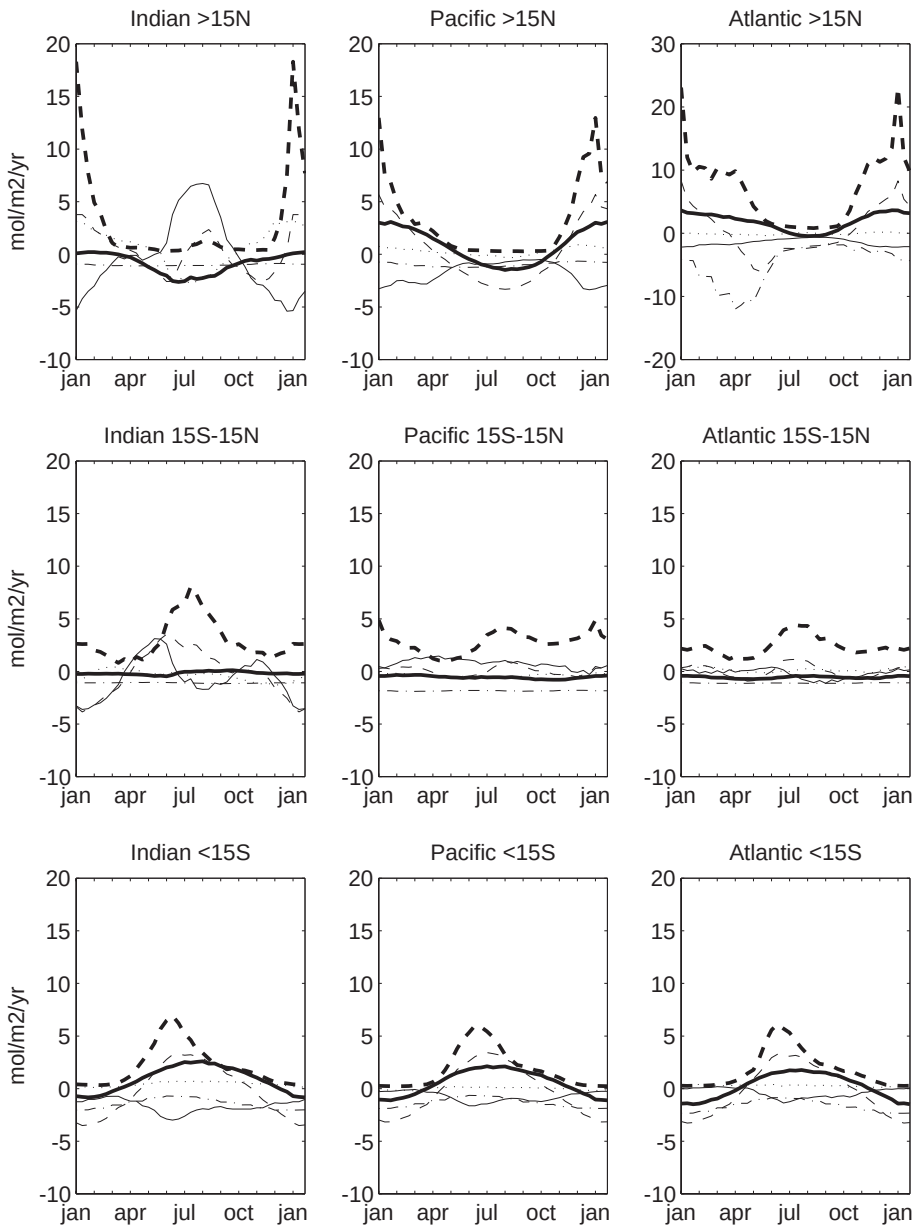

Figure 4-14: Components of the mean seasonal cycle of DIC in nine ocean regions. Plotted are the impacts on the DIC concentration in the top 50m of the ocean by advection (solid), convection (bold dash), biology (dash-dot), internal change or dDIC/dt (dash), freshwater (dotted), and air-sea flux (bold solid). Model fluxes are averaged over regions bounded by 15°S and 15°N and the major land masses. Note that the Atlantic north of 15°N is plotted on a different scale. Air-sea fluxes are positive to the ocean.

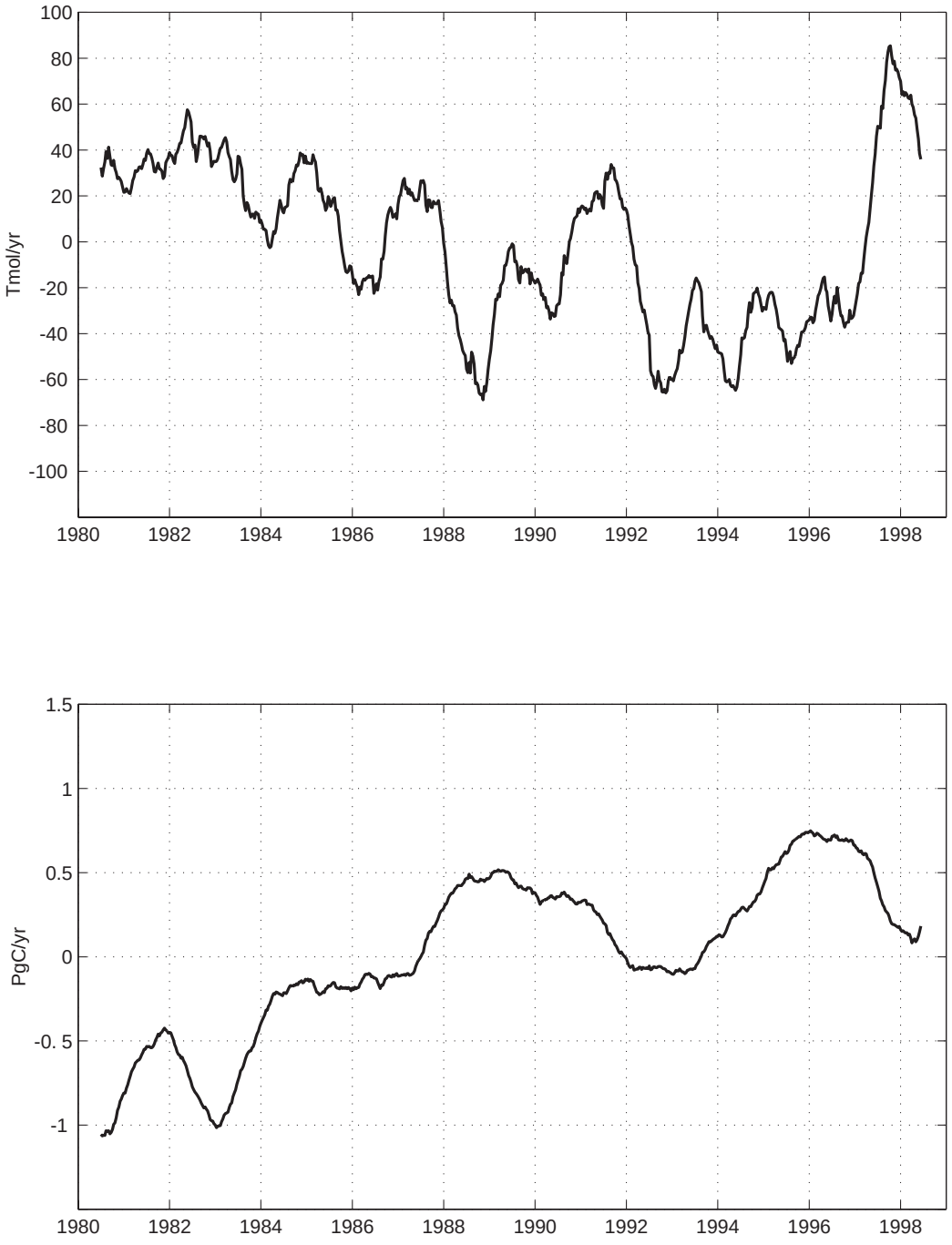

Figure 4-15: Undetrended global mean net air-sea fluxes for the 19 year model run. O_2 flux in Tmol/yr (top) and CO_2 flux in PgC/yr (bottom). The timeseries has been smoothed to remove timescales shorter than one year. Positive fluxes are to the atmosphere.

adjustment.

The temporal trend is calculated by a linear fit to the deseasonalized data at each point in space. When globally averaged, the linear trend results in the final model year having a mean outgassing that is 53 Tmol/yr less than in year 1. This trend results in a total of 477 Tmol less efflux over the course of the 19 model years than if there were no trend.

Approximately 70% of this trend is due to model adjustment in relation to the boundary conditions of the model via upwelling and mixing with deep waters that are still impacted by initial and boundary conditions. This adjustment occurs mostly in the Southern Ocean at latitudes <30°S. The physical model also has drift, evidenced by the necessity for salinity restoration

The upper 250m of the model ocean cools by 0.28°K over the 19 year model run. *Manning* [2001] find that the temperature dependence of O_2 solubility is -5.8x10^{-6} molkg$^{-1}\circ K^{-1}$ following *Weiss* [1970]. If it is assumed that the top 250m of the ocean can equilibrate with the atmosphere over the 19 year run, then the solubility reduction due to the 0.28°K model cooling results in an influx of 145 Tmol, or 7.7 Tmol/yr. This is approximately 30% of the trend in the O_2 flux.

Trends in the ocean O_2 budget in the recent decades due to warming and stratification change may occur along with global-warming induced changes to the ocean O_2 budget [*Keller et al.*, 2002; *Emerson et al.*, 2001; *Plattner et al.*, 2001; *Keeling and Garcia*, 2002; *Matear et al.*, 2000; *Sarmiento et al.*, 1998]. It is possible that some of the trend in the model is due to such forcing, but, as with the model mean, it is not possible to directly separate model drift and an actual signal. Further, the fact that this model cools in the surface ocean instead of warms would make the detection of any real trend extremely difficult. Therefore, for discussions of the interannual variability in air-sea fluxes of O_2, the linear trend has been removed.

Carbon Dioxide

The model indicates a significant trend toward less CO_2 uptake into the oceans toward the end of the model run, or a positive anomaly compared to the 1980-1998 mean (Figure 4-15). The work of the Intergovernmental Panel on Climate Change (IPCC) [*Prentice et al.*, 2001] indicates that the CO_2 sink into the oceans in the 1990's was 0.2 PgC/yr smaller than in

the 1980's. However, *Plattner et al.* [2001] suggest that, due to net O_2 outgassing, the IPCC estimate for the 1990's [*Manning*, 2001] should be revised upward such that ocean takes up 0.7 PgC/yr more in the 1990's than in the 1980's. Clearly, the temporal change in the actual ocean CO_2 sink over the period of the model run is an issue of active debate. There is not clear evidence to support the magnitude of the CO_2 flux trend in these results. In fact, the long-term trend can be shown to be due primarily to model adjustment with the initial conditions.

The model trend is calculated by a linear fit to the deseasonalized data at each point in space. When globally averaged, it results in the final model year having a mean influx that is 1.3 PgC/yr less than in year 1, or a total of 11.7 PgC less influx over the course of the 19 model years. The trend is due to a reduction in the rate of CO_2 storage in the model over the 19 year run, most likely due to model adjustment away from initial conditions. Most of the reduction in CO_2 storage rate occurs in the Southern Subtropics between 50-14°S.

If the physical model were not cooling, the long-term change in the model would be larger. A flux sensitivity to temperature (-3x10^{-13} molkg$^{-1}s^{-1}{}^{\circ}K^{-1}$) for carbon is calculated following *Wanninkhof* [1992], and assuming an average wind speed of 7.4 m/s. Applied to the cooling of 0.28°K over the 19 model years in the upper 250m of the ocean, this indicates that approximately 2.1 PgC was ingassed to the model due to the surface cooling. Thus, it is estimated that the model trend would have been approximately 20% larger if the model was not cooling at the surface.

For the following discussions of the interannual variability in air-sea fluxes of CO_2 and for the calculation of the land and ocean CO_2 sinks in Chapter 6, the linear trend is removed from the flux estimates.

Sensitivity to initial conditions

Although it is possible to calculate, explain, and remove trends from the flux timeseries, the existence of the trend raises questions about the reliability of the interannual air-sea flux estimates due to dependence on initial conditions. In order to begin to answer this question, the 19-year varying model run was restarted at 1980 using the end of 1998 from the original model run as the initial condition. This run was continued through 1985. After the first three years (1980-1982), the interannual variability of O_2 and CO_2 fluxes from the

repeated model run is practically identical to the original run, once the trend calculated with the original run is removed. Thus, the flux variability early in the time-varying run is sensitive to the initial conditions, but this sensitivity is dissipated after approximately three years. Therefore, model flux variability estimates for the first three years of the model run are considered to be less reliable than estimates from later in the run.

4.3 Interannual Variability in Air-Sea Fluxes of O_2 and CO_2

The detrended timeseries of interannual variability in air-sea O_2 and CO_2 fluxes is presented in Figure 4-16. Interannual variability in the air-sea O_2 flux has interannual extremes of -70 to +100 Tmol/yr, with a root-mean-square (RMS) of 35 Tmol/yr. I note the appearance of a biennial cycle in the O_2 flux variability. I can offer no explanation for this feature, in large part because the dominant regional fluxes presented in Figure 4-17 are controlled by processes that do not, to my knowledge, have a biennial cycle. For CO_2, the flux has extremes of $\pm$0.5 PgC/yr, and RMS of 0.28 PgC/yr.

While this model estimate of CO_2 flux interannual variability agrees qualitatively with the ocean GCM results of *LeQuéré et al.* [2000], it is notably larger in magnitude. *LeQuéré et al.* [2001] update the work of *LeQuéré et al.* [2000] by replacing their particle export scheme with a multi-compartment ecosystem model in their OGCM, but find only a small increase in air-sea flux interannual variability due to increased biological variability. The MITgcm estimate has approximately the same interannual extremes as does *LeQuéré et al.* [2001].

In both *LeQuéré et al.* [2000, 2001], the temperature and salinity of the OGCM is relaxed toward climatological observations below the mixed layer to the north of 10°N and south of 10°S with a timescale of 1 month. Their semidiagnostic model is likely to damp physical variability at the high latitudes, such as variability in mode water formation. The model used for this study is fully prognostic, and therefore is likely to have greater physical variability outside the 10°S to 10°N band than the model used in *LeQuéré et al.* [2000] and *LeQuéré et al.* [2001]. This greater physical variability is likely to be responsible for the larger global average air-sea CO_2 flux interannual variability in this model than in *LeQuéré et al.* [2000]. Nevertheless, it was illustrated in Section 3.1 that this model does

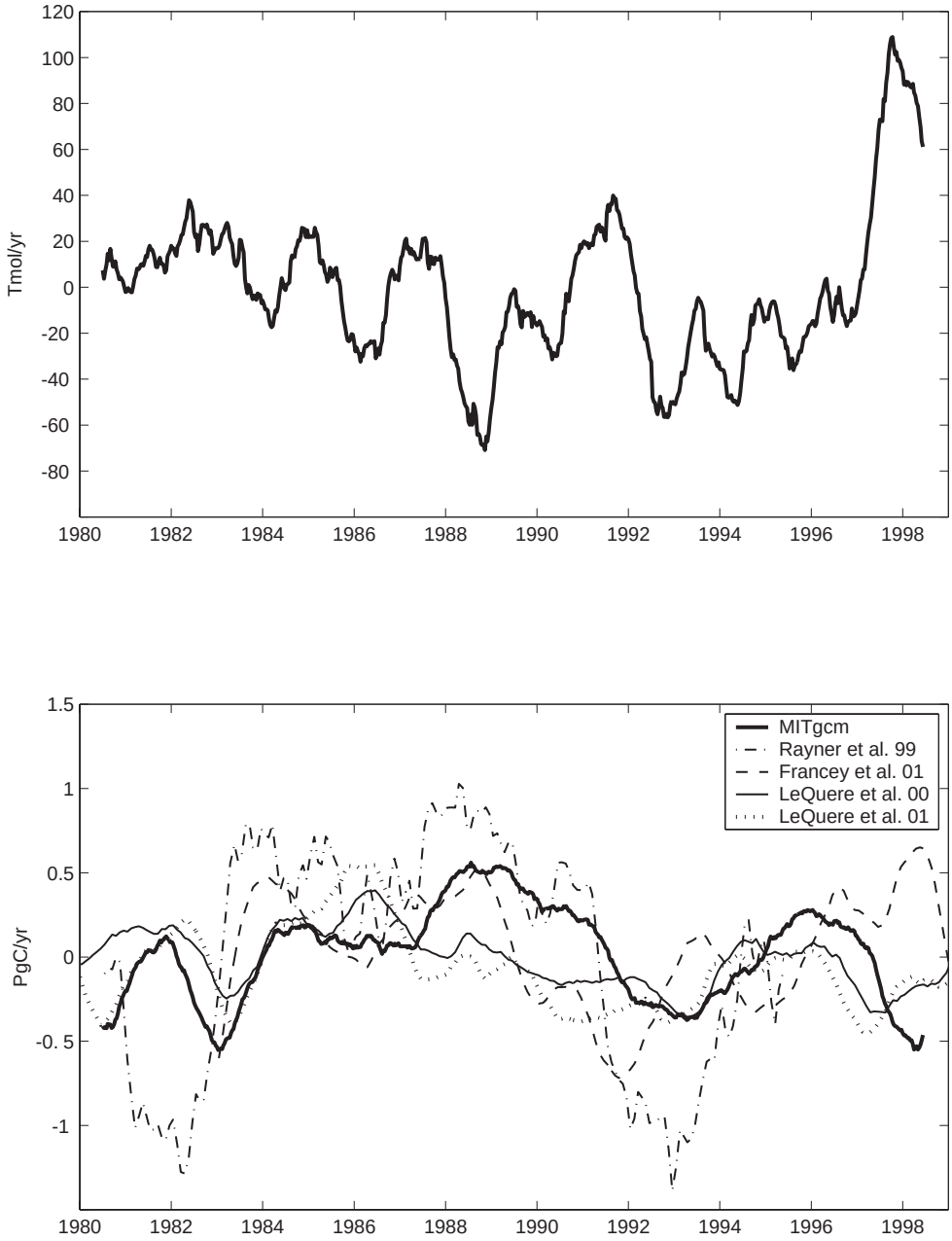

Figure 4-16: Global mean net air-sea fluxes for the 19 year model run (bold solid). O_2 flux in Tmol/yr (top) and CO_2 flux in PgC/yr (bottom). The CO_2 flux is compared to the atmospheric data inversions of *Rayner et al.* [1999] and *Francey et al.* [2001] and the ocean GCM estimates of *LeQuéré et al.* [2000] and *LeQuéré et al.* [2001]. The mean seasonal cycle and the long term trend have been removed from the model. All timeseries have been smoothed to remove timescales shorter than one year.

underrepresent the observed physical variability of the global ocean, and therefore all model estimates may still be lower bounds.

The work of *LeQuéré et al.* [2001] indicates that if a multi-compartment ecosystem model were implemented in the MITgcm, only a slight increase in the air-sea flux variability would result. It can be expected that qualitative changes in the results would be minimal.

Rayner et al. [1999] and *Francey et al.* [2001] use atmospheric observations of δ^{13}C and CO_2, with O_2/N_2 as a long-term constraint, to estimate the interannual variability in the land and ocean sinks of CO_2. The study of *Francey et al.* [2001] is an update of *Rayner et al.* [1999] that includes (1) a recalibration of the Cape Grim δ^{13}C record; (2) re-smoothing of the NOAA CO_2 data and Cape Grim δ^{13}C to account for their northern hemisphere and southern hemisphere biases, respectively; and (3) better estimates of the gross CO_2 flux due to different response times of surface exchange to atmospheric perturbations in ^{12}C and ^{13}C (R. Francey, personal communication). These adjustments of the data processing and gross flux estimates result in the smaller estimate for the ocean air-sea CO_2 flux variability.

In summary, the model estimate of the interannual variability in the global CO_2 flux has a larger variability than the model of *LeQuéré et al.* [2000], and a similar magnitude variability of as *LeQuéré et al.* [2001]. Concurrent work on atmospheric inversions estimates of the land and ocean CO_2 sinks [*Francey et al.*, 2001] gives smaller estimates than older efforts [*Rayner et al.*, 1999] for the ocean air-sea flux variability of CO_2, and has extremes similar in magnitude to this model estimate.

It can be concluded that the model estimate of the global air-sea flux variability of CO_2 is reasonable in comparison to the other available studies. This author is not aware of any studies for comparison to the model's O_2 flux variability estimate.

4.3.1 Mechanisms of regional flux variability

In this section, the regions dominating the global air-sea flux variability of O_2 and CO_2 are described. Then, the driving mechanisms are illustrated and discussed. The regions for this discussion are the same as used previously: the major ocean basins and the latitude lines of >15°S and >15°N.

A regional breakdown of the annual anomalies in O_2 and CO_2 fluxes (Figure 4-17) illustrates that the global flux variability of both gases is strongly influenced by the equatorial

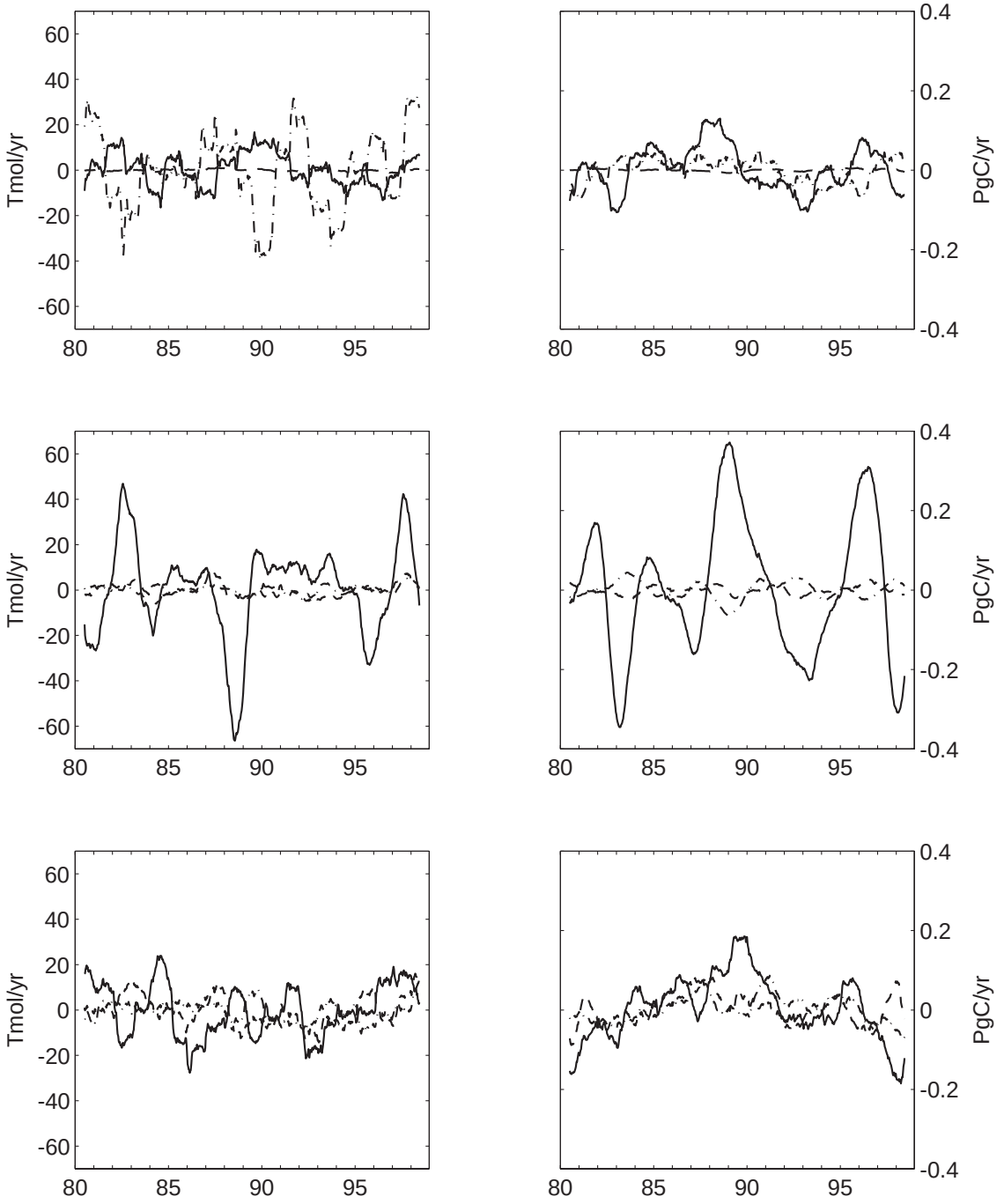

Figure 4-17: Regional breakdown of O_2 (left) and CO_2 (right) fluxes. Regions are separated by the major land masses (Pacific, solid; Atlantic, dash-dot; Indian, dash), and at 15°S and 15°N.

Pacific. For O_2, the North Atlantic is also particularly important to the global flux interannual variability. Despite significant physical variability in the North Atlantic, CO_2 flux variability is not significant in this region because carbonate reactions in seawater damp its air-sea exchange. Other regions of the globe have significant contributions to the global net interannual variability in some years, notable is the Pacific region of the Southern Ocean for both O_2 and CO_2. The dominance of the equatorial Pacific to global integrated CO_2 flux variability agrees with the previous modeling studies of *LeQuéré et al.* [2000] and *Winguth et al.* [1994].

In the following sections, the mechanisms driving the regional flux variability are presented. These are provided in units of mol/m^2/yr, as opposed to the spatially integrated units of Tmol/yr and PgC/yr used for previous flux estimates. Therefore, in Figures 4-18 through 4-26, an area of large fluxes may have only a weak impact on global air-sea fluxes because of its small area. Since the consideration is the balance of the tracers in the top 50m of the ocean, here positive fluxes are into the ocean.

Oxygen

As was found for the North Atlantic in Chapter 2, convective changes drive the air-sea flux variability of O_2 at first order across the global oceans (Figures 4-18 to 4-20). Advective changes are also of significant importance in the equatorial Pacific (Figure 4-19), where they tend to have the same sign as the convective flux. It is the ENSO cycle that drives these significant changes in both vertical advection and mixing in this region (see Section 4.3.2).

In the North Atlantic (Figure 4-20), variability in export production by biology in the subpolar North Atlantic, a region with a very short export timescale (τ), reduces the net air-sea O_2 flux variability by countering the effects of convective variability. When increased convection brings up waters both low in O_2 and high in nutrients, the increased nutrient supply rapidly leads to increased O_2 production. The biological production of O_2 to some degree counters the supply of low O_2 water to the surface by convection. In the period 1985-1987, this positive biological flux successfully counters the negative convective flux and there is almost no net air-sea flux anomaly. Generally, the biology is not able to fully compensate, and air-sea flux anomalies occur in response to convective variability.

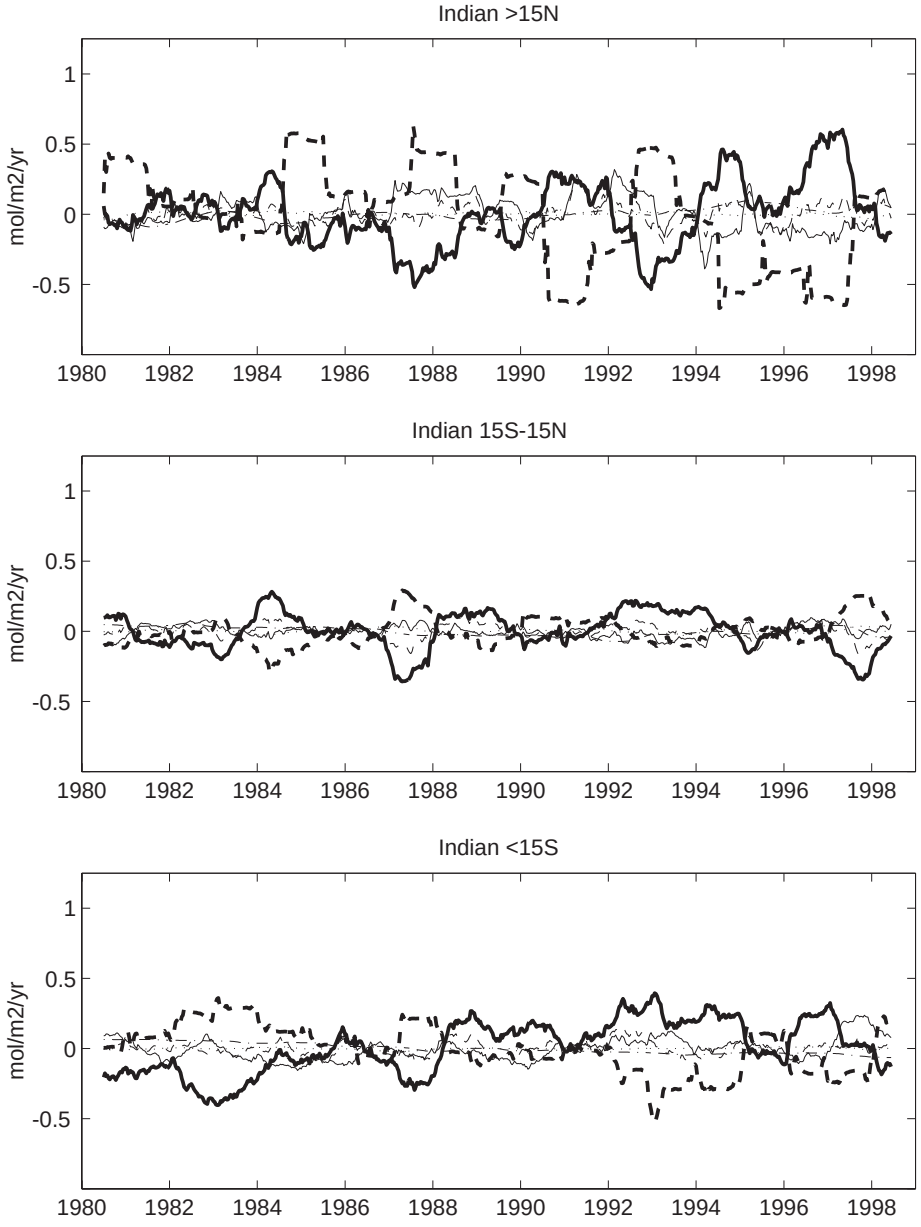

Figure 4-18: Components of the interannual variability around the mean cycle (Figure 4-11) in the O_2 air-sea flux in the Indian Ocean: >15°N (top), 15°S-15 °N (middle), and <15°S (bottom). Components, integrated over 0 to 50m, are advection (solid), convection (bold dash), biology (dash-dot), internal change or dO_2/dt (dash), freshwater (dotted), and undetrended air-sea flux (bold solid). The timeseries have been smoothed to remove timescales shorter than 1 year. Fluxes are positive to the ocean.

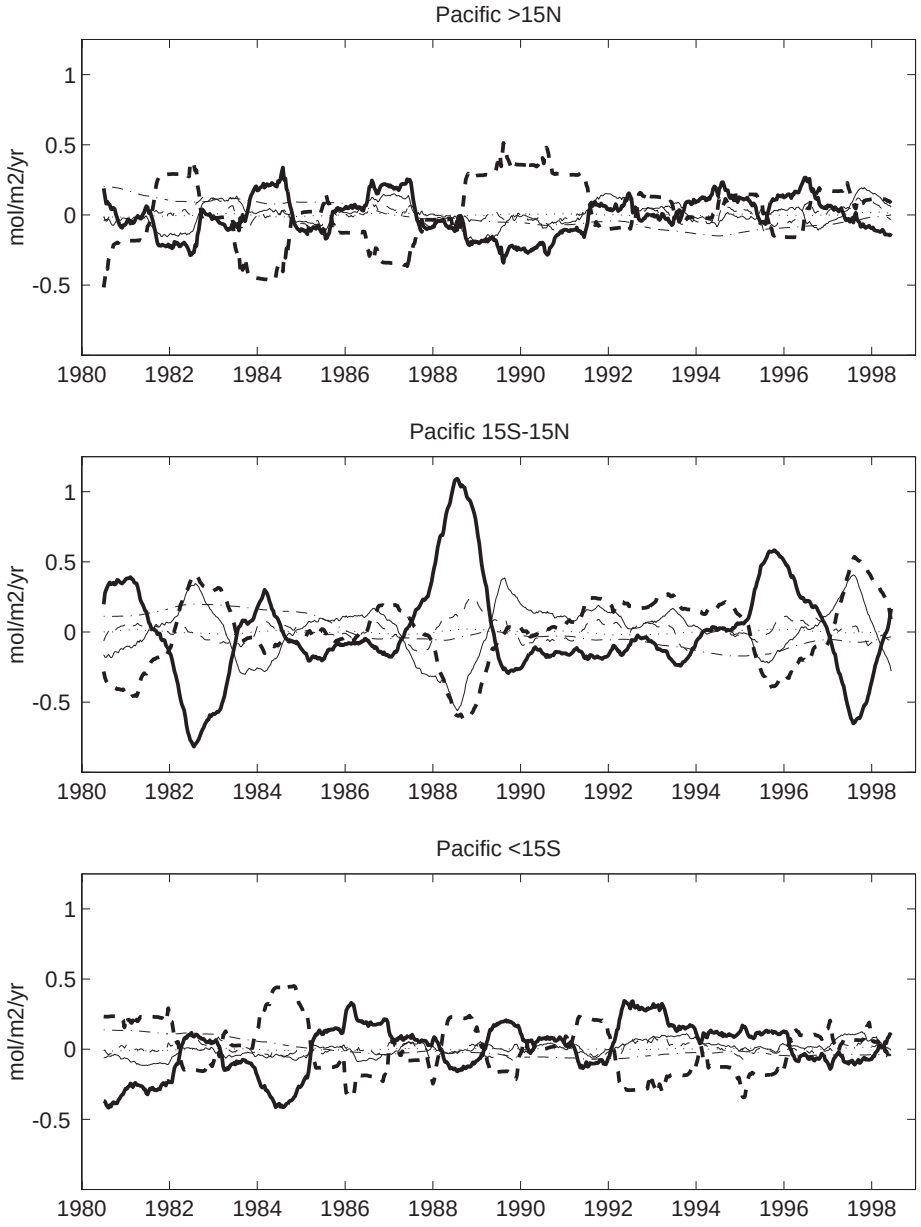

Figure 4-19: Same as Figure 4-18 for O_2 in the Pacific Ocean.

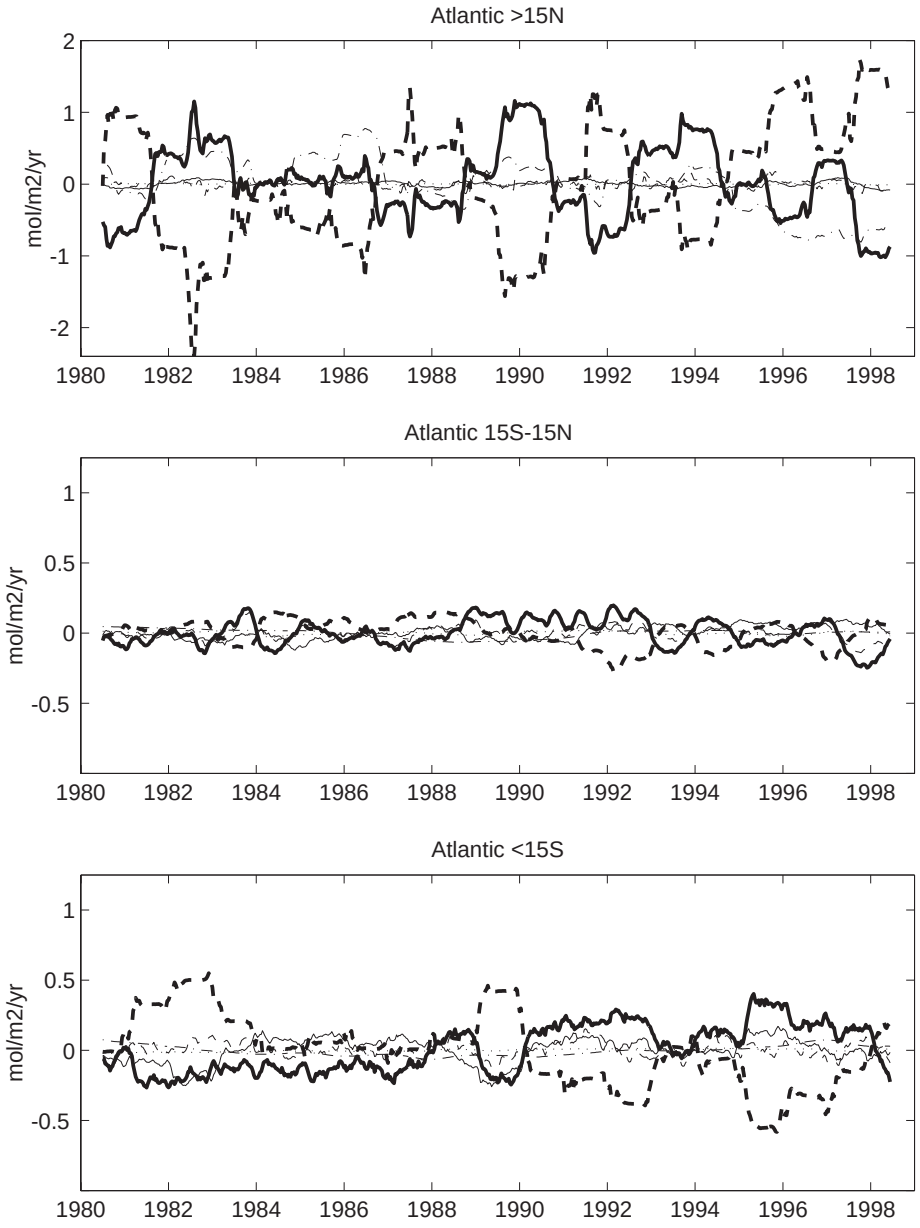

Figure 4-20: Same as Figure 4-18 for O_2 in the Atlantic Ocean. Note that the region >15°N has been plotted on a different scale than the other panels in this series.

Carbon Dioxide

Variability in ocean surface pCO_2 drives CO_2 flux variability. Thus, I begin this section with an evaluation of the regional mechanisms driving pCO_2 variability around the globe. After finding that the surface DIC concentration is a primary driver for pCO_2 variability, I continue by considering the regional mechanisms determining the surface DIC concentration.

In Figure 4-21, it can be seen that in the North and tropical Indian Ocean interannual variability in the ocean pCO_2 is driven by a combination of DIC, temperature and alkalinity. Alkalinity and temperature changes counter DIC changes and together create relatively small pCO_2 change despite large individual variability of DIC, temperature, and alkalinity in these regions.

Figures 4-22 and 4-23 illustrate that DIC drives pCO_2 variability in the North Pacific and North Atlantic regions, although at some points, temperature and / or alkalinity are also of first order importance to determining the surface pCO_2 . In the tropical Pacific, DIC variability determines pCO_2 variability, and temperature counters the effect of DIC with about half the magnitude of impact. Alkalinity variability is of minor importance. These findings in the tropical Pacific are consistent with the work of *LeQuéré et al.* [2000]. In the tropical Atlantic, the effect of temperature variability on pCO_2 has approximately an equal effect as does the variability of DIC. Alkalinity also has a smaller role, but is more important to the overall balance than in the tropical Pacific.

In the Southern Ocean for all three basins (Figures 4-21 to 4-23), the control of pCO_2 is based on a mix of temperature and DIC dominance. In some regions and time periods, temperature dominates, in others DIC dominates. Alkalinity is generally of secondary importance to the determination of pCO_2 variability in the Southern Ocean.

It is noted that the linear relationship of alkalinity to salinity used in this model [*Campbell*, 1983] should damp alkalinity variability. Such damping is likely to be more important to air-sea CO_2 flux variability in the high latitudes where alkalinity variability is relatively more important to determining pCO_2 variations. However, since there is still only a small importance of alkalinity variability to the determination of pCO_2 variability in most regions, the inclusion of prognostic alkalinity would be unlikely to fundamentally change model results for CO_2 flux variability on the global scale.

The control of DIC on the surface ocean pCO_2 in most regions makes the surface balance

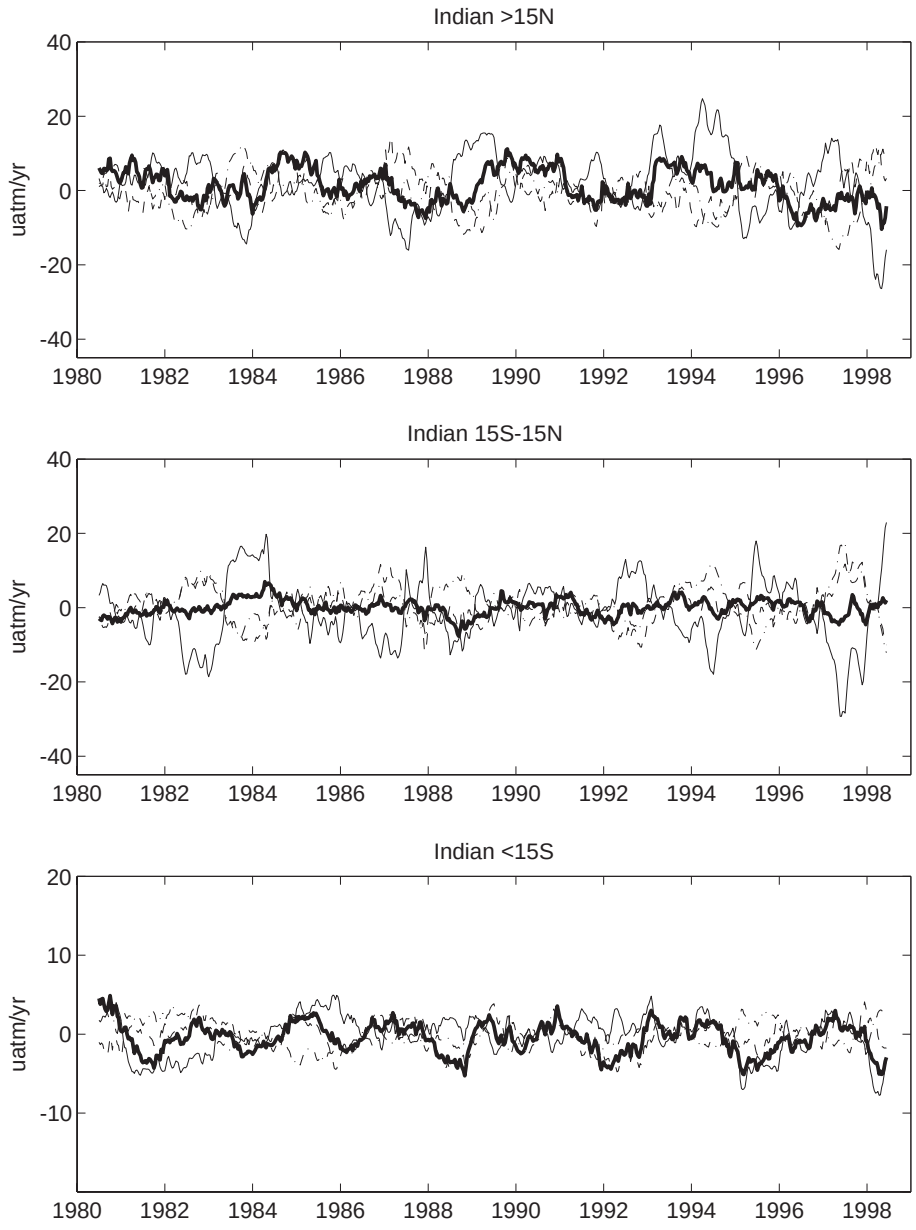

Figure 4-21: Components of the interannual variability around the mean cycle (Figure 4-13) of ocean pCO_2 in the Indian Ocean: >15°N (top), 15°S-15 °N (middle), and <15°S (bottom). Components, integrated over 0 to 50m, are ($\delta pCO_2/\delta DIC$)(dDIC/dt) (solid), ($\delta pCO_2/\delta T$)(dT/dt) (dash), ($\delta pCO_2/\delta ALK$)(dALK/dt) (dash-dot), and $dpCO_2/dt$ (bold solid). The timeseries are smoothed to remove timescales <1 year. Fluxes are positive to the ocean. The regions 15°S-15°N and >15°N are plotted on a different scale than the other panels in this series.

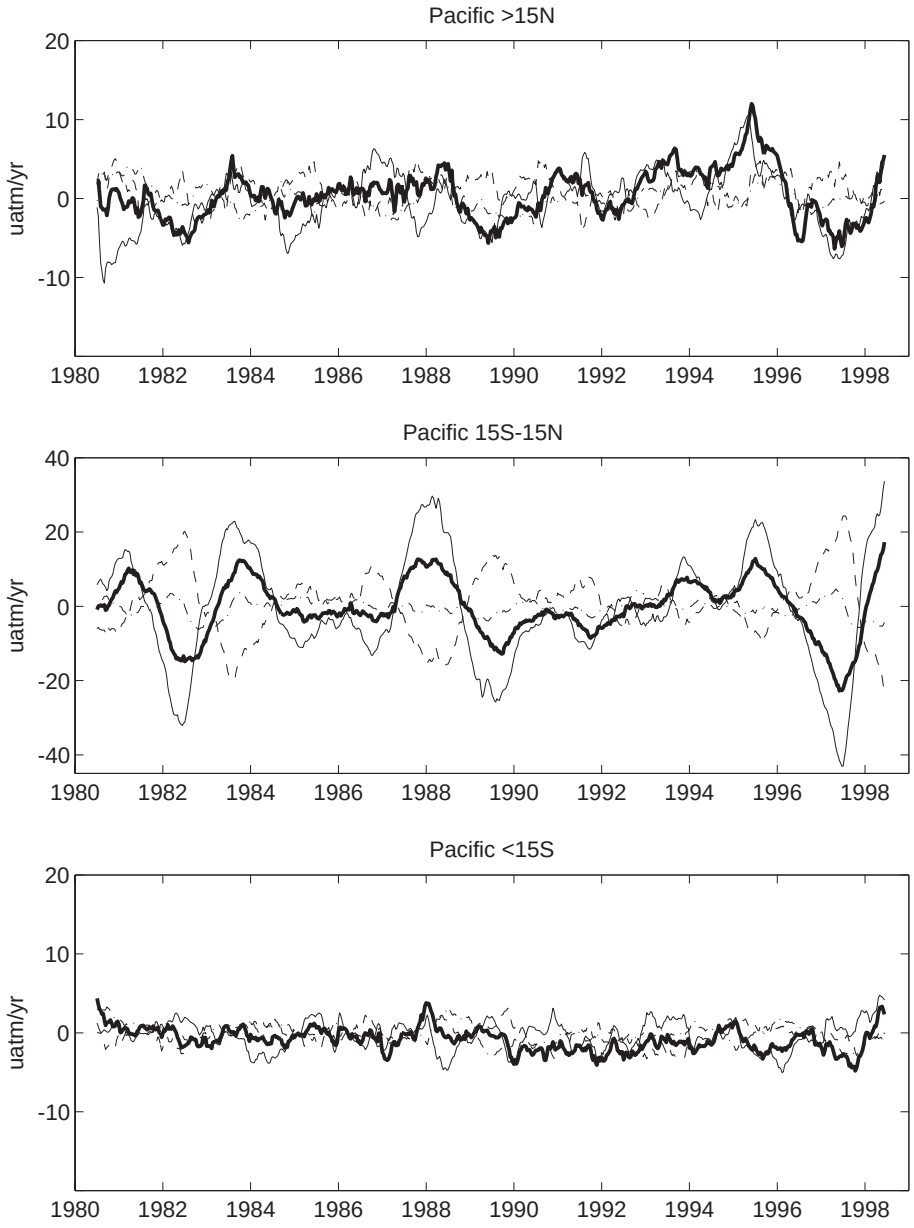

Figure 4-22: Same as Figure 4-21 for pCO_2 in the Pacific Ocean. Note that the region 15°S-15°N has been plotted on a different scale than the other panels in this series.

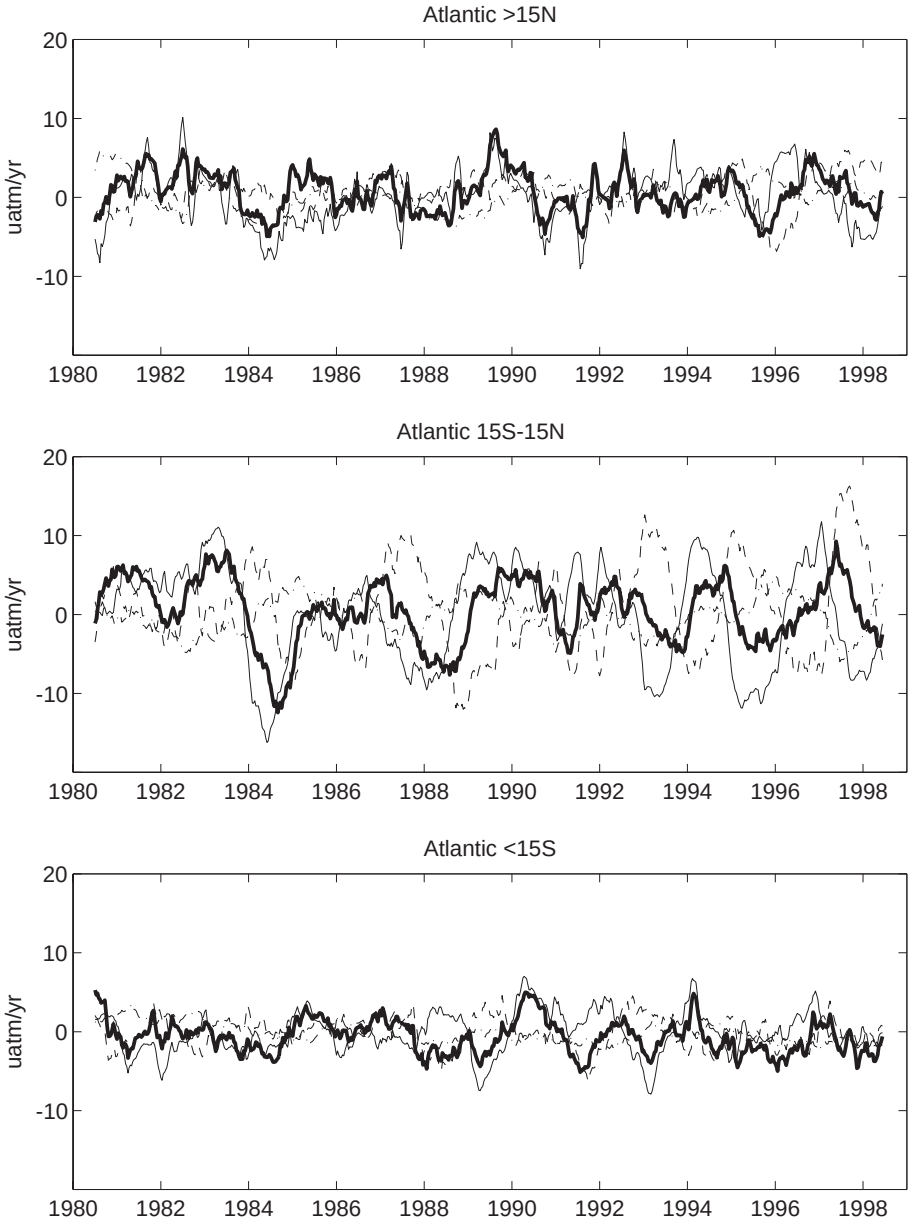

Figure 4-23: Same as Figure 4-21 for pCO_2 in the Atlantic Ocean.

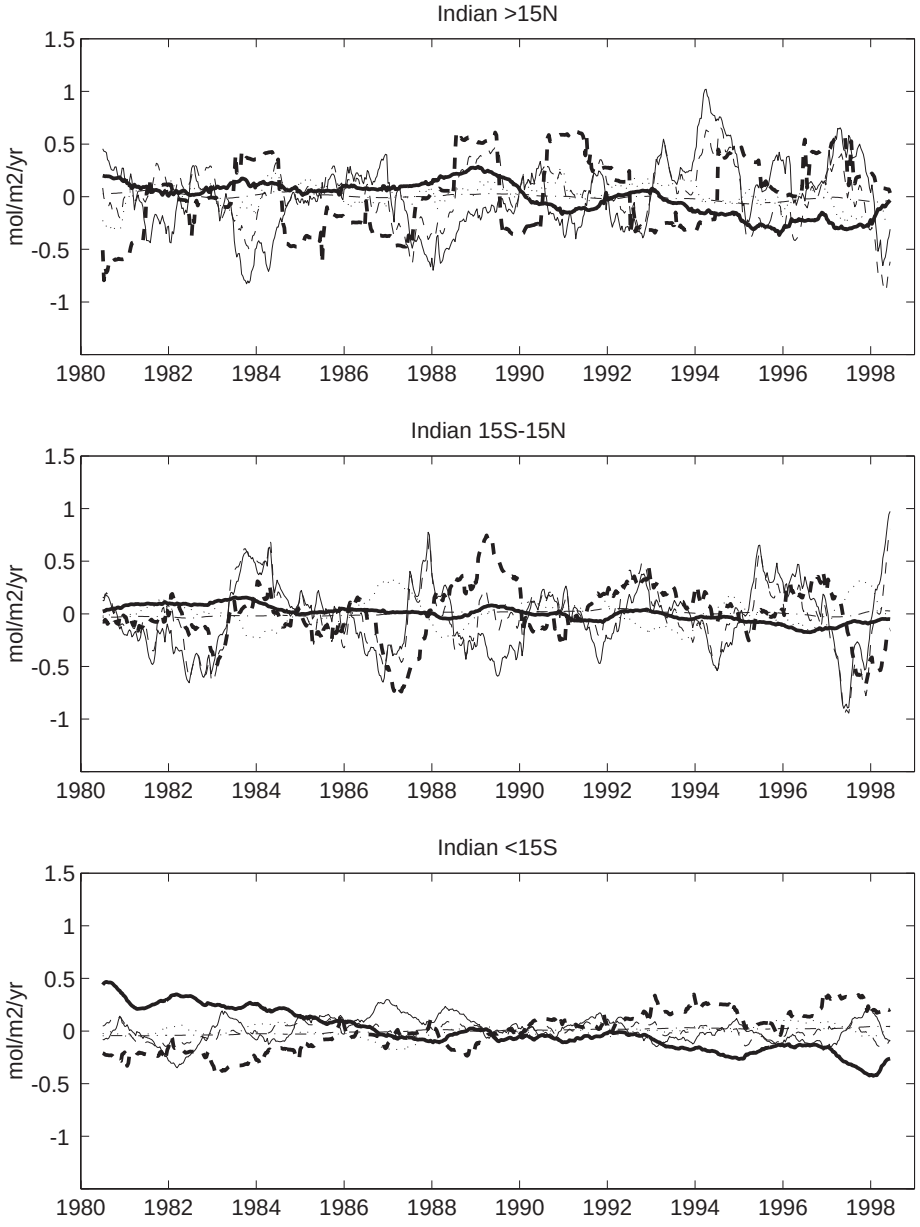

Figure 4-24: Components of the interannual variability around the mean cycle (Figure 4-14) in the surface DIC concentration in the Indian Ocean: >15°N (top), 15°S-15 °N (middle), and <15°S (bottom). Components, integrated over 0 to 50m, are advection (solid), convection (bold dash), biology (dash-dot), internal change or dDIC/dt (dash), freshwater (dotted), and undetrended air-sea flux (bold solid). The timeseries have been smoothed to remove timescales shorter than 1 year. Fluxes are positive to the ocean.

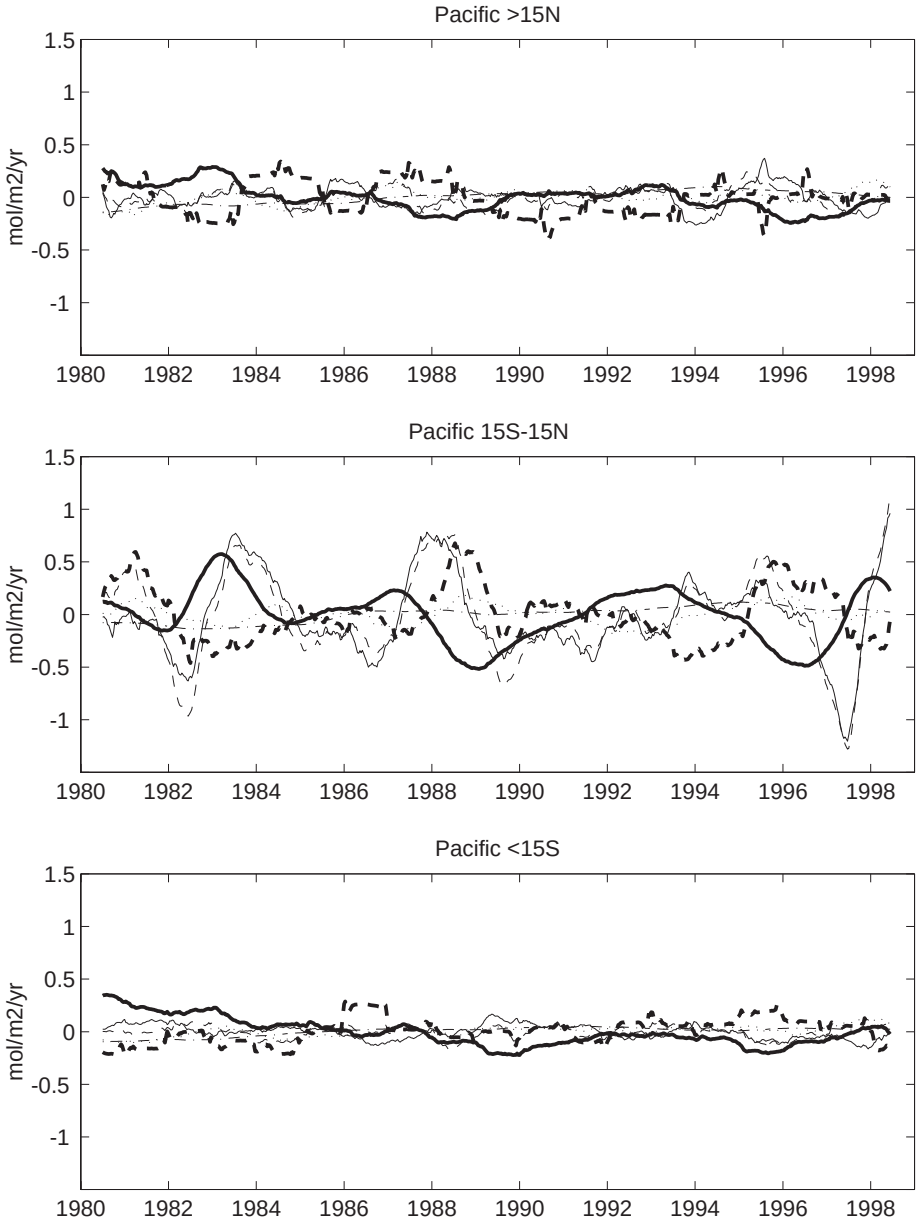

Figure 4-25: Same as Figure 4-24 for DIC in the Pacific Ocean.

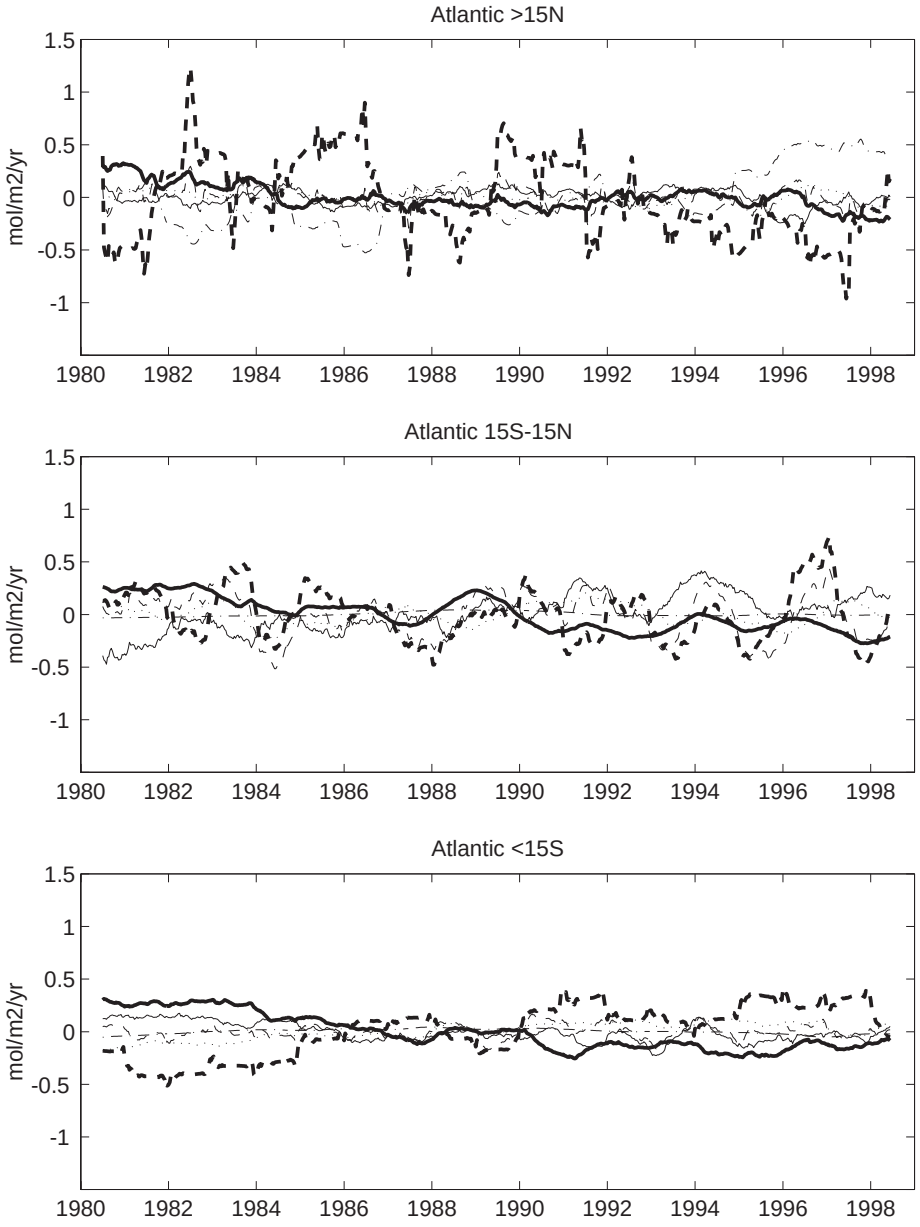

Figure 4-26: Same as Figure 4-24 for DIC in the Atlantic Ocean.

of DIC important to analyze further. Controls on temperature will be considered in relation to the ENSO and NAO cycles in the following section. Figures 4-24 through 4-26 show that DIC is primarily dynamically controlled (convection and advection) in all regions of the global ocean. In the North Indian and Tropical regions, variability in the freshwater flux is of some importance. Figure 4-25 indicates that the air-sea flux is of significant importance to the surface DIC balance in the Equatorial Pacific. Biology is important in the North Atlantic (Figure 4-26) where, as seen with O_2, it counters the convective supply of high DIC waters with the biological export of carbon. However, the slow air-sea exchange timescale for CO_2 allows the biological export more time to address the DIC excess and the impact on the air-sea flux via pCO_2 changes is ultimately small. Though biogenic export counters anomalies of surface O_2 and pCO_2 on the same timescale, the air-sea flux responses of the two gases are different. The rapid O_2 exchange timescale allows a gas flux response to convective anomalies, but the slow CO_2 exchange timescale prevents a significant flux response.

As discussed before, the air-sea CO_2 flux trend is largest in Southern Ocean. As illustrated in Figure 4-25, the trend is driven by changes in the convective supply of DIC which are, in turn, due to model adjustment.

4.3.2 Dominant regions

In this Section, air-sea fluxes in the equatorial Pacific and the North Atlantic are considered in greater detail because these are the regions most important to determining the global air-sea flux variability of O_2 and CO_2 in the model. In particular, flux variability related to the dominant modes of basin-scale variability in physical conditions of these regions, El Nino / Southern Oscillation (ENSO) and North Atlantic Oscillation (NAO), is examined.

The first EOFs of the air-sea fluxes of CO_2 and O_2 in these dominant regions are presented in Figure 4-27. High correlations of the normalized principle components (PC1) with the SOI and NAO indices demonstrate that the ENSO and NAO cycles drive flux interannual variability.

EOF1 for CO_2 in the equatorial Pacific explains 50% of the interannual variance. The corresponding PC1 has maximum correlation with the SOI at ($r = 0.84$) when the flux lags by 1 or 2 months. The maximum correlation occurs with a lag because carbonate chemistry

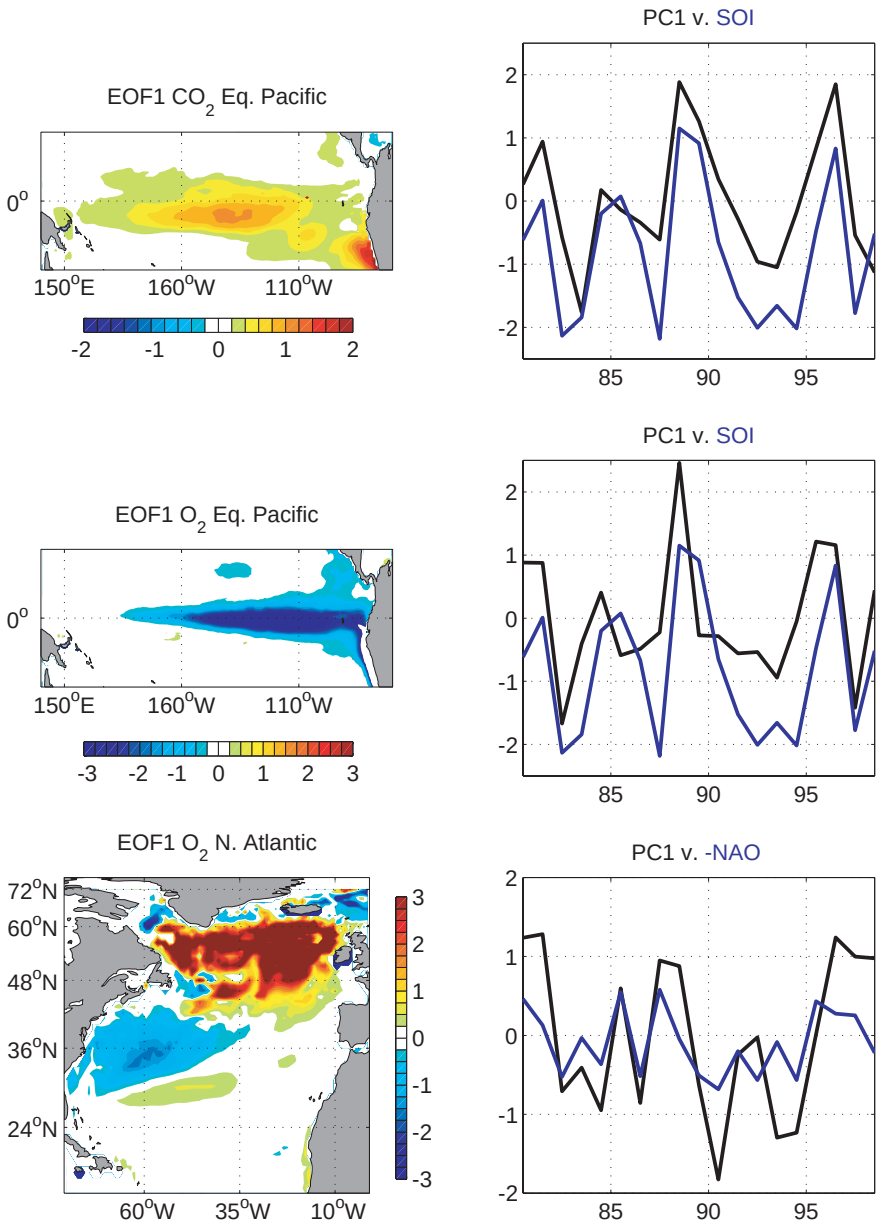

Figure 4-27: First Empirical Orthogonal Functions in mol/m^2/yr (EOF1, left) and the principle component normalized by the standard deviation (PC1) v. climate indices (right) for the regions dominant to the CO_2 and O_2 flux variability: the equatorial Pacific for CO_2 (top) and O_2 (middle), and the North Atlantic for O_2 (bottom). Climate indices are the Southern Oscillation Index (SOI) [*Trenberth*, 1984] and North Atlantic Oscillation (NAO) [*Hurrell*, 1995]. Air-sea fluxes are positive to the atmosphere.

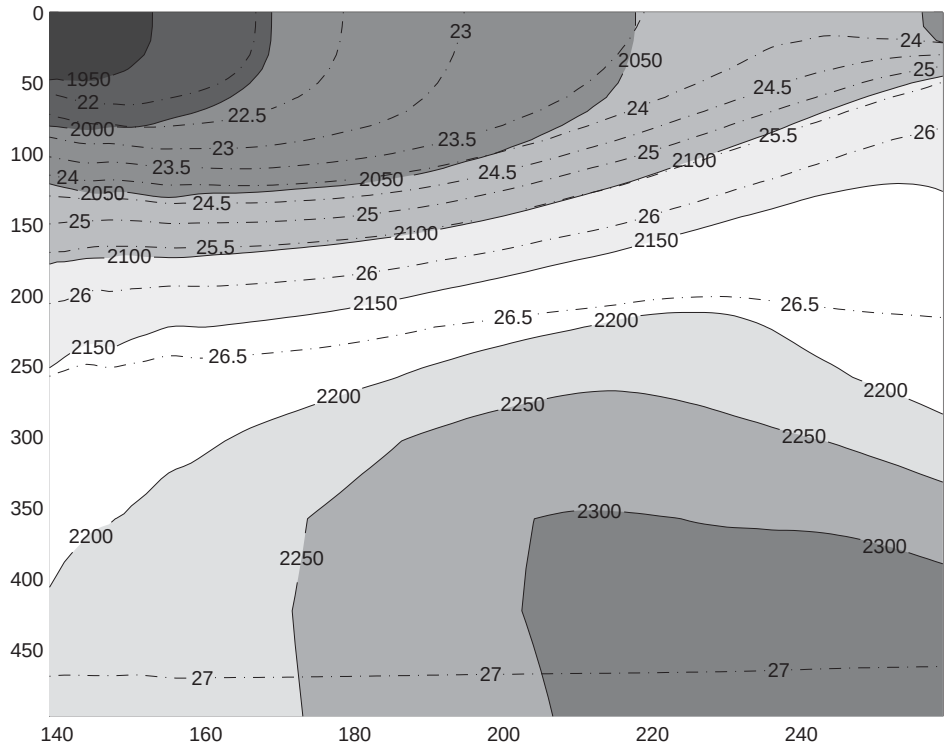

Figure 4-28: Mean DIC (solid contours and shading) with σ_θ (dash-dot contours) along the Equator in the equatorial Pacific.

in seawater slows the CO_2 air-sea exchange response to ENSO forcing. With no lag, the correlation is r = 0.82.

For O_2 in the equatorial Pacific, EOF1 explains 73% of the interannual variance. PC1 has a maximum correlation with the SOI (r = 0.80) when the flux leads by 2 or 3 months. The rapid air-sea exchange timescale for O_2 allows it to respond immediately to changes in the physical state of the equatorial Pacific, even before the atmospheric response is established and becomes evident in the SOI. Even with no lag, the correlation remains high (r = 0.69).

In the North Atlantic, EOF1 explains 28% of the interannual O_2 flux variance. The maximum correlation of the PC1 with the NAO (r = 0.73) occurs when there is no lag between the flux and the index.

Equatorial Pacific

ENSO impacts air-sea fluxes of O_2 and CO_2 primarily by changes in upwelling strength and the depth of low O_2 and high DIC waters below the thermocline (Figure 4-28). Under normal conditions in the equatorial Pacific, the thermocline shallows from west to east and strong upwelling occurs due to Ekman divergence at the equator. [*McPhaden et al.*, 1998] This supplies high DIC and low oxygen waters to the surface, resulting in net influx of O_2 and efflux of CO_2 as seen in Figures 4-5 and 4-7. [*Feely et al.*, 1987, 1995, 1999; *Chavez et al.*, 1999; *Radenac et al.*, 2001]

In the El Niño phase shown in Figure 4-29, the thermocline in the east is depressed by eastward propagating Kelvin waves generated by anomalous westerly wind bursts in the western Pacific. [*Webster and Palmer*, 1997; *McPhaden et al.*, 1998] This downward displacement of the thermocline moves the supply of high DIC (and also low O_2) waters further away from the surface. At the same time, the atmospheric response to El Niño causes slackening of the trade winds and reduced Ekman divergence at the equator. This results in reduced upwelling at the equator which also reduces the supply of high DIC (and low O_2) to the surface.

The combined effects of a depressed thermocline and reduced upwelling are to significantly alter the amount of high DIC (and low O_2) waters exposed to contact with the atmosphere. Air-sea gas fluxes of CO_2 fluxes experience a negative anomaly (less CO_2 outgassed to the atmosphere) and O_2 has a positive anomaly (less O_2 removed from the atmosphere), as seen in Figure 4-27. The response of CO_2 to El Niño has been previously documented based on in-situ observations by *Feely et al.* [1987, 1995]; *Chavez et al.* [1999]; *Feely et al.* [1999].

In the La Niña phase, the upward slope of the thermocline to the east is enhanced, both bringing high DIC and low O_2 waters closer to the surface and increasing the efficiency of divergence-driven upwelling along the equator. This results in a positive CO_2 flux anomaly and a negative O_2 flux anomaly.

As seen in Figure 4-22, the ENSO cycle also impacts temperature in such a way as to oppose DIC changes to pCO_2. Decreased DIC supply during El Niño reduces pCO_2, but the warm SST anomaly increases it. The opposite is true during La Niña when increased DIC supply drives up pCO_2 and the cold SST anomaly reduces it.

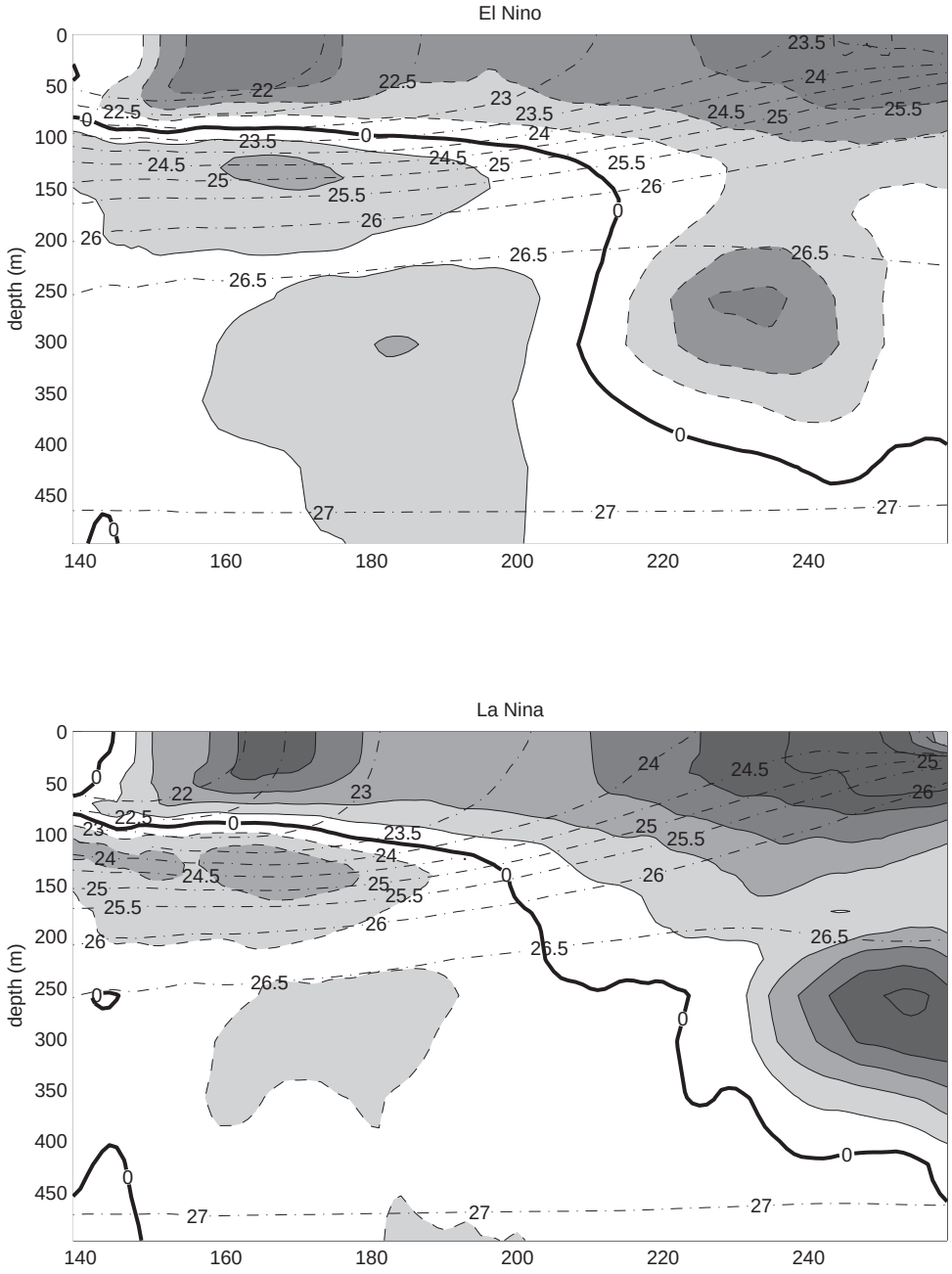

Figure 4-29: DIC anomalies (solid contours and shading) with σ_θ (dash-dot contours) along the Equator in the equatorial Pacific in the El Niño (top) and La Niña (bottom) phases of the ENSO cycle. The El Niño (La Niña) phase plot is a composite of all model months from 1980-1998 when the SST anomaly in the Niño 3.4 region (5°N - 5°S, 120°- 150°W) exceeds 0.4°C (falls below -0.4°C) [*Trenberth*, 1997]. Contours are every 4 μmol/kg, with dashed contours being negative.

Although not evident in this composite figure, it is important to mention that each El Niño and La Niña is different in its strength and in the consequent changes to air-sea gas fluxes [*Feely et al.*, 1999]. The El Niño events of 1982-1983 and 1997-1998 were far stronger than the 1991-1994 series of weak events. Impacts of variability in the strength of El Niño are particularly evident in the O_2 flux anomalies of the tropical Pacific presented in Figure 4-17.

In summary, I note that differences in surface DIC and vertical displacement of isotherms between extremes of the ENSO cycle are apparently small (<50 μmol/kg, ≈50m) and confined to the upper few hundred of the eastern equatorial Pacific (Figure 4-29). Yet, these small changes are responsible for the bulk of global air-sea CO_2 flux variability in the model.

North Atlantic

As shown in Figure 4-20, convection is the dominant forcing for O_2 flux variability in this region. Changes in air-sea heat fluxes and storm tracks with the NAO [*Hurrell*, 1995; *Cayan*, 1992] alter convective mixing in the North Atlantic region. The response in terms of the O_2 flux is essentially an imbalance in the local balance mechanism which proposes an annual balance between biological O_2 production in the summer months and wintertime drawdown of O_2 due to convective supply of low O_2 waters to the surface [*Bender et al.*, 1996; *Keeling et al.*, 1993]. It is clearly seen in Figure 4-20 that convective variability is not completely balanced by the biological flux as postulated by this mechanism, and net interannual variability in the O_2 air-sea flux results. This same result was found using the North Atlantic regional model described in Chapter 2.

For CO_2 in the North Atlantic, it can be seen in Figure 4-23 that temperature and DIC changes generally oppose each other in the creation of surface pCO_2 anomalies. This is consistent with NAO forcing where enhanced cooling in the high phase of the NAO drives more mixing and supplies more DIC to the surface ocean, increasing pCO_2. At the same time, the cooling decreases pCO_2. This counterbalancing of pCO_2 tendencies, along with the slow air-sea exchange timescale of CO_2 that allows the biological response to counter convective DIC fluxes (Figure 4-20), combine to cause the low air-sea flux variability of CO_2 in the North Atlantic.

4.3.3 Summary

Using an offline biogeochemical ocean model, I find that physical variability primarily determines variability in surface concentrations of O_2 and DIC, and is therefore the primary driver for interannual variability of global CO_2 and O_2 air-sea fluxes. Variability in surface pCO_2 is also significantly influenced by temperature variations in some regions of the globe.

Physical variability in the equatorial Pacific associated with ENSO is the primary driver of global air-sea flux variability of O_2 and CO_2. Alterations to the slope of the thermocline across the equatorial Pacific and changes to the efficiency of upwelling significantly alter the supply of DIC and O_2 to the surface over a large ocean area. These changes drive the substantial flux variability.

In the North Atlantic, changes to biogenic export counter flux tendencies created by convective variability associated with the NAO. The rapid air-sea exchange timescale of O_2 allows for a 3-way balance between convection, export, and air-sea exchange, and the result is significant O_2 flux variability. However, the slowing of CO_2 air-sea exchange by carbonate reactions means that the balance for CO_2 is essentially between convection and export, resulting in little CO_2 air-sea flux variability from this region.

For the period 1980-1998, the global air-sea flux variability of O_2 is found to have interannual extremes of -70 to +100 Tmol/yr (RMS = 35 Tmol/yr), and the CO_2 flux has extremes of $\pm$ 0.5 PgC/yr (RMS = 0.28 PgC/yr). The magnitude of the CO_2 flux variability is consistent with other recent estimates from both ocean models and atmospheric data inversions.

Chapter 5

Air-Sea Flux Variability from the Model Constrained with Altimetry

In this chapter, an additional modeling experiment is described. Here, the physical output from a experimental version of the MITgcm constrained with TOPEX/Poseidon satellite altimetry was used to force the biogeochemical model and estimate air-sea fluxes of O_2 and CO_2 for 1997-1998.

It has been shown in the previous section that physical variability is the primary forcing for O_2 and CO_2 air-sea flux interannual variability in the model. The objective of this effort is to understand whether the physical state of the constrained model is significantly altered, and if so, how this impacts gas fluxes.

For the purpose of the following discussion, the model used to estimate air-sea fluxes of O_2 and CO_2 for 1980-1998 in the previous sections will be referred to as 'unconstrained' to distinguish it from the 'constrained' run for 1997-1998.

5.1 Model Description

The MITgcm model version used in this experiment is the same as described previously except that it has been constrained with satellite altimetry over the period 1993-1998. To accomplish this data assimilation, three steps are used: (1) an approximate Kalman filter model run; (2) a smoothing procedure; and (3) a forward run with forced with the wind field resulting from the smoothing.

First, as the model is run, the Kalman filter is used to periodically adjust barotropic velocity, which acts to displace horizontal isolines adiabatically in order to bring the model SSH toward agreement with the satellite data. Below the mixed layer, this adjustment is essentially equivalent to changing the surface wind stress. [*Fukumori*, 2000; *Fukumori et al.*, 1999] Next, a smoothing is applied in order to make physical changes from the Kalman filter adjustments consistent with model physics. Finally, the model is run in forward mode, forced by the wind stress field resulting from the previous two steps. (D. Menemenlis, personal communication)

In this section, a model run using physical results from the forward model forced with Kalman-filter derived winds is described. Model results for 1997-1998 are used to force the biogeochemical model. This run was initialized at the end of 1996 from a test run that used the unsmoothed Kalman filter model results.

5.2 Change to the Physical Model Variability

It has been shown that the Equatorial Pacific is the primary driver for the global net variability of air-sea fluxes of both O_2 and CO_2 . Therefore, physical changes in this region should be most important to changes in air-sea gas flux variability.

In Figure 5-1, it can be seen that the alteration of the wind field via the assimilation procedure does significantly improve the model's representation of the observed SSH variability. The high SSH associated with the strong El Niño of 1997-1998 is significantly stronger in the constrained model than in the unconstrained. The low of the 1998 La Niña is also more realistically captured due to the constraint.

However, Figure 5-2 illustrates that the differences between the physical state at depth of the unconstrained and constrained model are actually quite small in the Equatorial Pacific. The unconstrained model already does a good job of capturing the changes to the depth of the 20°C isotherm (D20) as the Equatorial Pacific shifts from an El Niño to La Niña regime. The constrained model only improves this representation to a small degree at some points, and to the same degree worsens the comparison at other times.

In Figure 5-3, timeseries mixed layer depths at four locations across the globe are shown. The SSH constraint makes little difference to the model physical state at these locations.

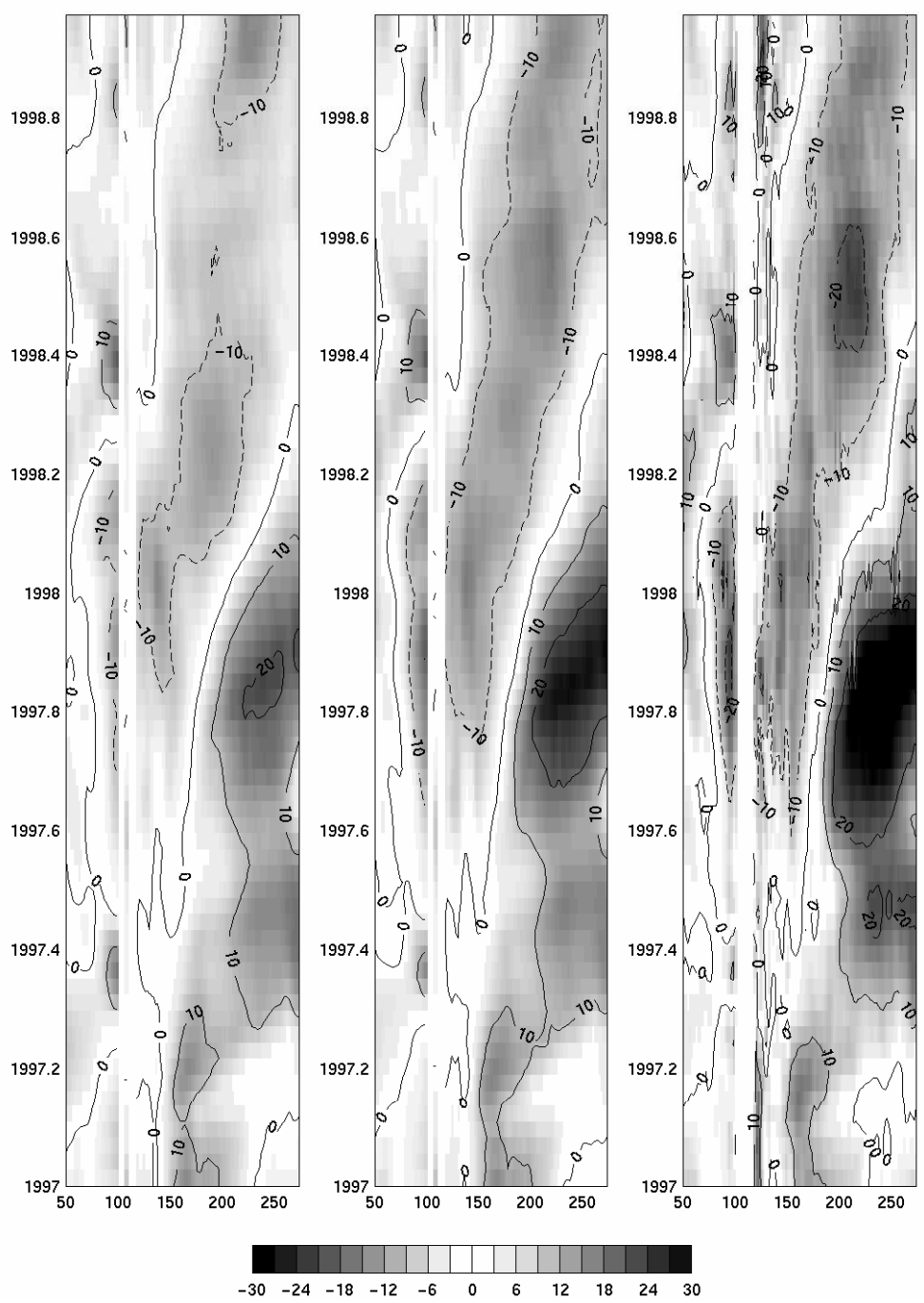

Figure 5-1: Time-longitude diagram for 1997-1998 of the SSH anomaly at the equator between 50°E and 260°E in the unconstrained model (left), the constrained model (middle), and TOPEX/Poseidon satellite altimetry (right). Dashed contours indicate a negative anomaly.

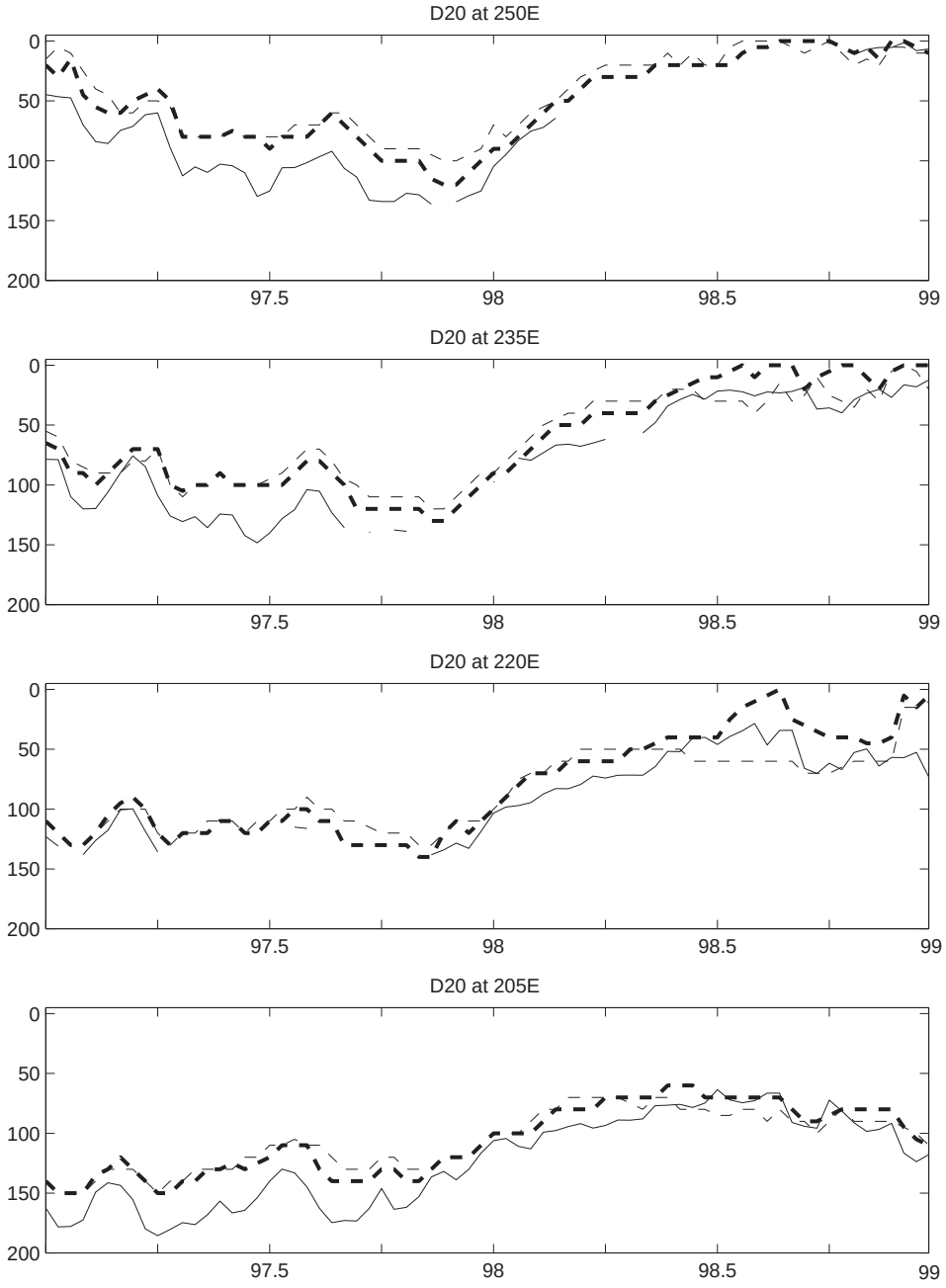

Figure 5-2: The depth of the 20°C isotherm (D20) for 1997-1998 in the unconstrained model (dash), constrained model (bold dash), and TAO moorings (solid) [*McPhaden et al.*, 1998] at the equator and 250°E, 235°E, 220°E, and 205°E.

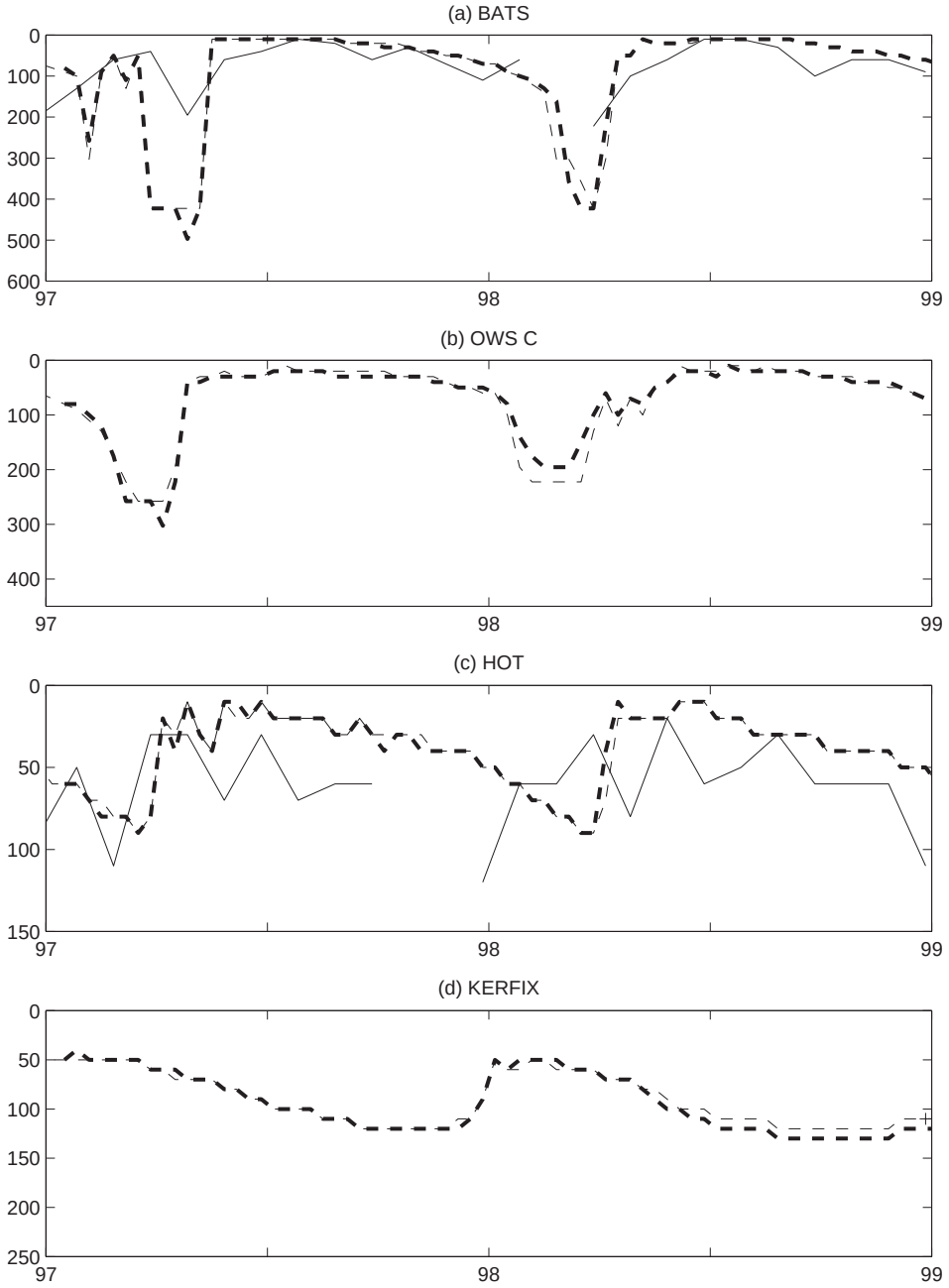

Figure 5-3: Mixed layer depths for 1997-1998 in the unconstrained model (dash), constrained model (bold dash), and at timeseries stations (solid): (a) BATS, (b) OWS C, (c) HOT, and (d) KERFIX.

Mixed layer depth comparisons for the entire length of the unconstrained model run are presented and discussed in Section 3.1.1.

In addition, analysis of the global SSH variance in the unsmoothed Kalman filter result for 1993-1998 indicates that the constrained model captures only 40% of the variance observed by TOPEX/Poseidon. It was shown in Section 3.1.1 that the unconstrained model already captures approximately 35% of the observed SSH variance. Thus, despite the significant improvement seen in Figure 5-1, the global change in total SSH variance is actually relatively small between the unconstrained and constrained model.

5.3 Comparison of Interannual Variability in Air-Sea Fluxes

Figure 5-4 illustrates that the change to air-sea flux variability is quite small. This is not unexpected given the lack of significant physical change in the model interior.

The regional breakdown of the O_2 and CO_2 fluxes shown in Figure 5-5 indicates that there are no significant changes to the location of the fluxes due to the SSH constraint. Both O_2 and CO_2 fluxes are slightly different in magnitude in the Equatorial Pacific, likely due to slight changes in the model behavior as it switches from the El Niño to the La Niña state in this time period. The constrained model illustrates some shifts of mixing regions in the Southern Ocean that alters the magnitude of anomalies in the Indian and Pacific sectors, but these changes are cancellatory for both O_2 and CO_2. Overall, changes are very small, particularly in comparison to the magnitude of the anomalies over the 1980-1998 period from the unconstrained run (Figures 4-16 and 4-17).

5.4 Summary

No significant change to interannual variability in air-sea fluxes of O_2 and CO_2 is found due to the constraint of the physical model with TOPEX/Poseidon satellite altimetry.

However, these results should be considered preliminary for several reasons. First, the method of constraining the physical model with the satellite data is still under development. In addition, the basic physical model continues to be improved in its capacity to represent of the ocean's mean state. It is believed that these changes will allow the SSH constraint to more effectively impact the model's interior. (D. Menemenlis, personal communication)

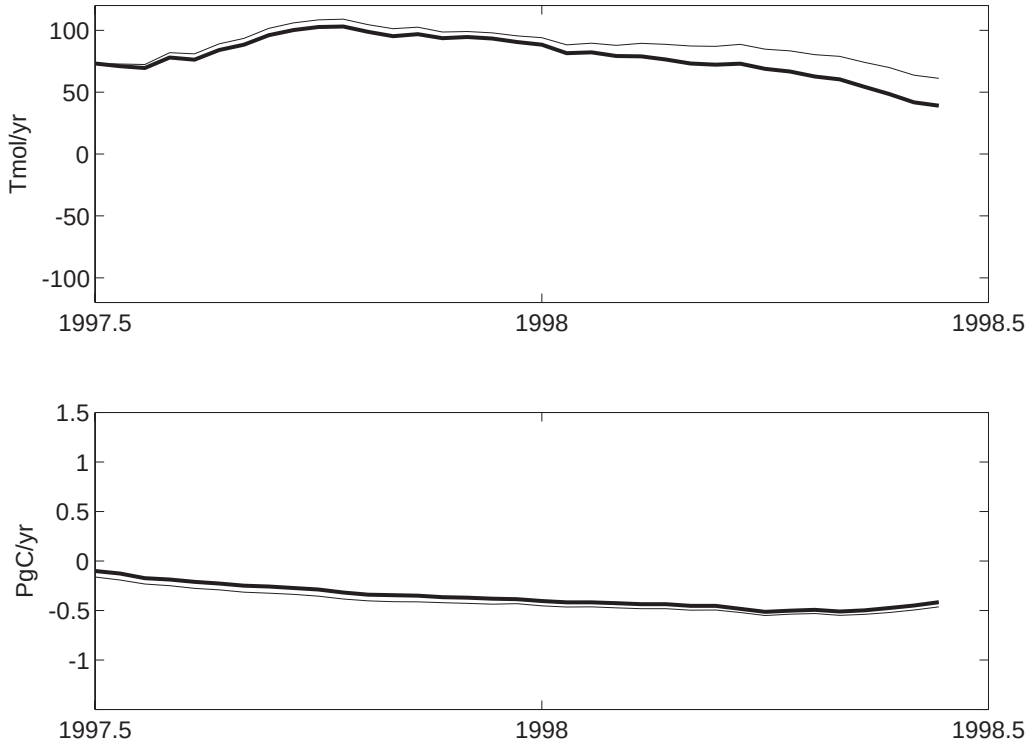

Figure 5-4: Global average fluxes from the 1997-1998 constrained model run (bold solid) compared to the unconstrained model (solid): O_2 flux (top) and CO_2 flux (bottom). The mean seasonal cycle and the trend from the unconstrained model (1980-1998) have been removed from the timeseries, and smoothing to remove timescales shorter than one year has been performed.

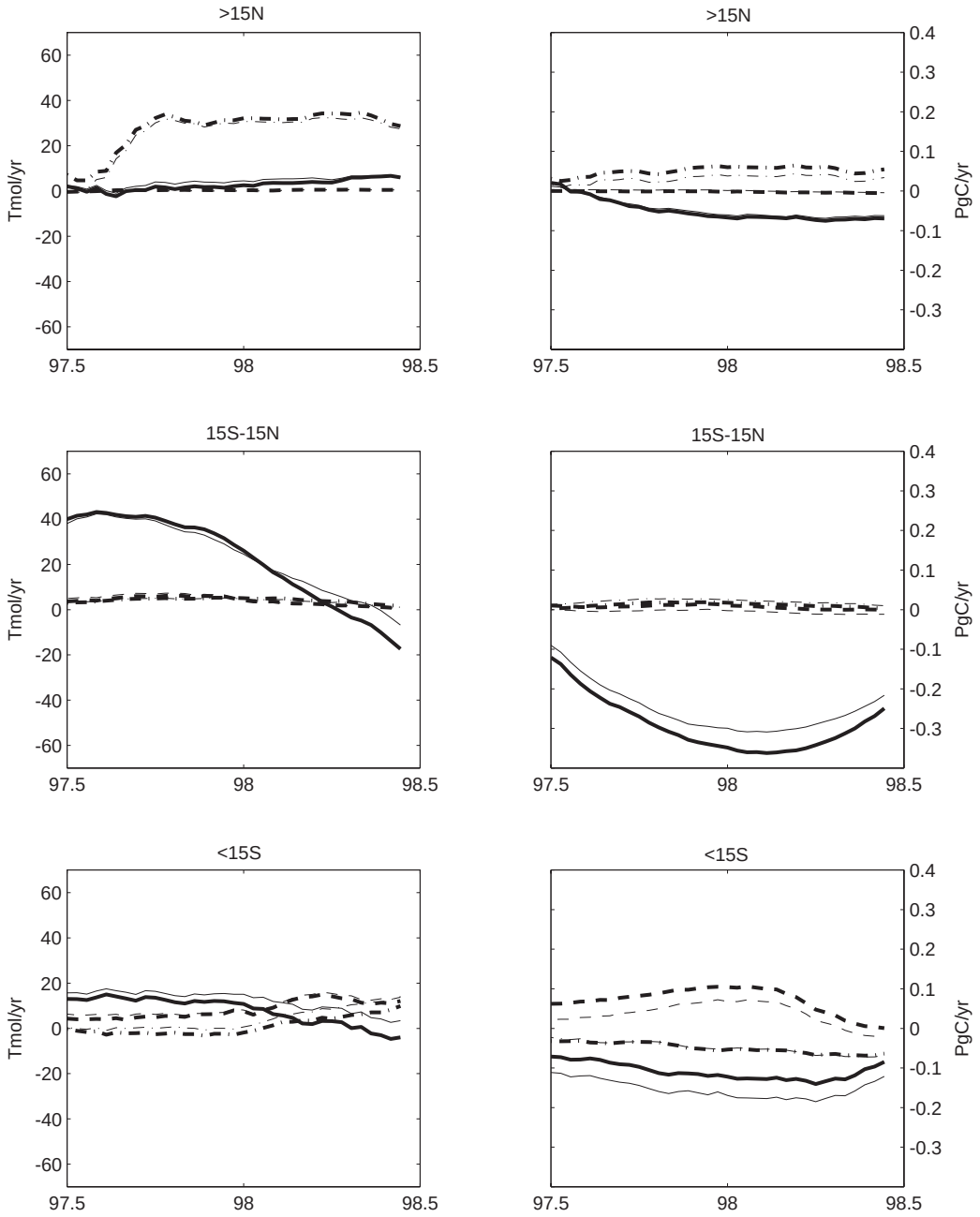

Figure 5-5: Regional breakdown of O_2 (left) and CO_2 (right) fluxes in the Pacific (solid), Atlantic (dash-dot), and Indian (dash). The constrained model is shown in bold and the unconstrained model is not bolded.

In addition, the run presented here is too short to draw any profound conclusions. More effort is clearly needed to explore the potential for improving this type of biogeochemical ocean models with data assimilation.

Chapter 6

Interannual Variability of Land and Ocean Sinks of Carbon Dioxide

When determining the global sinks of CO_2 , the global budget for atmospheric CO_2 can be estimated by:

$$\Delta CO_2 = F - O - B \tag{6.1}$$

The observed global change in the atmospheric CO_2 concentration (ΔCO_2) is measured at sites across the globe. The global source of CO_2 due from the burning of fossil fuels (F) is known from industry data [*Marland et al.*, 2001]. O is the ocean sink of CO_2, and B is the sink of CO_2 into the terrestrial biosphere. Evidently, one of these two sinks needs to be known in order to solve Equation 6.1 for the other sink.

In Figure 6-1, the solution of Equation 6.1 for the land CO_2 sink is shown graphically. Here, the ocean sink is taken from the offline biogeochemical model for 1980-1998. In the atmospheric O_2/N_2 method, the observed atmospheric change in O_2 is used to estimate the land CO_2 sink, and then Equation 6.1 is used to find the ocean sink. Despite valiant efforts to quantify global CO_2 sinks using these and other methods, the combination of sparse data and many simplifying assumptions has resulted in a wide range of CO_2 sink estimates with large error bars. Estimates for the mean land sink range from from 0.4 $\pm$ 1.1 PgC/yr for 1977-1985 [*Battle et al.*, 1996] to 3.3 $\pm$ 1.6 PgC/yr [*Bender et al.*, 1996] for 1991 to 1994; and for the mean ocean sink from <1.0 PgC/yr [*Tans et al.*, 1990] for 1981 to 1987 to 2.3

± 0.7 PgC/yr [*Langenfelds et al.*, 1999] for April 1978 - January 1997.

In the coming sections, estimates of O_2 and CO_2 air-sea flux variability generated from the MITgcm are used with Equation 6.1 to provide new estimates of the land and ocean CO_2 sinks. Using the atmospheric O_2/N_2 method, estimates of the mean and interannual variability of CO_2 sinks are made that, for the first time, include an estimate of the interannual variability in air-sea O_2 fluxes. These sink estimates are compared to the model estimates of ocean CO_2 flux variability and the inferred land sink variability. All estimates are compared to the recent atmospheric data inversion of *Francey et al.* [2001].

6.1 Impact of Variability in the Air-Sea Flux of O_2 on O_2/N_2 Sink Estimates

The sinks of CO_2 in the ocean and land biosphere can be estimated based on atmospheric observations of O_2/N_2 and CO_2 by taking advantage of the differing characteristics of O_2 and CO_2 exchange with the ocean [*Keeling et al.*, 1996; *Bender et al.*, 1996; *Battle et al.*, 2000; *Manning*, 2001]. In this method, it is assumed that over the time period of data averaging, there is no net flux of O_2 into or out of the global ocean. The solubility of CO_2 in seawater allows a net CO_2 exchange with the ocean. Fossil fuel burning is assumed to increase atmospheric CO_2 and decrease atmospheric O_2 in a fixed ratio. Similarly, terrestrial photosynthesis is assumed to use atmospheric CO_2 and generate atmospheric O_2 in a fixed ratio. Equation 6.1 is used for the global budget for atmospheric CO_2. Following *Keeling et al.* [1996], *Bender et al.* [1996], *Battle et al.* [2000] and *Manning* [2001], the global budget for atmospheric O_2 can be estimated by:

$$\Delta O_2 = \alpha_F F - \alpha_B B \tag{6.2}$$

Here, ΔO_2 is the observed global change in the atmospheric O_2 concentration, F is the global source of CO_2 due to the burning of fossil fuels, O is the sink of CO_2 in the ocean, and B is the sink of CO_2 into the terrestrial biosphere. The factors α_F and α_B are the O_2:C molar ratios describing O_2 utilization with fossil fuel burning and O_2 production with terrestrial photosynthesis, respectively. Based on previous works, *Manning* [2001] estimates α_F = -1.39±0.04 and α_B = -1.1±0.05. ΔO_2 is measured as O_2/N_2 in the atmosphere, and

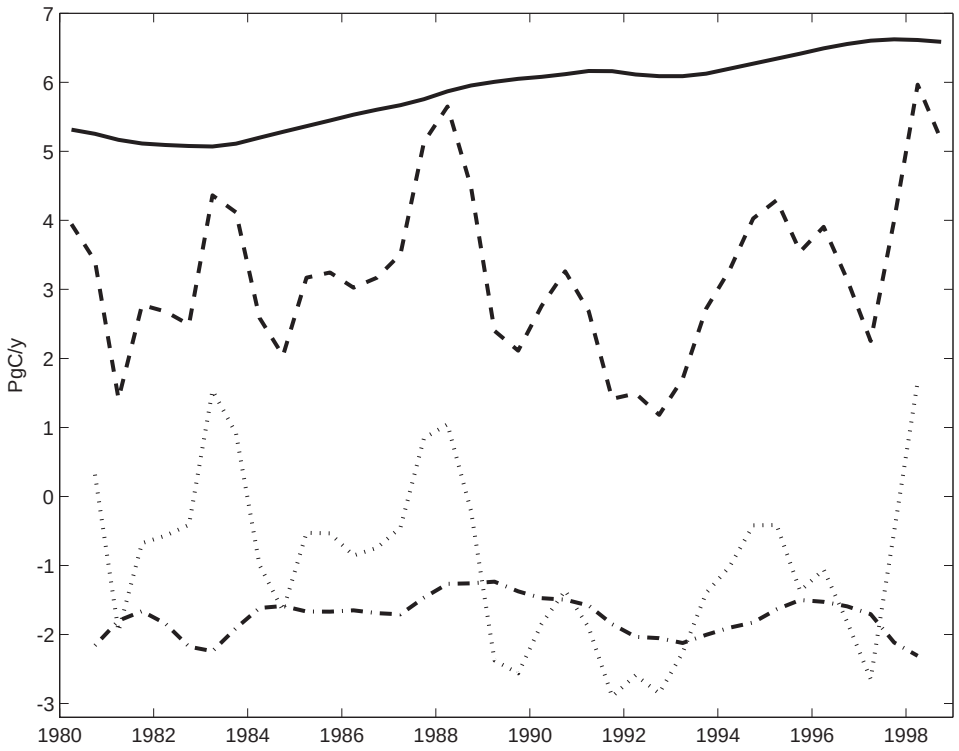

Figure 6-1: Estimating interannual variability in land and ocean CO_2 sinks using Equation 6.1: Fossil fuel emissions (F, solid), observed atmospheric CO_2 trend (ΔCO_2, dash), ocean sink (O, dash-dot), and land sink (B, dot). The observed atmospheric CO_2 change presented is SIO flask data from Barrow, Mauna Loa and South Pole [*Keeling and Whorf*, 2001] for 1980-1999, and Cape Grim data from *Conway et al.* [1994a] for 1985-1992 and from the NOAA/CMDL network for July 1991 to 1999 (Andrew Manning, personal communication). Fossil fuel data is from *Marland et al.* [2001]. The ocean sink is taken from the model.

translated to an atmospheric O_2 concentration by the factor (0.027 per meg O_2/N_2)/(1 Tmol O_2).

It is stressed that in Equation 6.2, there is no term for the ocean interaction with O_2. This is because it is assumed that over the time period these equations are applied, there is no net air-sea O_2 flux. Yet, it has been shown in Chapter 4 that there is a quantifiable interannual variability of O_2 fluxes across the global ocean. These fluxes are due primarily to the ENSO and NAO phenomena. To account for this variability in the estimates of CO_2 sinks, Equation 6.2 can be rewritten as:

$$\Delta O_2 = \alpha_F F - \alpha_B B - O_2{}' \tag{6.3}$$

Where $O_2{}'$ is the model-estimated interannual variability of the air-sea flux of O_2 shown in the top panel of Figure 4-16. The interannual variability in the air-sea flux of N_2 is assumed negligibly small [*Keeling et al.*, 1998; *Garcia and Keeling*, 2001].

In Figure 6-2, the land and ocean sinks calculated with and without interannual variability in the air-sea flux of O_2 are shown. For this calculation, fossil fuel data (F) is from *Marland et al.* [2001], and CO_2 and O_2/N_2 atmospheric data are from NOAA/CMDL data at Alert, La Jolla, and Cape Grim (Andrew Manning, personal communication). All data and model O_2 flux estimates are averaged over 12 months, centered on April 1 and October 1 of each year.

The impact of CO_2 data sparsity on the error of these results is estimated by comparing the global CO_2 trend estimates using different combinations of stations from the NOAA/CMDL network for the period 1984-1990 [*Conway et al.*, 1994a]. In each combination of data sources, equal numbers of stations from the Northern and Southern Hemispheres are used. Between 10 stations (5 each hemisphere) and 2 stations (1 each hemisphere) are used in various combinations. It is found that the estimates of the interannual variability in the global CO_2 trend differ by 0.2 to 0.3 ppm/yr, which translates into an error of approximately 0.5 PgC/yr. This error estimate, combined with the error estimates for α_F (± 0.04), α_B(± 0.05), and fossil fuel burning (± 0.38) found in Table 2.5 of *Manning* [2001], allow the calculation of the error bars shown as the bold solid vertical lines in Figure 6-2 (Land = $\pm$ 0.63 PgC/yr ; Ocean = $\pm$ 0.81 PgC/yr).

While there are only minor differences between the two estimates of land and ocean

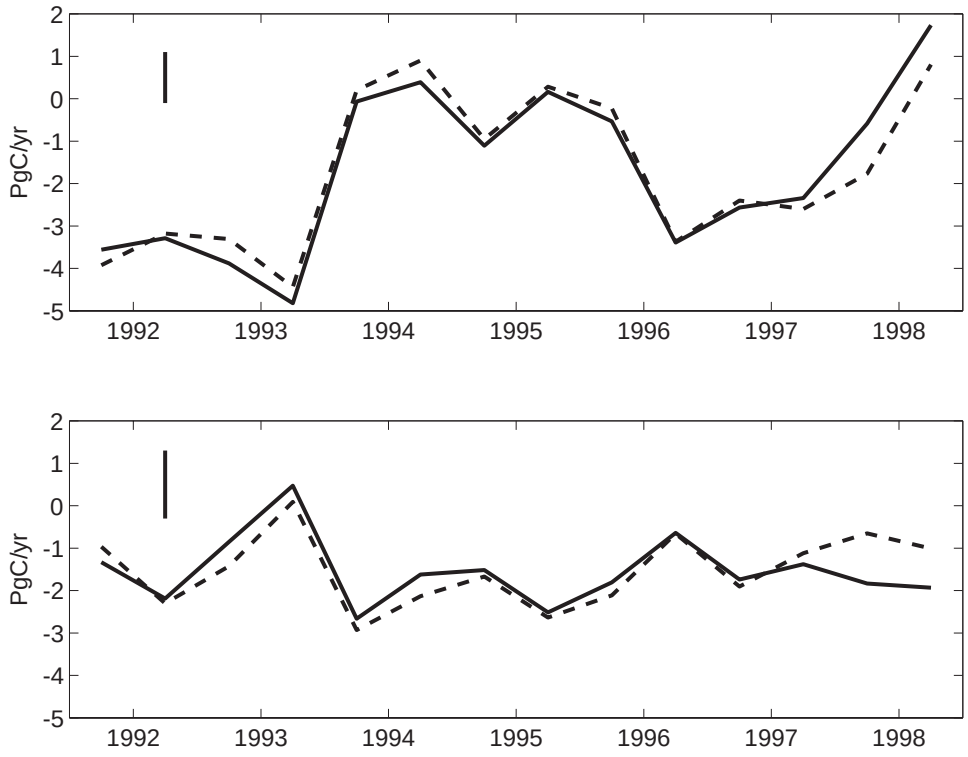

Figure 6-2: Land (top) and ocean (bottom) sinks of CO_2 for October 1991 to April 1998. Shown are sinks estimated by the O_2/N_2 method based on Equations 6.1 and 6.2 (bold dashed), and the O_2/N_2 method with model-estimated interannual variability in the air-sea O_2 flux (bold solid) (i.e. Equations 6.1 and 6.3). The error bar for the O_2/N_2 method does not include error for the neglect of air-sea O_2 flux variability (bold solid vertical line).

Table 6.1: Mean CO_2 sinks calculated with and without O_2'

Mean CO_2 Sink Estimates for October 1991 to April 1998 (PgC/yr)		
-	Land Sink	Ocean Sink
without O_2'	1.71 ± 0.63	1.53 ± 0.81
with O_2'	1.70 ± 0.63	1.54 ± 0.81

sinks shown in Figure 6-2 over most of October 1991 to April 1998, there is a significant difference during 1997-1998 when both the equatorial Pacific was in a period of a strong El Niño, reducing O_2 influx into the ocean, and the low phase of the NAO reduced convection, also reducing the influx of O_2 into the global ocean. Together, these phenomena created a large positive (to the atmosphere) O_2 flux anomaly. When the air-sea O_2 flux variability was assumed negligible, this source of O_2 to the atmosphere was attributed to the land biosphere, and a proportional land sink of CO_2 was inferred. With the inclusion of the model O_2 flux variability, this O_2 flux is accounted for as a net ocean O_2 efflux, and this results in an estimate for the land CO_2 sink that is approximately 1 PgC/yr smaller and an ocean sink estimate that is larger by the same amount. Thus, for estimates of the interannual variability in CO_2 sinks using the atmospheric O_2/N_2 method, the interannual variability in air-sea flux of O_2 should not be neglected. The error in these estimates should be largest during periods when the NAO and ENSO cycles create O_2 flux anomalies of the same sign. The RMS error in the interannual sink estimate is 0.38 PgC/yrdue to O_2 air-sea flux variability.

In Table 6.1, it is shown that when the calculations illustrated in the Figure 6-2 are performed using mean values for October 1991 to April 1998 for all variables, there is little difference in the sink magnitude estimates. This indicates that while there is significant error in estimates of the interannual variability in CO_2 sinks using the O_2/N_2 method and not accounting for air-sea O_2 flux variability, the O_2/N_2 method does not appear have a significant error due to O_2 flux variability when it is used to estimate the mean sinks over from October 1991 to April 1998.

Admittedly, I have removed the long-term change in the O_2 flux as part of the air-sea flux trend because it was not possible to separate from model drift (see Section 4.2.3). This prevents this work from estimating the impact of such trends on CO_2 sink estimates. *Plattner et al.* [2001] and *Keeling and Garcia* [2002] indicate that O_2 outgassing induced by ocean warming may significantly change estimates of mean CO_2 sinks in the 1990's.

6.2 Sink Estimates Using CO_2 Data and Model Results

An alternative method for the calculation of variability of the land sink of CO_2 is to use Equation 6.1 with the model CO_2 sink variability as the estimate for O (Figure 6-3). Despite error in this mean estimate due to the temporal trend in the model estimate of the 19-year mean CO_2 sink, it is retained because of its close comparison to the data estimate of *Takahashi et al.* [1999]. The same atmospheric data for CO_2 (ΔCO_2) and fossil fuel burning (F) data are used as in the previous calculation.

The study of *Francey et al.* [2001] shown in Figure 6-3 is an update of the work of *Rayner et al.* [1999] that uses atmospheric observations of $\delta^{13}C$ and CO_2, with O_2/N_2 as a long-term constraint, to estimate the land and ocean CO_2 sinks (see Section 4.3). The error of the *Francey et al.* [2001] result is estimated to be ± 1 PgC/yr (Roger Francey, personal communication).

The comparison of several sink estimates in Figure 6-3 illustrates a general agreement in that the land sink has a larger variability than does the ocean sink. The O_2/N_2 estimates estimate a significantly larger variability in the ocean CO_2 sink than do the direct ocean model estimate or the atmospheric inversion of *Francey et al.* [2001]. However, the large error bars, particularly for the ocean sink, means that these estimates are essentially indistinguishable. Additionally, considering that the model underrepresents physical variability and therefore likely provides lower bound estimates of O_2 flux variability, the additional error in the O_2/N_2 method due to O_2 flux variability may actually be larger than estimated here. Some of the land sink variability clearly lies outside the error bars, and there is evidence of coherent multi-year trends in the land sink variability that are captured by all the estimates.

In Figure 6-4, the CO_2 sinks estimate for the entire model period is shown. As indicated

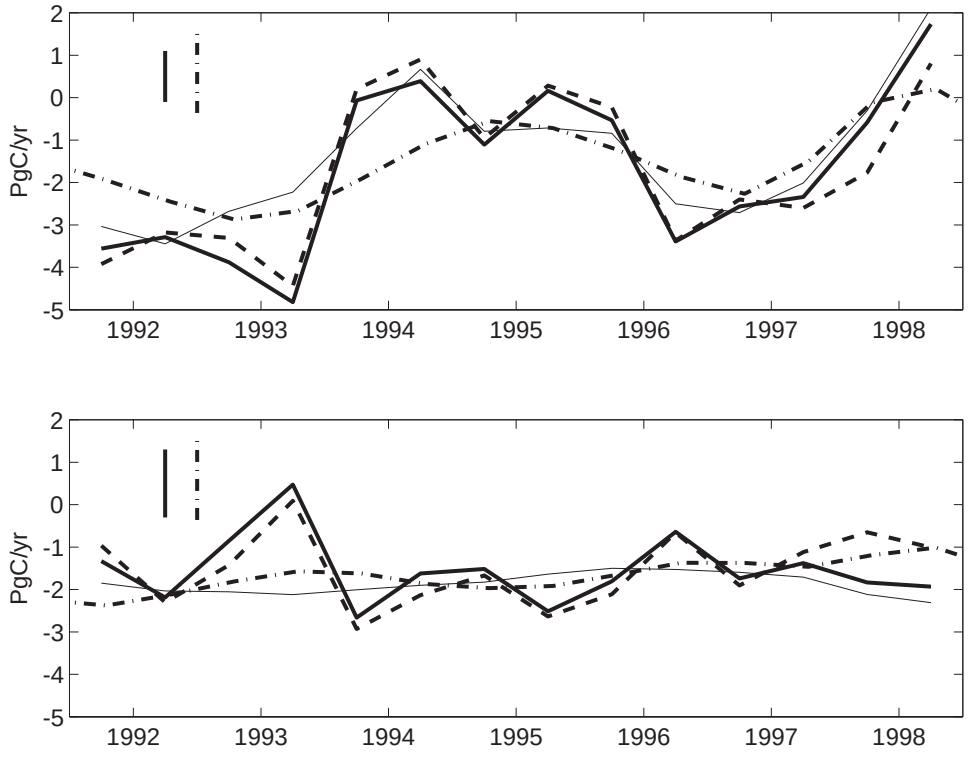

Figure 6-3: Land (top) and ocean (bottom) sinks of CO_2 for 1992-1998. As in Figure 6-2, shown are sinks estimated by the O_2/N_2 method without (bold dashed), and with model-estimated O_2 flux interannual variability (bold solid). In addition, this model's CO_2 ocean sink variability estimate and the land sink inferred from Equation 6.1 (solid), and the result of *Francey et al.* [2001] (bold dash-dot) are shown.

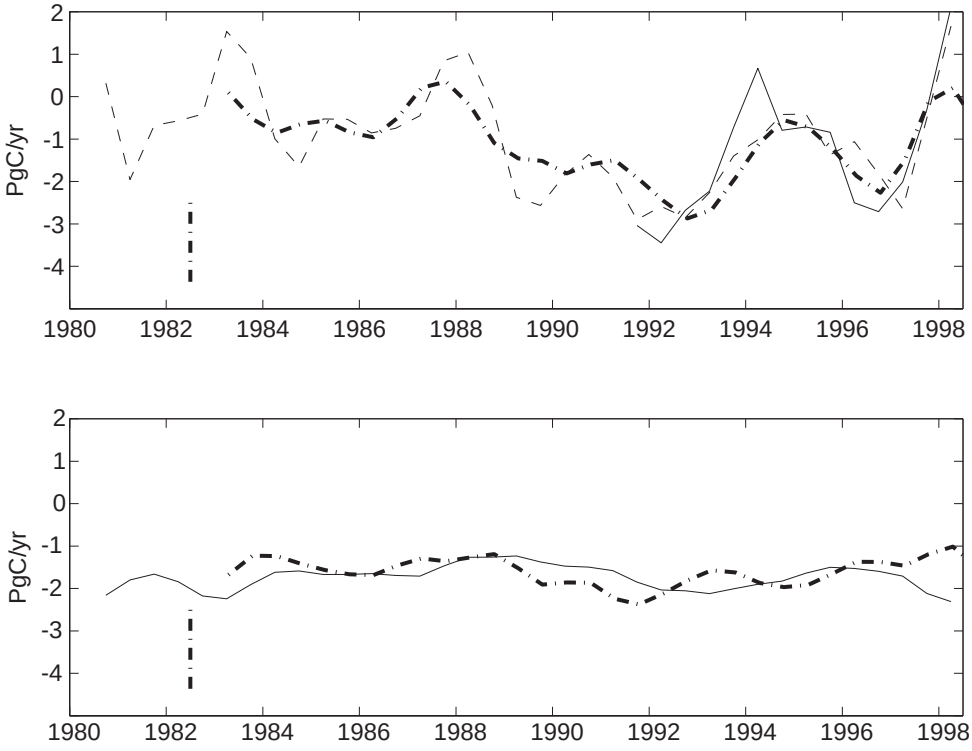

Figure 6-4: Land (top) and ocean (bottom) sinks of CO_2 for 1980-1998. This model's CO_2 ocean sink variability estimate (solid). The land sink is inferred from Equation 6.1 with the observed CO_2 trend from Alert, La Jolla, and Cape Grim in the 1990's (solid); and from the data source quoted in Figure 6-1 (dash). The result of *Francey et al.* [2001] (bold dash-dot) for both the land and ocean sinks is also shown.

in the caption, different data source for the atmospheric CO_2 trend was used since Alert, La Jolla and Cape Grim CO_2 data is not available for the entire 1980-1998 time period. For 1980-1998, the model indicates a mean CO_2 ocean sink of 1.79 PgC/yr with interannual extremes of ± 0.5 PgC/yr . The land sink is estimated to be 0.95 PgC/yr with interannual extremes of ± 1.9 PgC/yr.

Here, it is important to note the impact of the different CO_2 data sources in the land sink estimates for the 1990's. The only difference between the solid and dashed line in the land sink estimate in Figure 6-4 is the atmospheric CO_2 data used. The error is larger at some points than the ± 0.5 error estimated when considering data sparsity only in the NOAA/CMDL network, indicating potentially significant calibration differences between the different networks (Roger Francey, personal communication). Caution is clearly needed when using atmospheric CO_2 data and when comparing sink estimates based on different subsets of atmospheric data sources.

Figure 6-4 illustrates that the model-derived land sink estimate compares well to the atmospheric inversion study of *Francey et al.* [2001] over the period July 1982 to April 1998. Model error bars are difficult to estimate, but are likely to be at least as large as the ± 1 PgC/yr estimated by *Francey et al.* [2001] when combined with error in the atmospheric CO_2. Given these large error bars, the estimates for both the land and ocean sinks are indistinguishable.

6.3 Summary

A convergence of estimates of the magnitude of the land and ocean sink variability between the most recent atmospheric inversions and ocean model estimates is found. Both ocean model and atmosphere inversion studies find that the land sink variability is approximately ± 2 PgC/yr, and ocean sink variability is less than ± 1 PgC/yr. The temporal structure of the ocean sink variability differs significantly between methods, and error bars remain large, indicating that much work remains to be done to more precisely estimate the variability of these sinks.

Given the likelihood that the MITgcm underestimates O_2 flux variability, it is possible that CO_2 sink estimates using the atmospheric O_2/N_2 method under the assumption of

negligible air-sea O_2 flux variability have a larger error than estimated here. These results indicate that this error is likely to be more significant on shorter timescales, and to be reduced when atmospheric O_2/N_2 is used as a long-term constraint on sink estimates.

Chapter 7

Conclusions

Using a modestly high-resolution ocean general circulation model, I investigate mechanisms driving interannual variability in air-sea fluxes of CO_2 and O_2. This work indicates that convective and advective processes are the primary drivers of air-sea flux variability for both O_2 and CO_2.

In the global model, variability in the global air-sea O_2 flux is primarily forced by temporal changes in ocean circulation and mixing associated with the ENSO cycle in the equatorial Pacific. Changes to the east-west slope of the thermocline and to wind-driven upwelling alter the supply of low O_2 waters from the thermocline to a large area of the surface equatorial Pacific. El Niño reduces this supply and promotes a large reduction in the net O_2 ingassing in this region; La Niña has the opposite effect.

In addition, both the regional and global modeling studies presented here suggest that there is significant air-sea O_2 flux variability in the North Atlantic sector. Variability is forced primarily by convective anomalies, typically associated with the NAO, that alter the supply of low O_2 waters from the deep ocean to the surface. These variations are counterbalanced to some degree by changes in biogenic export which respond to nutrient variability driven by the same convective forcing. Nevertheless, the rapid O_2 air-sea exchange timescale allows a net air-sea flux anomaly to occur before anomalies in biogenic export can remove the entire O_2 flux anomaly.

Model results suggest that the interannual variability in the air-sea flux of O_2 has extremes of -70 to +100 Tmol/yr in the period 1980-1998. This variability implies a significant error of up to $\pm$ 1 PgC/yr (RMS = 0.38 PgC/yr) in estimates of the interannual variability

of land and ocean CO_2 sinks using atmospheric O_2/N_2 under the assumption of negligible air-sea O_2 flux variability. The error is greatest in periods when extremes of the ENSO and NAO cycles create O_2 flux anomalies of the same sign, as occurred in 1997-1998. However, when estimates of mean CO_2 sinks between October 1991 and April 1998 are made using atmospheric O_2/N_2, the explicit inclusion of this model estimate of air-sea O_2 flux variability has a negligible impact on results.

Variability in modeled global CO_2 air-sea fluxes is forced primarily by changes in surface DIC due to variations in thermocline depth and upwelling associated with the ENSO cycle in the equatorial Pacific. Temperature variability also due to ENSO damps CO_2 flux variability. Despite significant physical variability in the North Atlantic associated with the NAO, CO_2 flux variability is minimal in this region. Damping of CO_2 air-sea exchange by carbonate chemistry allows biogenic export to remove convectively-generated DIC anomalies before significant air-sea flux anomalies occur.

The model estimates interannual extremes in the CO_2 sink to be ± 0.5 PgC/yr over the period 1980-1998. Combining this estimate with observations of atmospheric CO_2 and fossil fuel emissions data allows the estimate of interannual extremes in the sinks into the terrestrial biota of $\pm$ 1.9 PgC/yr for the same period. The magnitude and pattern of the land sinks compare well to the recent atmosphere inversion estimate of *Francey et al.* [2001].

This work was undertaken in part because previous ocean general circulation models were apparently unable to capture extratropical variability in the air-sea CO_2 flux because of coarse resolution or strong physical restoring below the mixed layer in the middle and high latitudes [*Winguth et al.*, 1994; *LeQuéré et al.*, 2000]. Yet, I find, as do the previous modeling studies, that the equatorial Pacific is the region dominant in the variability of the air-sea CO_2 flux. Improvement to model physical variability in the high latitudes with this model does not substantially change the global air-sea CO_2 flux variability from that of *LeQuéré et al.* [2000], and, overall, there is only slightly more variability in the global flux estimate from this model. However, both this model and almost certainly the model of *LeQuéré et al.* [2000] substantially underestimate the physical variability of the real ocean, and thus both may still underestimate air-sea flux gas variability. On the other hand, it may be that additional large scale variability and the ocean's small scale variability are not first order controls on the air-sea flux variability of CO_2.

In parallel with this work, *Francey et al.* [2001] have been refining their method for the inversion of atmospheric CO_2, $\delta^{13}C$ and O_2/N_2 for CO_2 sinks. Through their independent work, they find a much smaller ocean sink variability than their previous estimate [*Rayner et al.*, 1999]. Together with this work, there is the indication that ocean models and atmospheric data studies are converging toward agreement upon a relatively small variability of the ocean CO_2 sink of $\pm$ 0.5 to 1 PgC/yr, and a larger land sink variability of approximately $\pm$ 2 PgC/yr. This convergence indicates that neither method is likely to be missing processes essential to the CO_2 sink variability in the real ocean. Yet, despite agreeing on the amplitude of the sink variability the two estimates are quite different in their temporal structure (Figure 6-4). There are many improvements to be made to both ocean biogeochemical models and the atmospheric inversion techniques.

7.1 Key Model Issues

There is a significant underestimation of variability at the large scale in the physical model used in this study. It is shown in Section 3.1 that the model captures only 35% of the variance of sea surface height as measured by the TOPEX/Poseidon satellite altimeter and averaged to 2°x2°. This estimate does not account for the upper ocean physical variability that occurs due to mesoscale eddies which the model does not explicitly resolve, although the 0.3°x1° resolution in the tropics is eddy-permitting. Thus, the high frequency variability of the physical model is little like the real ocean. It is unclear how much this underrepresentation, either at the large or small scale, impacts air-sea gas flux estimates. Yet, the convergence of the model estimated air-sea CO_2 flux variability with the atmospheric inversion estimate of *Francey et al.* [2001] provides some confidence in the capacity of the model to capture the key mechanisms driving air-sea flux interannual variability. These model results indicate that the gas flux variability responds primarily to the large-scale physical phenomena such as ENSO, and it is these features that the model does capture reasonably well.

In the high latitudes of the North Atlantic, deep mixing in the model is too great, which may lead to an overestimate of the net CO_2 and O_2 fluxes. In addition, mean export is overrepresented in the North Atlantic which may contributes to overestimates of mean gas

fluxes. The fact that the model estimates of the mean fluxes in this region agree with independent data-based estimates is encouraging, but given the large areas over which both model and data estimates are made, there is potential for the compensation of errors.

The export parameterization of this model is highly idealized. Comparisons of the mean seasonal cycle of the O_2 anomaly and ΔpCO_2 indicate that seasonal nutrient cycles are underrepresented by the model across most of the ocean. An explicit ecosystem model should improve nutrient cycling, and may lead to better estimates of air-sea gas flux interannual variability. However, the fact that *LeQuéré et al.* [2001] find that an explicit ecosystem only slightly increases CO_2 air-sea flux variability in the model of *LeQuéré et al.* [2000] may indicate that the underrepresentation of annual nutrient cycles is not crucial to capturing interannual variability of air-sea fluxes. Clearly, it will be important to explicitly test the impact of improved representation of model nutrient cycles, and presumably of O_2 anomaly and ΔpCO_2 cycles, on air-sea flux variability.

There is a significant trend in the model flux estimates for both O_2 and CO_2 and a significant mean O_2 efflux, although the mean CO_2 flux influx compares well to *Takahashi et al.* [1997, 1999]. The difference of the mean comparisons may be explained by *Stephens et al.* [1998] who indicate that O_2 fluxes are more sensitive to the properties of an ocean general circulation model than are CO_2 fluxes. This sensitivity arises because biological and temperature drivers for air-sea fluxes are typically in sync over the annual cycle for O_2, but out of phase for CO_2. This means that errors in model processes that drive O_2 fluxes are likely to be cumulative, while errors in CO_2 fluxes are likely to be damped. Flux errors for CO_2 are further damped by a slow air-sea exchange timescale. For this work, the 19-year mean O_2 flux at each point is simply subtracted away, and air-sea flux trends are removed by a linear fit in time at each point in space. These features may be better addressed in future work by a longer model spin-up and improved representation of Southern Ocean physics. Also desirable would be to further study the impact of parameterizations for export, anoxic respiration, and remineralization on these fluxes and to improve the performance of these parameterizations. As computational power grows, these options will become increasingly feasible and should be explored.

7.2 Next Steps

In Chapter 5, it is shown that an offline model run for 1997-1998 that was forced with physical results from a model constrained with altimetric data exhibited little difference in air-sea gas flux variability in comparison to the unconstrained run presented in Chapters 3 and 4. This is because the physical changes at the surface of the model caused by the constraint do not propagate significantly into the interior and improve the structure of the mean thermocline or its variability. The reasons for this problem and possible solutions are active areas of research at the present time. The use of satellite altimetry to constrain physical models and increase their physical variability is an important direction for future work.

When the export parameterization described in Section 3.3 is used in future studies, it should be improved by choosing regions based on biogeochemical or dynamical regimes, instead of latitude bands. Smoothing of the transitions between the α regions would ameliorate the sharp gradients in mean gas fluxes, though this would be largely a cosmetic improvement and should not significantly alter the mean or variability of the gas fluxes estimated by the model.

As previously indicated, an explicit ecosystem model should help to improve nutrient cycling and, therefore, seasonal O_2 and CO_2 air-sea fluxes. It is possible that improving seasonal cycles of gas fluxes will have important implications for interannual variability in air-sea gas fluxes. The addition of iron limitation to an explicit ecosystem model may be crucial for the representation of nutrient cycling, especially in the equatorial Pacific and the Southern Ocean [*Moore et al.*, 2002]. With either a particle export scheme or an ecosystem model, an explicit alkalinity pool would likely increase ΔpCO_2 variability, particularly at high latitudes, and also improve model surface DIC concentrations. Along with improvements to model physics in the equatorial Pacific, the addition of a DOC pool may help to reduce the region of deep anoxia in the model that contributes to an overestimate of the global mean O_2 flux [*Aumont et al.*, 1999]. Finally, an ecosystem model that allows for long-term ecosystem change due to shifts in dominant species, nitrogen fixation, and other processes, although still on the scientific horizon, would likely be useful in this application for improving our understanding of the observed phenomena.

These results indicate a dominance of the equatorial Pacific to global air-sea flux variability of both CO_2 and O_2. Air-sea gas flux variability and its driving mechanisms in this region could be analyzed further and compared to available data. A regional model with greater resolution could be used to determine whether the resolution of this global model is adequate to capture regional dynamics [*Aumont et al.*, 1999], and to estimate the full extent of air-sea gas flux variability in the equatorial Pacific. Additional study could also be done to better understand how the different air-sea exchange timescales for O_2 and CO_2 interact with ocean physics to make the O_2 flux timeseries lead the SOI index while the CO_2 flux lags.

The impact of the physics and biogeochemistry of the Southern Ocean on O_2 and CO_2 air-sea flux variability is an important future direction. It is not fully clear if the Gent-McWilliams eddy parameterization in the model is damping mean fluxes and variability. Additional experiments with and more analysis of this model could be undertaken to understand the impacts of model physics in the Southern Ocean on air-sea gas fluxes. Biogeochemical variability, which is damped in this model, may become more realistic with the use of an ecosystem model that includes biological iron limitation and geochemical iron cycling [*Parekh et al.*, 2002]. Being such a large sector of the global ocean, the Southern Ocean may have a significant impact on gas flux variability that is perhaps only hinted at (Figure 4-17), but not fully captured, in this work. Thus, the physics and biogeochemistry of the Southern Ocean provides a fertile ground for future work.

Finally, there is a pressing need for additional data. Measurements of atmospheric CO_2 and O_2/N_2 are sparse, imparting significant error to atmospheric inversion efforts and complicating efforts to verify model results. If the O_2/N_2 method is to reliably estimate interannual variability in the land and ocean CO_2 sinks, error due to interannual variability in air-sea O_2 fluxes needs to be addressed. With appropriate measurements, particularly in the equatorial Pacific and North Atlantic, these model results indicate that there is a possibility of quantifying the bulk of the O_2 flux variability and constraining CO_2 fluxes using the atmospheric O_2/N_2 method on interannual timescales. The continuous O_2 analyzer of *Manning* [2001] could be used to expand the network of O_2/N_2 methods across the globe, and accomplish such quantification. Model estimates such as the one presented here might also be used to help interpret O_2/N_2 measurements on interannual timescales, but

they themselves have significant error that is difficult to quantify.

Ocean/atmosphere ΔpCO_2 measurements are also needed. Results from this model could be used to improve understanding of uncertainty due to data sparsity and interpolation in the ΔpCO_2 climatology of *Takahashi et al.* [1997, 1999], and could help to guide additional data collection. The ΔpCO_2 surveys discussed by *Chavez et al.* [1999] in the equatorial Pacific during various stages of the ENSO cycle have been highly informative and the continuation and expansion of this work is important. Physical and biogeochemical data from the Southern Ocean is particularly lacking despite indications that the region may be very important to many pieces of the global climate puzzle. Measurement campaigns designed to significantly increase the spatial and temporal density of the Southern Ocean observations should be seriously considered.

Appendix A

NPZD Model

In this appendix, I illustrate that an NPZ model similar in form to that of *Dutkiewicz et al.* [2001] can be reduced to the biological sink term in Equation 3.6 when a steady state assumption is made. There is evidence that the steady state approximation, although often made, may not be sufficient to capture the mean state of ocean biogeochemistry due to the influence of mesoscale eddies (G. Flierl, personal communication). I proceed acknowledging that important controls on export may be omitted.

In the below equations, four compartments are represented: inorganic phosphorus (P), dissolved organic phosphorus (DOP), phytoplankton (PHY) and zooplankton (Z). S is the supply of inorganic phosphorus; μ_P is the growth rate for phytoplankton on inorganic phosphorus; Po and PHYo are half-saturation constants; r is the rate of regeneration of DOP; g is the grazing rate of Z on PHY; e is the excretion rate of DOP; and m is the mortality of zooplankton. All dead zooplankton fall out of the surface layer, and thus mZ is the export rate.

$$\frac{dP}{dt} = -\mu_P \cdot PHY \cdot \frac{P}{P + Po} + rDOP + S \tag{A.1}$$

$$\frac{dPHY}{dt} = \mu_P \cdot PHY \cdot \frac{P}{P + Po} - gZ\frac{PHY}{PHY + PHYo} \tag{A.2}$$

$$\frac{dDOP}{dt} = -rDOP + eZ \tag{A.3}$$

$$\frac{dZ}{dt} = gZ\frac{PHY}{PHY + PHYo} - eZ - mZ \tag{A.4}$$

Assuming steady state and summing Equations A.1 to A.4, we find:

$$S = mZ \tag{A.5}$$

Or that export production and supply must be equal in steady state. From Equation A.1 in steady state:

$$S = \mu_P \cdot PHY \cdot \frac{P}{P + Po} - rDOP \tag{A.6}$$

Equating A.5 and A.6:

$$Z = \frac{1}{m}(\mu_P \cdot PHY \cdot \frac{P}{P + Po} - rDOP) \tag{A.7}$$

From equation A.2 in steady state:

$$\mu_P \frac{P}{P + Po} = gZ\frac{1}{PHY + PHYo} \tag{A.8}$$

Substituting A.7 in A.8:

$$\mu_P \frac{P}{P + Po} = \frac{g}{m}(\mu_P \frac{P}{P + Po} - \frac{rDOP}{PHY}) \cdot \frac{PHY}{PHY + PHYo} \tag{A.9}$$

I estimate recycled production as the rate of DOP remineralization normalized by the phytoplankton concentration, and thus can define the ratio of new (total - regenerated production) to total production:

$$f = \frac{\mu_P \frac{P}{P+Po} - \frac{rDOP}{PHY}}{\mu_P \frac{P}{P+Po}} \tag{A.10}$$

Substituting this definition into Equation A.9, we find the steady state phytoplankton concentration:

$$PHY = \frac{1}{\frac{g \cdot f}{m} - 1} \cdot PHYo \tag{A.11}$$

With Equation A.11 and the definition of $\mu_P = \mu_o \frac{I}{I+Io}$, a constant export parameter modified by light availability, Equation A.6 now becomes:

$$S = \frac{\mu_o}{\frac{g \cdot f}{m} - 1} \cdot PHYo \cdot \frac{I}{I + Io} \cdot \frac{P}{P + Po} \tag{A.12}$$

and thus:

$$\alpha = \frac{\mu_o}{\frac{g \cdot f}{m} - 1} \cdot PHYo \tag{A.13}$$

and

$$S = \alpha \cdot \frac{I}{I + Io} \cdot \frac{P}{P + Po} \tag{A.14}$$

Where S = export as shown above.

Below we present values from the literature for the NPZ model inputs that are required to solve Equation A.13. These values are found in the literature review of *Dutkiewicz et al.* [2001], *Six and Maier-Reimer* [1996] and *Sarmiento et al.* [1993].

Range of NPZ parameters for α calculation

parameter	symbol	range	units
phytoplankton maximum growth rate	μ_o	0.5 - 4	d^{-1}
zooplankton mortality rate	m	0.02 - 0.05	d^{-1}
zooplankton grazing rate	g	0.625 - 1.0	d^{-1}
f-ratio	f	0.1 - 1.0	
half-saturation for phytoplankton	PHYo	0.03 - 0.05	μmol PO_4 kg^{-1}

Given these values, a theoretical range for α is $4x10^{-9}$ to $1x10^{-5}$ μmol PO_4 kg^{-1} s^{-1}.

For the solution of a globally heterogeneous export parameter (Section 3.3, I make a rough calculation of a starting value for α given an average surface phosphate concentration of 0.5 μmol PO_4 kg^{-1} from the WOA98 climatology and a global fallout timescale of 9 months, and find an initial $\alpha = 2.3x10^{-8}$ μmol PO_4 kg^{-1} s^{-1}. This α is clearly consistent with the range suggested by this analysis.

Bibliography

Albritton, D., L. Meira Filho, et al., Summary for Policymakers: A Report of Working Group I of the Intergovernmental Panel on Climate Change, in *Climate Change 2001: The Scientific Basis*. Intergovernmental Panel on Climate Change, 2001.

Anderson, L. A., and J. L. Sarmiento, Redfield ratios of remineralization determined by nutrient data analysis, *Global Biogeochem. Cycles*, *8*, 65–80, 1994.

Arrhenius, S., On the influence of carbonic acid in the air upon the temperature of the ground, *London Edinburgh Dublin Philos. Mag. J. Sci.*, *41*, 237–276, 1896.

Aumont, O., J. Orr, and P. Monfray, Nutrient trapping in the equatorial Pacific: The ocean circulation solution, *Global Biogeochem. Cycles*, *13*(2), 351–369, 1999.

Bates, N., Interannual variability of oceanic CO2 and biogeochemical properties in the Western North Atlantic subtropical gyre, *Deep-Sea Res. II*, *48*(8-9), 1507–1528, 2001.

Battle, M., et al., Atmospheric gas concentrations over the past century measured in air from firn at the South Pole, *Nature*, *383*, 231–235, 1996.

Battle, M., M. Bender, P. Tans, J. White, J. Ellis, T. Conway, and R. Francey, Global carbon sinks and their variability inferred from atmospheric O_2 and $\delta^{13}C$, *Science*, *287*, 2467–2470, 2000.

Bender, M., T. Ellis, P. Tans, R. Francey, and D. Lowe, Variability in the O_2/N_2 ratio of southern hemispher air, 1991-1994: Implications for the carbon cycle, *Global Biogeochem. Cycles*, *10*, 9–21, 1996.

Bousquet, P., P. Peylin, P. Ciais, C. LeQuéré, P. Friedlingstein, and P. P. Tans, Regional changes in carbon dioxide fluxes of land and oceans since 1980, *Science*, *290*, 2000.

Boutin, J., and J. Etcheto, Climatology of K deduced from the satellite wind speeds, OCMIP protocal README.sat, 1995.

Buesseler, K., The decoupling of production and particle export in the surface ocean, *Global Biogeochem. Cycles*, *12*(2), 297–310, 1998.

Campbell, J., Geochemical oceans sections study, in *Chemical Oceanography*, edited by J. Riley, and R. Chester. Academic Press, 1983.

Cayan, D. R., Latent and sensible hear flux anomalies over the Northern Oceans: The connection to monthly atmospheric circulaton, *J. Climate*, *5*, 354–369, 1992.

Chavez, F., P. Strutton, G. Friederich, R. Feely, G. Feldman, D. Foley, and M. McPhaden, Biological and chemical response of the equatorial Pacific Ocean to the 1997-98 El Niño, *Science*, *286*, 2126–2131, 1999.

Conkright, M., S. Levitus, and T. Boyer, World Ocean Atlas 1994, Volume 1: Nutrients. NOAA Atlas NESDIS 1., Tech. rep., U.S. Department of Commerce, Washington, D.C., 1994.

Conkright, M., S. Levitus, T. O'Brien, T. Boyer, J. Antonov, and C. Stephen, World Ocean Atlas 1998 CD-ROM Data Set Documentation, Tech. Rep. 15, NODC Internal Report, Silver Spring, MD, 1998.

Conway, T., P. Tans, and L. Waterman, Atmospheric CO_2 records from sites in the NOAA/CMDL air sampling network. In Trends 1993: A Compendium of Data on Global Change. ORNL/CDIAC-65., Tech. rep., Carbon Dioxide Information Analysis Center, Oak Ridge National Laboratory, U.S. Department of Energy, Oak Ridge, Tenn. USA, 1994a.

Conway, T. J., P. P. Tans, L. S. Watermann, K. W. Thoning, D. R. Kitzis, K. A. Masarie, and N. Zhang, Evidence for interannual variability of the carbon cycle from the National Oceanic and Atmospheric Administration / Climate Monitoring and Diagnostics Laboratory Global Air Sampling Network, *J. Geophys. Res.*, *99*(D11), 22,831–22,855, 1994b.

Dickson, A., and F. Millero, A comparison of the equilibrium constants for the dissociation of carbonic acid in seawater media, *Deep-Sea Res.*, *34*, 173–184, 1987.

Dutkiewicz, S., M. Follows, J. Marshall, and W. W. Gregg, Interannual variability of phytoplankton abundances in the North Atlantic, *Deep-Sea Res. II*, *48*(10), 2323–2344, 2001.

Emerson, S., S. Mecking, and J. Abell, The biological pump in the subtropical North Pacific Ocean: Nutrient sources, Redfield ratios, and recent changes, *Global Biogeochem. Cycles*, *15*, 535–554, 2001.

Fan, S., M. Gloor, J. Mahlman, S. Pacala, J. Sarmiento, T. Takahashi, and P. Tans, A large terrestrial carbon sink in North America implied by atmospheric and ocean carbon dioxide data and models, *Science*, *282*, 1998.

Feely, R. A., R. H. Gammon, B. A. Taft, P. E. Pullen, L. S. Watterman, T. J. Conway, J. F. Gendron, and D. P. Wisegarver, Distribution of chemcial tracers in the eastern equatorial Pacific during and after the 1982-1983 El Niño/Southern Oscillation event, *J. Geophys. Res.*, *92*(C6), 6545–6558, 1987.

Feely, R. A., R. Wanninkhof, C. E. Cosca, P. P. Murphy, M. F. Lamb, and M. D. Steckley, CO_2 distributions in the equatorial Pacific during the 1991-1992 ENSO event, *Deep-Sea Res. Part II*, *42*, 567–601, 1995.

Feely, R. A., R. Wanninkohf, C. Goyet, D. E. Archer, and T. Takahashi, Variability of CO_2 distributions and air-sea fluxes in the central and eastern equatorial Pacific during the 1991-1994 El Niño, *Deep-Sea Res. II*, *44*(9-10), 1851–1867, 1997.

Feely, R. A., R. Wanninkhof, T. Takahashi, and P. Tans, Influence of El Niño on the equatorial Pacific contribution to atmospheric CO_2 accumulation, *Nature*, *398*, 365–386, 1999.

Follows, M., R. Williams, and J. Marshall, The solubility pump of carbon in the subtropical gyre of the North Atlantic, *J. Mar. Res.*, *54*(4), 605–630, 1996.

Francey, R., P. Tans, C. Allison, I. Enting, J. White, and M. Troller, Changes in oceanic and terrestrial carbon uptake since 1982, *Nature*, *373*, 326–330, 1995.

Francey, R., C. Allison, C. Trudinger, P. Rayner, I. Enting, and L. Steele, The interannual variation in global atmospheric δ^{13}C and its link to net terrestrial exchange., in *Extended Abstracts, 6th International Carbon Dioxide Conference, Sendai*. 2001.

Fukumori, I., Altimetric Data Assimilation, in *Satellite Altimetry: Theory, Measurements, and Geophysical Applications*, edited by L. Fu, and A. Cazenave. Academic Press (in press), 2000.

Fukumori, I., R. Raghunath, L. Fu, and Y. Chao, Assimilation of TOPEX/POSEIDON data into a global ocean circulation model: How good are the results?, *J. Geophys. Res*, *104*, 25,647–25,665, 1999.

Ganachaud, A. S., Large scale oceanic circulation and fluxes of freshwater, heat, nutrients, and oxygen., Ph.D. thesis, MIT / WHOI Joint Program in Physical Oceanography, 1999.

Garcia, H. E., and R. F. Keeling, On the global oxygen anomaly and air-sea flux, *J. Geophys. Res.*, *106*(C12), 31,155–31,166, 2001.

Gent, P., and J. McWilliams, Isopycnal mixing in ocean general circulation models, *J. Phys. Ocean.*, *20*, 150–155, 1990.

Goyet, C., R. Healy, and J. Ryan, Global Distribution of Total Inorganic Carbon and Total Alkalinity Below the Deepest Winter Mixed Layer Depths, Tech. Rep. NDP-076, Carbon Dioxide Information Analysis Center, Oak Ridge, TN, 2000.

Gregg, W., Tracking the SeaWiFS record with a coupled physical/biogeochemical/radiative model of the global oceans, *Deep-Sea Res. II*, *49*(1-3), 81–105, 2002.

Gruber, N., E. Gloor, S.-M. Fan, and J. L. Sarmiento, Air-sea flux of oxygen estimated from bulk data: Implications for the marine and atmospheric oxygen cycles, *Global Biogeochem. Cycles*, *15*, 783–803, 2001.

Hoffert, M., Y.-C. Wey, A. Callegari, and W. Broecker, Atmospheric response to deep sea injections of fossil fuel carbon dioxide, *Climate Change*, *2*, 53–68, 1979.

Hurrell, J. W., Decadal Trends in the North Atlantic Oscillation: Regional Temperatures and Precipitation, *Science*, *269*, 676–679, 1995.

Jeandel, C., et al., KERFIX, a time-series station in the Southern Ocean: A presentation, *J. Mar. Sys.*, *17*(1-4), 555–569, 1998.

Jenkins, W., and J. Goldman, Seasonal oxygen cycling and primary production in the Sargasso Sea, *J. Mar. Res.*, *43*, 465–491, 1985.

Joos, F., R. Meyer, M. Bruno, and M. Leuenberger, The variability in the carbon sinks as reconstructed for the last 1000 years, *Geophys. Res. Let.*, *26*(10), 1437–1440, 1999.

Karl, D., et al., The role of nitrogen fixation in biogeochemical cycling in the subtropical North Pacific, *Nature*, *388*, 533–538, 1997.

Karl, D., and R. Lukas, The Hawaii Ocean Time-series (HOT) program: Background, rationale and field implementation, *Deep-Sea Res. II*, *43*(2-3), 129–156, 1996.

Keeling, C., T. Whorf, M. Wahlen, and J. van der Plicht, Interannual extremes in the rate of rise of atmospheric carbon dioxide since 1980, *Nature*, *375*, 666–670, 1995.

Keeling, C. D., and T. P. Whorf, Atmospheric CO2 Concentrations - Mauna Loa Observatory, Hawaii, 1958-1999 (revised August 2000), Tech. Rep. NDP-001, Carbon Dioxide Information Analysis Center, Oak Ridge, TN, 2000.

Keeling, C. D., and T. P. Whorf, Atmospheric CO_2 records from sites in the SIO air sampling network. In Trends: A Compendium of Data on Global Change, Tech. rep., Carbon Dioxide Information Analysis Center, Oak Ridge, TN, 2001.

Keeling, R., and H. Garcia, The change in oceanic O_2 inventory associated with recent global warming, *Proc. US Natl. Acad. Sci. (in press)*, 2002.

Keeling, R. F., and S. R. Shertz, Seasonal and interannual variations in atmospheric oxygen and implications for the global carbon cycle, *Nature*, *358*, 723–727, 1992.

Keeling, R. F., R. P. Najjar, M. L. Bender, and P. P. Tans, What atmospheric oxygen measurements can tell us about the global carbon cycle, *Global Biogeochem. Cycles*, *7*(1), 37–67, 1993.

Keeling, R. F., S. C. Piper, and M. Heimann, Global and hemispheric CO_2 sinks deduced from changes in atmospheric O_2 concentration, *Nature*, *381*, 218–221, 1996.

Keeling, R. F., B. B. Stephens, R. P. Najjar, S. C. Doney, D. Archer, and M. Heimann, Seasonal variations in the atmospheric O_2/N_2 ratio in relation to the kinetics of air-sea gas exchange, *Global Biogeochem. Cycles*, *12*(1), 141–163, 1998.

Keller, K., R. Slater, M. Bender, and R. Key, Possible biological or physical explanations for decadal scale trends in North Pacific nutrient concentrations and oxygen utilization, *Deep-Sea Res. II*, *49*(1-3), 345–362, 2002.

King, C., D. Stammer, and C. Wunsch, The CMPO/MIT TOPEX/POSEIDON altimetric data set, Tech. Rep. 30, Center for Global Change Science, MIT, 1994.

Langenfelds, R., R. Francey, L. Steele, M. Battle, R. Keeling, and W. Budd, Partitioning of the global fossil CO_2 sink using a 19-year trend in atmospheric O_2, *Geophys. Res. Let.*, *26*(13), 1897–1900, 1999.

Large, W., J. McWilliams, and S. Doney, Oceanic vertical mixing: a review and a model with a nonlocal boundary layer parameterization, *Rev. of Geophys.*, *32*(4), 363–403, 1994.

Lee, K., R. Wanninkhof, T. Takahashi, S. C. Doney, and R. A. Feely, Low interannual variability in recent oceanic uptake of atmospheric carbon dioxide, *Nature*, *396*, 155–158, 1998.

Lee, T., I. Fukimori, D. Menemenlis, Z. Xing, and L. Fu, Effects of Indonesian throughflow on the Pacific and Indian ocean, *J. Phys. Ocean., in press*, 2001.

LeQuéré, C., J. C. Orr, P. Monfray, O. Aumont, and G. Madec, Interannual variability of the oceanic sink of CO_2 from 1979 to 1997, *Global Biogeochem. Cycles*, *14*(4), 1247–1265, 2000.

LeQuéré, C., O. Aumont, P. Monfray, and J. C. Orr, Climate-induced variability of ocean stratification, marine biology, and CO_2 during 1979 to 1999, *submitted to J. Geophys. Res.*, 2001.

Levitus, S., and T. Boyer, World Ocean Atlas 1994 Volume 4: Temperature, Tech. Rep. 4, NOAA Atlas NESDIS, Washington D.C., 1994.

Lewis, M., N. Kuring, and C. Yentsch, Global patterns of ocean transparency: Implications for the new production of the open ocean, *J. Geophys. Res*, *93*, 6847–6856, 1988.

Mahlman, J., Science and nonscience concerning human-caused climate warming, *Annual Review: Energy Environment*, *23*, 83–105, 1998.

Maier-Reimer, E., Geochemical cycles in an ocean general circulation model. Preindustrial tracer distributions, *Global Biogeochem. Cycles*, *7*(3), 645–677, 1993.

Manabe, S., and R. Wetherald, Thermal equilibrium of the atmosphere with a given distribution of relative humidity, *J. Atmos. Sci*, *24*, 241–259, 1967.

Manning, A. C., Temporal variability of atmospheric oxygen from both continuous measurements and a flask sampling network: Tools for studying the global carbon cycle, Ph.D. thesis, University of California, San Diego, 2001.

Marland, G., T. Boden, and R. Andres, Global, Regional, and National Annual CO_2 Emissions from Fossil-Fuel Burning, Cement Production, and Gas Flaring: 1751-1998. In Trends: A Compendium of Data on Global Change, Tech. rep., Carbon Dioxide Information Analysis Center, Oak Ridge National Laboratory, U.S. Department of Energy, Oak Ridge, Tenn. USA, 2001.

Marshall, J., and F. Molteni, Toward a dynamical understanding of planetary-scale flow regimes, *J. Atmos. Sci.*, *50*(12), 1792–1818, 1993.

Marshall, J., A. Adcroft, C. Hill, L. Perelman, and C.Heisey, A finite volume, incompressible Navier-Stokes model for studies of the ocean on parallel computers, *J. Geophys. Res*, *102*, 5753–5766, 1997a.

Marshall, J., C. Hill, L. Perelman, and A. Adcroft, Hydrostatic, quasi-hydrostatic and non-hydrostatic ocean modeling, *J. Geophys. Res*, *102*, 5733–5752, 1997b.

Martin, J. H., Glacial-interglacial CO_2 change: The iron hypothesis, *Paleoceanography*, *5*(1), 1–13, 1990.

Matear, R., A. Hirst, and B. McNeil, Changes in dissolved oxygen in the Southen Ocean with climate change, *Geochem. Geophys. Geosyst.*, *1*(Paper no. 2000GC000086), 2000.

McGillicuddy, D., A. Robinson, D. Seigel, H. Jannasch, R. Johnson, T. Dickey, J. McNeil, A. Michaels, and A. Knap, Influence of mesoscale eddies on new production in the Sargasso Sea, *Nature*, *394*, 263–266, 1998.

McKinley, G. A., M. J. Follows, and J. C. Marshall, Interannual variability of the air-sea flux of oxygen in the North Atlantic, *Geophys. Res. Let.*, *27*(18), 2933–2936, 2000.

McPhaden, M. J., et al., The Tropical Ocean-Global Atmosphere observing system: A decade of progress, *J. Geophys. Res.*, *103*(C7), 14,169–14,240, 1998.

Melillo, J. M., A. D. McGuire, D. W. Kicklighter, B. Moore III, C. J. Vorosmarty, and A. L. Schloss, Global climate change and terrestrial net primary production, *Nature*, *363*, 1993.

Millero, F. J., K. Lee, and M. Roche, Distribution of alkalinity in the surface waters of the major oceans, *Mar. Chem.*, *60*, 111–130, 1998.

Moore, J., S. Doney, J. Kleypas, D. Glover, and I. Fung, An intermediate complexity marine ecosystem model for the global domain, *Deep-Sea Res. II*, *49*(1-3), 403–462, 2002.

Morel, A., Available, usable, and stored radiant energy in relation to marine photosynthesis, *Deep-Sea Res.*, *25*, 673–68, 1978.

Najjar, R., and R. Keeling, Analysis of the mean annual cycle of the dissolved oxygen anomaly in the World Ocean, *J. Mar. Res.*, *55*, 117–151, 1997.

Najjar, R., and R. Keeling, Mean annual cycle of the air-sea oxygen flux: A global view, *Global Biogeochem. Cycles*, *14*(2), 573–584, 2000.

Najjar, R. G., J. L. Sarmiento, and J. Toggweiler, Downward transport and fate of organic matter i the ocean: Simulations with a general circulation model, *Global Biogeochem. Cycles*, *6*(1), 45–76, 1992.

North, G., R. Cahalan, and J. Coakley, Energy balance climate models, *Rev. of Geophys. and Space Phys.*, *19*, 91–121, 1981.

Ono, S., A. Ennyu, R. Najjar, and N. Bates, Shallow remineralization in the Sargasso Sea estimated from seasonal variations in oxygen, dissolved inorganic carbon and nitrate, *Deep-Sea Res. II*, *48*, 1567–1582, 2001.

Orr, J., OCMIP evaluation of deep ocean circulation, *Research GAIM*, *4*(2), 5, 2001.

Orr, J., R. Najjar, C. Sabine, and F. Joos, *Ocean Carbon-Cycle Model Intercomparison Project 2: Abiotic-HOWTO (http://www.ipsl.jussieu.fr/OCMIP/)*, 2000.

Oschlies, A., and V. Garçon, Eddy-induced enhancement of primary production in a model of the North Atlantic Ocean, *Nature*, *394*, 266–269, 1998.

Paltridge, G., and C. Platt, *Radiative Processes in Meteorology and Climatology*. Elsevier, Amsterdam, 1976.

Parekh, P., M. Follows, E. Boyle, and J. Marshall, Controls on deep water iron distribution: Scavenging vs. complexation, *in preparation*, 2002.

Parsons, T., M. Takahashi, and B. Hargrave, *Biological Oceanographic Processes, 3rd Ed.* Pergamon Press, New York, 1984.

Pickard, G. L., and W. J. Emery, *Descriptive Physical Oceanography*. Butterworth Heinemann, Great Britain, 5th ed., 1990.

Plattner, G.-K., F. Joos, and T. F. Stocker, Revision of the global carbon budget due to changing air-sea oxygen fluxes, *submitted to Global Biogeochem. Cycles*, 2001.

Prentice, I., et al., *Climate Change 2001, The Scientific Basis*, chap. 3. Intergovernmental Panel on Climate Change, 2001.

Radenac, M., C. Menkes, J. Vialard, Y. Dandonneau, T. Delcroix, C. Dupuoy, A. Stoens, and P.-Y. Deschamps, Modeled and observed impacts of the 1997-1998 El Niño on nitrate and new production in the equatorial Pacific, *J. Geophys. Res.*, *106*(C11), 26,879–26,898, 2001.

Rayner, P., I. Enting, R. Francey, and R. Langenfelds, Reconstructing the recent carbon cycle from atmospheric CO_2, $\delta^{13}C$ and O_2/N_2 observations, *Tellus*, *51B*, 213–232, 1999.

Reynolds, R., and T. Smith, Improved global sea surface temperature analyses, *J. Climate*, *7*, 929–948, 1994.

Sarmiento, J., R. Slater, M. Fasham, H. Ducklow, J. Toggweiler, and G. Evans, A seasonal three-dimensional ecosystem model of nitrogen cycling in the North Atlantic euphotic zone, *Global Biogeochem. Cycles*, *7*(2), 417–450, 1993.

Sarmiento, J. L., and E. Sundquist, Revised budget for the oceanic uptake of anthropogenic carbon dioxide, *Nature*, *356*, 589–593, 1992.

Sarmiento, J. L., T. M. Hughes, R. J. Stouffer, and S. Manabe, Simulated response of the ocean carbon cycle to anthropogenic climate warming, *Nature*, *393*, 245–2494, 1998.

Schimel, D., et al., Radiative forcing of climate change, in *Climate Change, 1995: The Science of Climate Change*, edited by Houghton, et al., pp. 76–86. University Press, Cambridge, UK, 1995.

Schimel, D., et al., Contribution of increasing CO_2 and climate to carbon storage by ecosystems in the United States, *Science*, *287*, 2000.

Simonot, J.-Y., and H. LeTreut, A climatological field of mean optical properties of the world ocean, *J. Geophys. Res*, *91*(C5), 6642–6646, 1986.

Six, K. D., and E. Maier-Reimer, Effects of plankton dynamics on seasonal carbon fluxes in an ocean general circulation model, *Global Biogeochem. Cycles*, *10*(4), 559–583, 1996.

Stammer, D., R. Tokmakian, A. Semtner, and C. Wunsch, How well does a 1/4° global circulation model simulate large-scale oceanic observations?, *J. Geophys. Res*, *101*(C10), 25,779–25,811, 1996.

Stephens, B., R. Keeling, M. Heimann, K. Six, R. Murnane, and K. Caldiera, Testing global carbon cycle models using measurements of atmospheric O_2 and CO_2 concentration, *Global Biogeochem. Cycles*, *12*, 213–230, 1998.

Takahashi, T., W. Broecker, and A. Brainbridge, The alkalinity and total carbon dioxide concentrations in the world oceans, in *Carbon Cycle Modelling*, edited by B.Bolin. John Wiley and Sons, New York, 1981.

Takahashi, T., W. Broecker, and S. Langer, Redfield ratio based on chemical data from isopycnal surfaces, *J. Geophys. Res*, *90*, 6907–6924, 1985.

Takahashi, T., J. Olafsson, J. G. Goddard, D. W. Chipman, and S. Sutherland, Seasonal variation of CO_2 and nutrients in the high-latitude surface oceans: A comparative study, *Global Biogeochem. Cycles*, *7*(4), 843–878, 1993.

Takahashi, T., R. A. Feely, R. F. Weiss, R. H. Wanninkhof, D. W. Chipman, S. C. Sutherland, and T. T. Takahashi, Global air-sea flux of CO_2: An estimate based on measurements of sea-air pCO_2 difference, *Proc. Natl Acad. Sci. USA*, *94*, 8292–8299, 1997.

Takahashi, T., R. H. Wanninkhof, R. A. Feely, R. F. Weiss, D. W. Chipman, N. Bates, J. Olafsson, C. Sabine, and S. C. Sutherland, Net sea-air CO_2 flux over the global oceans: An improved estimate based on the sea-air pCO_2 difference, in *Proceedings of the 2nd International Symposium: CO_2 in the Oceans*, pp. 9–15. 1999.

Tans, P. P., I. Y. Fung, and T. Takahashi, Observational constraints on the global atmospheric CO_2 budget, *Science*, *247*, 1990.

Tomczak, M., and J. S. Godfrey, *Regional Oceanography: An Introduction*. Pergamon, 1994.

Trenberth, K. E., Signal versus Noise in the Southern Oscillation, *Mon. Wea. Rev.*, *112*, 326–332, 1984.

Trenberth, K. E., The Definition of El Niño, *Bull. Amer. Meteor. Soc.*, *78*(12), 2771–2777, 1997.

Wanninkhof, R., Relationship between wind speed and gas exchange over the ocean, *J. Geophys. Res*, *97*, 7373–7382, 1992.

Webster, P. J., and T. N. Palmer, The past and the future of El Niño, *Nature*, *390*, 562–564, 1997.

Weiss, R., The solubility of nitrogen, oxygen, and argon in water and seawater, *Deep-Sea Res.*, *17*, 721–735, 1970.

Weiss, R., Carbon dioxide in water and seawater: The solubility of a nonideal gas, *Mar. Chem.*, *2*, 203–215, 1974.

Williams, R. G., and M. J. Follows, The Ekman transfer of nutrients and maintenance of new production over the North Atlantic, *Deep-Sea Res.*, *45*, 461–489, 1998.

Winguth, A., M. Heimann, K. Kurz, E. Maier-Reimer, U. Milolajewicz, and J. Segschneider, El Niño - Southern Oscillation related fluctuations in the marine carbon cycle, *Global Biogeochem. Cycles*, *8*, 39–93, 1994.

Worthington, L., On the North Atlantic circulation, *Johns Hopkins Oceanographic Studies*, *6*, p.110, 1976.

Zhang, R., M. Follows, J. Grotzinger, and J. Marshall, Could the Late Permian deep ocean have been anoxic?, *Paleoceanography*, *16*(3), 317–329, 2001.